

PH.D. THESIS

**zCOSMOS survey galaxy groups:
exploring the effect of group environment on galaxy properties**

Candidato:
Valentina Presotto

Matricola **710649**

Relatore:
Dott.ssa Angela Iovino

Correlatore:
Dott. Marco Scodiggio

Contents

Contents	iii
List of Tables	v
List of Figures	viii
Abstract	ix
1 Introduction	1
1.1 An evolving Universe: cosmological model and structure formation	1
1.2 The last snapshot: Galaxies in the Local Universe	4
1.3 The role of environment: <i>Nature</i> or <i>Nurture</i> ?	6
1.4 Processes active in groups/clusters	9
1.5 Segregation effects in groups	11
1.6 Outline of the Thesis	14
2 The zCOSMOS survey and its data set	17
2.1 Survey description	17
2.1.1 zCOSMOS survey	17
2.1.2 zCOSMOS bright: design and data reduction	18
2.1.3 The final sample: 20K galaxy catalog and its properties	20
2.1.4 Spectroscopic group catalog	25
2.1.5 Spectroscopic field sample	29
2.2 Photometric redshifts	30
3 Mock catalogs construction	35
4 The Algorithm	37
4.1 Adding photo-zs to the spectroscopic group catalog	37
4.1.1 Strategy	37
4.1.2 Tests on the mocks	41
4.2 Defining the group centers	46

Contents

4.2.1	Strategy	46
4.2.2	Tests on the mocks	47
4.3	Conclusions	54
5	The Stacked Group	57
5.1	Applying the algorithm to the 20K final sample	57
5.2	Volume-mass limited samples	60
5.3	Group rescaling	62
5.4	Low-z and High-z Stacked-Groups	64
5.5	Conclusions	67
6	Segregation effects in the zCOSMOS 20k groups: colors and masses	69
6.1	F_{blue} and galaxy stellar masses in groups vs field	69
6.2	Color segregation: F_{blue} as a function of the group-centric distance . . .	72
6.3	Large scale trend	75
6.4	Galaxy stellar mass and group richness dependence	77
6.5	Mass segregation	79
6.6	Migration from blue to red: the effects of group environment	83
6.7	Conclusions	86
7	Segregation effects: further insights from spectra and morphologies	89
7.1	Morphologies	89
7.2	Spectra	91
7.2.1	Co-adding spectra: the procedure	91
7.2.2	SSP fitting and line measuring	94
7.3	Morphological and Spectral segregation	95
7.3.1	Morphological changes as a function of group-centric distance . . .	98
7.3.2	The 'strangled' red-spirals population	101
7.3.3	Star forming galaxies at fixed environment and stellar mass . . .	104
7.4	Low mass galaxies: the key to understand the rapid <i>nurture</i> effects . . .	110
7.5	Conclusions	112
8	Conclusions and future prospects	115
8.1	Conclusions	115
8.2	Future plans	117
	Bibliography	126
	Acknowledgements	127

Contents

CV of Valentina Presotto	129
List of publications	133

List of Tables

2.1	<i>z</i> COSMOS confidence class flag scheme	19
4.1	Median and VW center distance to the central galaxy	51
5.1	Volume- and mass-volume-limited sample sizes	62
5.2	Radial range of different group regions	66
6.1	F_{blue} in groups and field for different stellar mass bins	71
6.2	F_{blue} for different group regions, group masses, and stellar mass bins	74
6.3	KS test probabilities for mass distribution in group and field	81
7.1	ZEST Classification Scheme	90
7.2	F_{early} for different group regions and stellar mass bins	99

List of Figures

1.1	Fraction of galaxies in groups at different redshifts	2
1.2	Distribution of broad-band galaxy properties in the SDSS	5
1.3	The morphology density relation	7
1.4	Group regions where physical mechanisms operate	13
2.1	Ra-Dec distribution of the zCOSMOS-bright galaxies	21
2.2	Redshift distribution of the zCOSMOS-bright galaxies	22
2.3	Distribution along the line of sight of the zCOSMOS-bright galaxies . .	23
2.4	B band absolute magnitudes for the zCOSMOS-bright galaxies	24
2.5	Color-mass diagram in bins of redshift for the zCOSMOS-bright galaxies	26
2.6	Statistics of the "multi-pass" FOF group-finding algorithm	28
2.7	Comparison between photo-z from Ilbert et al. (2009) and Oesch (2011)	31
2.8	Comparison between photo-z and spec-z	33
4.1	Selection functions for photo-zs candidate members	38
4.2	Distribution of the center-shift in mock groups	40
4.3	Distribution of the completeness in mock groups	41
4.4	Completeness and interlopers distribution for small center-shift	42
4.5	Completeness and interlopers distribution for big center-shift	43
4.6	Fraction of interlopers as a function of group-centric distance	45
4.7	Examples of Voronoi Tessellation	48
4.8	Median and VW centers performances	49
4.9	Distribution of VW center distance to the central galaxy in mock groups	50
4.10	RCG probability distribution in mock groups	52
4.11	Same as Fig. 4.10 for different RCG configurations	53
4.12	Distribution of the RCG distance to the central galaxy	54
5.1	Example of sky distribution of a typical group	58
5.2	Same as Fig. 4.11 for observed RCG	59
5.3	Redshift distribution and color-mass diagram of our sample	60

List of Figures

5.4	Comparison of group global properties at different redshifts	64
5.5	Sky distribution of the composite groups	65
6.1	Mass distribution and F_{blue} for group and field galaxies	70
6.2	F_{blue} as a function of the group-centric distance	72
6.3	F_{blue} in the near field	76
6.4	F_{blue} dependence on group richness and stellar mass	78
6.5	Galaxy radial distribution for different stellar mass bins	79
6.6	Same as Fig. 6.5 for poor and rich groups	82
7.1	Composite spectrum for different galaxy types	93
7.2	Example of SED fitting with GOSSIP	96
7.3	F_{late}^{GR} and F_{early}^{GR} as a function of the group-centric distance	97
7.4	Same as Fig. 7.3 for different stellar mass bins	100
7.5	Bulge type distribution for different stellar mass bins	102
7.6	Fraction of red passive late-type galaxies	103
7.7	Composite spectrum of a typical galaxy in the low-z bin	105
7.8	Same as Fig. 7.7 but in the high-z bin	106
7.9	EW of the typical galaxy as a function of the group-centric distance . .	107
7.10	Distribution of EWs of blue active galaxies	109

Abstract

The evolution of galaxies in groups may have important implications for the global evolution of the galaxy population as a whole. The fraction of galaxies bound in groups at $z \sim 0$ is as high as 60% and many processes operating in groups may concur in shaping galaxy evolution.

The rich zCOSMOS spectroscopic data (about 20000 galaxies with $I_{AB} \leq 22.5$ up to $z \sim 1$) and its excellent group catalog (~ 200 groups with more than 5 members up to $z \sim 1$) coupled with the wide photometric coverage of the COSMOS survey, can shed new light on this topic, enabling us to study in a continuous way, up to $z \sim 1$, the complex interplay between environment and galaxy evolution.

In this thesis I present the new results I have obtained on this topic by exploring the group-centric dependence of galaxy colors, masses, morphologies and star formation.

In brief, by building two composite groups at intermediate ($0.2 \leq z \leq 0.45$) and high ($0.45 < z \leq 0.8$) redshifts, I was able to study in detail how galaxy stellar masses, colors, morphologies, and spectral features vary as a function of the distance from the group center. My analysis was performed in narrow bin of stellar masses/colors, in order to disentangle the obvious galaxy stellar mass/color dependencies.

To build the composite group I developed an algorithm to incorporate the galaxies brighter than $I_{AB} = 22.5$ and missing a secure spectroscopic redshift, thus improving the statistics of the sample. To confidently determine all galaxy projected distance and rescale them into the composite group, I defined a new centering technique.

From the color/mass analysis I found that the evolution of most massive galaxies ($\log(\mathcal{M}_{gal}/\mathcal{M}_{\odot}) > 10.6$) is mainly driven by internal processes, as no strong group-centric environment dependence is visible.

For galaxies of lower masses ($9.8 \leq \log(\mathcal{M}_{gal}/\mathcal{M}_{\odot}) \leq 10.6$) there is a radial dependence in the changing mix of red and blue galaxies, red galaxies residing preferentially in the group center. Such dependence is most evident in poor groups, whereas richer groups do not display any obvious color trend.

Interestingly mass segregation shows the opposite behavior: it is visible only in rich groups, while poorer groups have a constant mix of galaxy stellar masses as a function of radius.

Abstract

The morpho-spectral analysis showed the presence of a mild morphological segregation at fixed galaxy stellar mass, with massive early-type galaxies preferentially located in the core of groups. Galaxies with $9.8 \leq \log(\mathcal{M}_{gal}/\mathcal{M}_{\odot}) \leq 10.6$ exhibit the strongest morphological differences between group and field environment. These galaxies also have an excess of red-passive spirals in the group with respect to the field.

Despite the presence of a significant segregation of the spectral properties of group galaxies, such that the typical core galaxy have less intense emission lines, the star forming galaxies share the same level of activity at fixed stellar mass irrespective of the environment they reside in.

This findings can be explained in a simple scenario where color/SFR and mass segregation originates from different physical processes.

Mass segregation is driven by dynamical phenomena within groups, and therefore its presence/absence in rich/poor groups is a possible indication that poorer groups start to assemble later in cosmic time than richer structures.

The parallel absence/presence of color segregation in rich/poor groups hints to the fact that nurture effects are still in action in poorer structures, whereas in richer systems are already largely over, so that all galaxies are red irrespective of their position within the group (at least down to the galaxy stellar masses we explored).

Poorer groups hold the smoking gun of environmental effects in action superimposed to secular galaxy evolution: galaxies display gradually redder colors as a consequence of the still recent accretion history of these groups.

The physical processes causing these environmental effects should act on rather short timescales, 1.5-2 Gyrs, because they are not able to erase the striking bi-modality of galaxy color distribution and, moreover, we are not able to observed blue active galaxies showing less intense star formation activity in groups than in the field.

1 Introduction

"An important feature in the non-uniform distribution of galaxies is the occurrence of many physical groups..." "A dozen or more groups of galaxies are now known in which the members exceed two hundred in number. Some of these systems are spheroidal in form, centrally concentrated and of rather definite boundary. The majority of the groups, however, are of irregular form, with indefinite boundaries, and small in membership." (Shapley 1933). The tendency of galaxies to aggregate into larger systems was known since the early '30s and this peculiarity immediately attracted the attention of the astronomers. After nearly a century the study of these large and massive structures still plays a key role in modern astronomy. On one hand galaxy clusters and groups are extreme/special environments: they are characterized by a high density and this may influence the evolution of their member galaxies. On the other hand their distribution in nodes and filaments forms the so-called large scale structure of the universe, which is sensitive to the cosmological model adopted. In other words clusters and groups are excellent laboratories both to study galaxy evolution and to test cosmology.

In this thesis I will focus on the first topic: the effect of the group environment on its member galaxies.

1.1 An evolving Universe: cosmological model and structure formation

Modern cosmology is based on the assumption that the Universe is homogeneous and isotropic and that it is described by Einstein's general theory of relativity. The *concordance* cosmological model assumes that we live in a flat cold dark matter (CDM) universe with a cosmological constant, the so-called standard Λ CDM model. The main elements of this model are baryons, cold dark matter, and dark energy and their abundance is defined by a set of parameters, Ω_i , that is the density of the i^{th} element, $\rho_i(t)$, normalized to the critical density, $\rho_c(t)$:

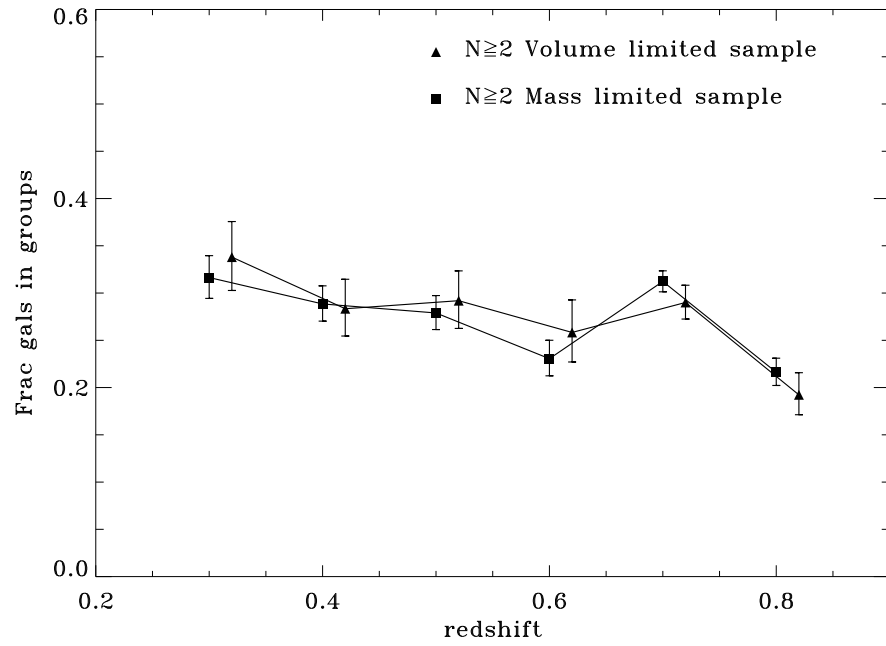


Figure 1.1: Fraction of galaxies in groups in the central region of the zCOSMOS field of view. The points show the fraction of galaxies in groups with richness, $\mathcal{N} \geq 2$ in the 20K volume limited sample up to $z=0.8$ (triangles), and in the 20K mass limited sample down to $\log(\mathcal{M}_{gal}/\mathcal{M}_{\odot}) = 10.6$ (squares).

1.1 An evolving Universe: cosmological model and structure formation

$$\Omega_i = \frac{\rho_i(t)}{\rho_c(t)}, \quad \rho_c(t) = \frac{3H^2(t)}{8\pi G} \quad (1.1)$$

where $H(t)$ is the Hubble's constant, the expansion rate. The present value of the Hubble's constant can be expressed using the adimensional parameter h as: $H_0 = 100 \cdot h$ $\text{km s}^{-1} \text{Mpc}^{-1}$). The final set of parameters is composed by Ω_Λ , the cosmological constant parameter, Ω_m , the total matter parameter, and Ω_b , the baryonic matter parameter.

Current estimations of the present day cosmological parameters yield to: $h \simeq 0.7$, $\Omega_\Lambda \simeq 0.73$, $\Omega_m \simeq 0.27$, where the baryonic contribution to the total matter is $\Omega_b \simeq 0.046$ (Komatsu et al. 2011).

This means that $\Omega = \sum_i \Omega_i = 1$, the required condition by Friedmann equation for a flat universe. Another direct consequence of this model is that the Universe contains only a small percentage of baryonic matter, while it is dominated by Ω_Λ , the so called Dark Energy. This energy acts in the opposite way of the gravitational force: it generates the pressure/repulsion that makes the Universe expand. Not only baryons contribute only marginally to the total density in the Universe, but they also represent only a small percentage of the total matter density. The model assumes that the mass density in the universe is dominated by a weakly interacting massive particle, the so called Dark Matter (DM), and the relative gravitational effects produce the build-up of structure, starting from an initial distribution of density perturbations (Press & Schechter 1974; Peebles 1982; Mo & White 2002).

Dark matter halos (DMHs) are the main bricks that form the structures we observe in the universe. These DMHs are quasi-equilibrium systems of dark matter particles formed by non-linear gravitational collapse. In other words the initial distribution of density perturbation has the greatest power on small scales. Low mass dark matter halos are formed at high redshift and larger halos are produced later through the merging, or accretion, of smaller halos. This is the so-called hierarchical structure formation and the final results of the structure growth are groups and clusters. Galaxies are assumed to develop by cooling and condensation of baryons falling into the DMHs (White & Rees 1978), in other words the large-scale distribution of galaxies is determined by the distribution of DMHs (Mo & White 2002). Therefore, halo clustering is a strong function of halo mass, with more massive halos more strongly clustered.

In this model, groups of galaxies are a gravitationally bound, virialized systems, i.e., their member galaxies inhabit the same DMH. The typical mass of groups are: $M_{group} \sim 10^{12-14} M_\odot$ and their velocity dispersions range from 200 km s^{-1} , for the less massive systems, to 800 km s^{-1} for the largest groups.

1 Introduction

There are many observational evidences of this structure growth: in the Local Universe galaxies reside mostly in groups rather than at higher redshifts, i.e. $z \sim 1/1.5$ (Huchra & Geller 1982; Eke et al. 2004; Berlind et al. 2006; Knobel et al. 2009), while only a small fraction of galaxies live in denser environment such as core clusters. Fig. 1.1 shows the fraction of galaxies in groups in the central region of the zCOSMOS field of view (see Chapt. 2.1.3 for details on the zCOSMOS survey) for groups with richness, $\mathcal{N} \geq 2$ in the 20K volume limited sample up to $z=0.8$, and in the 20K mass limited sample down to $\log(\mathcal{M}_{gal}/\mathcal{M}_{\odot}) = 10.6$. Where richness, \mathcal{N} , is defined as the number of member galaxies surviving to the absolute rest-frame magnitude cut-off for a volume limited sample up to $z=0.8$, see Sect. 5.2 for details on the adopted cut off.

There is a clearly increase of galaxies residing in groups from $z \sim 0.8$ to $z \sim 0.2$ for each explored sample. The percentage of group galaxies rises from less then 20% up to nearly 40%, making the group the most common environment in which galaxies spend their lives. At low redshift zCOSMOS covers a small volume, i.e., $Vol \sim 8 \cdot 10^3 h_{70}^{-3} Mpc^3$ at $z \sim 0.1$, for this reason in Fig. 1.1 we limit the lower redshift to be $z=0.25$.

1.2 The last snapshot: Galaxies in the Local Universe

The picture that raises from the *concordance* cosmological model is the one of an evolving Universe. We can think about the Universe evolution as a movie, this way the Local Universe can be regarded as the last snapshot. This last frame clearly corresponds to the most evolved Universe, from the theoretical point of view, and to the best studied Universe, from the observational point of view. Our understanding of the Local Universe is a starting point in rewinding the tape of this movie and comprehending its evolution.

The plenty of observations at redshift zero has provided a well defined picture of the distribution of galaxy properties. Recent surveys such as the Sloan Digital Sky Survey (SDSS) have explored many dimensions of galaxy properties simultaneously and homogeneously, in order to put galaxy scaling relationships in reciprocal context.

Fig. 1.2 shows the distribution of broad-band galaxy properties in the SDSS (Blanton & Moustakas 2009). The diagonal panels show the distribution of four properties independently: absolute magnitude M_r , g-r color, Sersic index n , and half-light radius r_{50} . The grayscale and contours reflect the number of galaxies in each bin (darker means larger numbers).

These properties reveal a variety of correlations, the strongest ones between the absolute magnitude M_r and the other properties. Given that M_r correlates well with stellar mass as well as with dynamical mass (Rix & Rieke 1993; Gavazzi et al. 1996; Cowie et al. 1996; Kauffmann & Charlot 1998), this means that most of the properties

1.2 The last snapshot: Galaxies in the Local Universe

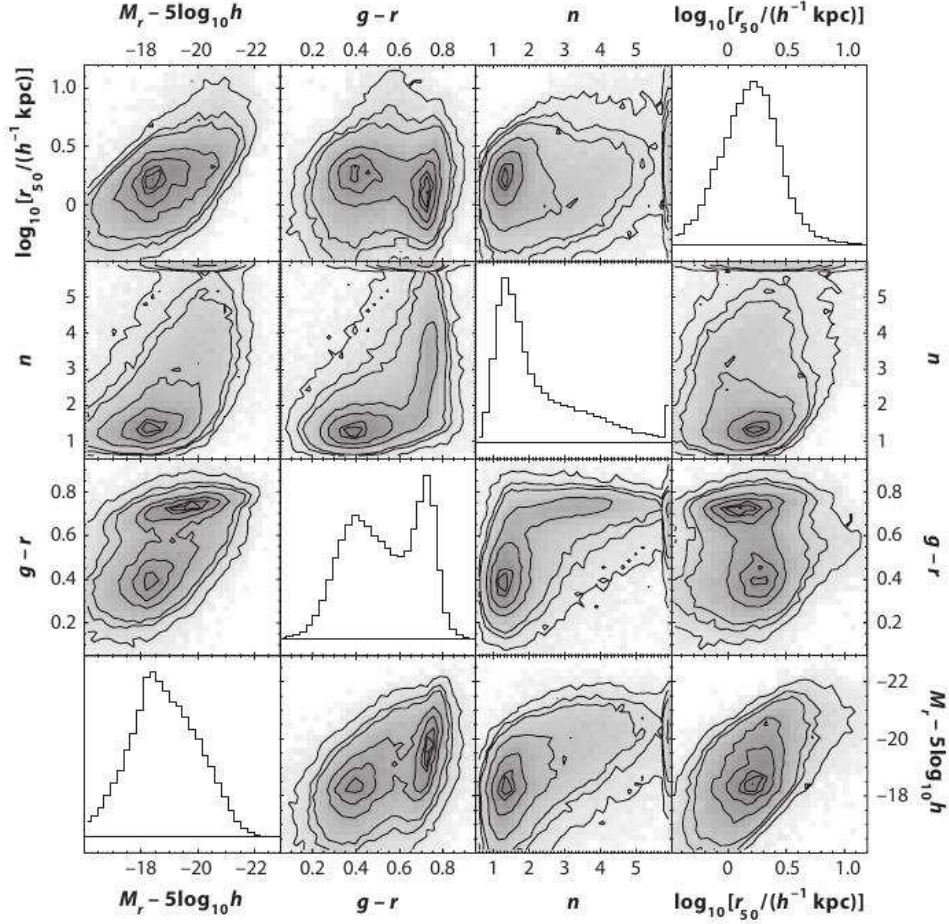


Figure 1.2: Distribution of broad-band galaxy properties in the SDSS (Blanton & Moustakas 2009). The diagonal panels show the distribution of four properties independently: absolute magnitude M_r , $g-r$ color, Sersic index n , and half-light radius r_{50} . A bimodal distribution in $g-r$ is apparent. The grayscale and contours reflect the number of galaxies in each bin (darker means larger number).

1 Introduction

of a galaxy are a strong function of its mass. Many of the plots in Fig. 1.2, particularly those involving g-r color, show a bimodal distribution. Generally speaking galaxies show a bimodal behaviour dividing into two main classes: blue, star-forming, disk-dominated galaxies and red, inactive, elliptical galaxies.

The color-magnitude/color-mass diagram (CMD) is the most common way to show this striking bimodality (First plot of the third row in Fig. 1.2). This plot shows the distribution of galaxy colors as a function of the galaxy absolute magnitude M_r /stellar mass. In this plot galaxies populate mainly two different regions that correspond to the two classes described above: galaxies with low masses inhabit preferentially the so-called blue cloud, whereas galaxies with high masses are disposed along a narrow string, the so-called red sequence.

As long as galaxies are star forming they are dominated by gas and young stellar population and they emit most of their light in the blue part of the spectrum. As galaxy mass increases, the change in color reflects both the increased reddening due to dust and the decreased fraction of recent star formation. Once they have *consumpted* their gas, their stellar mass grows, and they become red due to their old population.

This striking bi-modality raises important questions for galaxy formation and evolution. Which are the physical processes responsible for the sharp partition into blue cloud/red sequence galaxies? On which timescales does the quenching of star formation occur? Does the environment, in which galaxy live, play a key role in this process by boosting the transition into the red sequence region by removing part of the gas?

1.3 The role of environment: *Nature or Nurture?*

As far as we have understood, galaxy stellar mass and redshift play a key role in shaping galaxy properties and their evolution. There is still a further variable that must be taken into account: the environment. By environment we mean the DMH the galaxy resides in, but in literature it has mainly been characterized in terms of local density (using the number of neighboring galaxies within a cylinder (Blanton et al. 2005; Cucciati et al. 2006; Kovač et al. 2010a, and references therein)), or cluster/group catalogs (Abell et al. 1989; Snowden et al. 2008; Hao et al. 2010; Gerke et al. 2005; Yang et al. 2007; Knobel et al. 2009, and references therein)

The original work of Dressler (1980) is a milestone in exploring the dependence of galaxy properties on the environment: studying 55 galaxy clusters in the low redshift universe he showed that the central parts of the clusters are rich in elliptical galaxies, whilst the lower density region among the clusters are populated by spirals.

This so-called morphology-density relation (MDR) inspired a lot of subsequent stud-

1.3 The role of environment: Nature or Nurture?

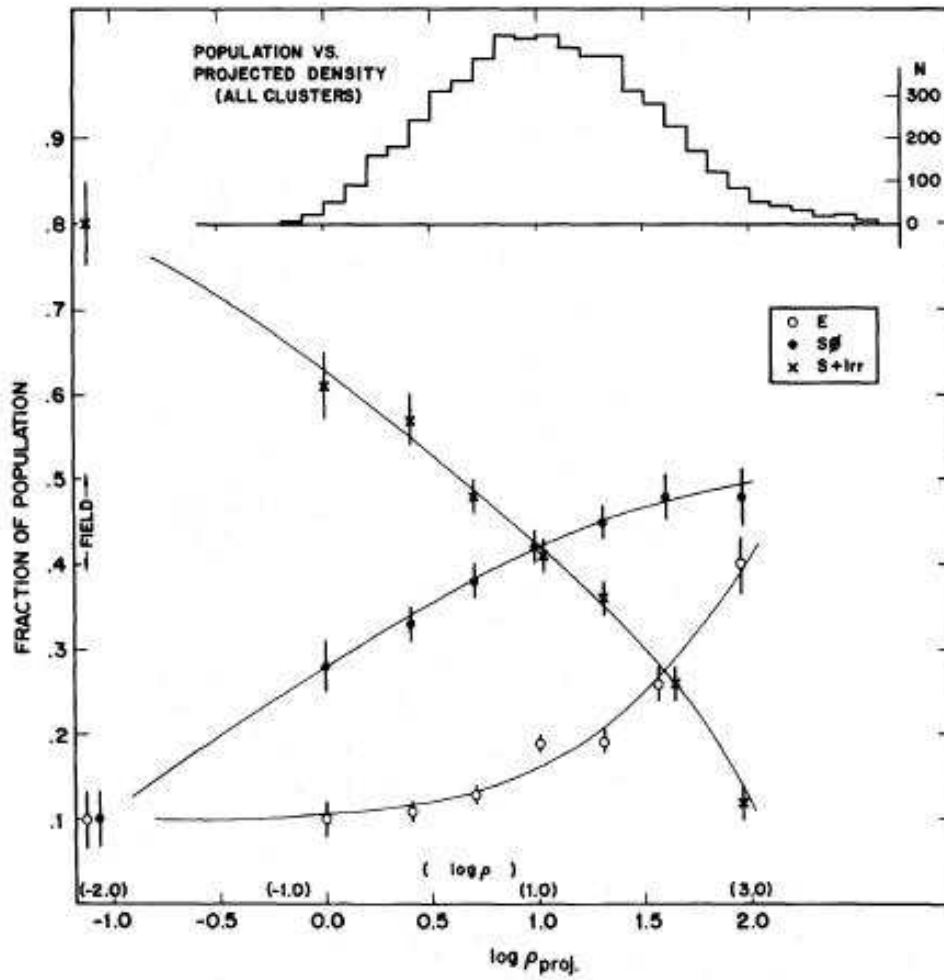


Figure 1.3: Fraction of ellipticals, spheroidals and spirals as a function of the log of the projected density, in galaxies Mpc^{-2} (Dressler 1980)

1 Introduction

ies extending it to: a wider range of environment, including groups (Postman & Geller 1984), higher redshift (Dressler et al. 1997; Capak et al. 2007a), and other galaxy properties (Cucciati et al. 2006). The global picture that has arisen is that, generally speaking, blue star-forming disk-dominated galaxies reside preferentially in low-density environment whereas red inactive elliptical galaxies favor high-density environment.

However we must consider the complication due to the strong correlation between galaxy properties such as colors, morphologies and star formation, with galaxy stellar mass (Cowie et al. 1996; Gavazzi et al. 1996; Blanton et al. 2003; Kauffmann et al. 2003; Brinchmann et al. 2004; Baldry et al. 2004) and the further correlation between galaxy stellar mass itself and environment: galaxies in less dense environment tend to be less massive than those located in denser environment (Hogg et al. 2003; Kauffmann et al. 2004; Blanton et al. 2005; Bolzonella et al. 2010). Thus any study performed on samples of galaxies containing a wide range of stellar masses cannot disentangle between true environmental effects and effects simply induced by the changing of the mass distributions of galaxies with environment. To isolate the true environmental effect the analysis must be performed in narrow galaxy stellar mass bins.

Much of the earlier works were mixing these effects and, as a consequence, led to strong artificial trends. This originated the so-called *nature/nurture* debate: Are the evolution of the galaxy population in clusters and the differences of the galaxy population between the field and the groups a result of the particular group environment (*nurture*), or do they just reflect the initial conditions and general evolution of galaxies irrespective of environment (*nature*)? For instance, the morphology-density relation could just be the consequence of variations of the stellar mass function in different environments, due to the formation process of the corresponding group and to a correlation between the stellar mass and the morphology of a galaxy.

Recent studies have allowed to perform a detailed analysis in bins of galaxy stellar mass, avoiding so any correlation between galaxy properties, galaxy stellar mass and environment. The original MDR of Dressler (1980) has now been confirmed at low redshift using a galaxy sample of different stellar mass bins: morphology at fixed stellar mass does show density dependence (Bamford et al. 2009; van der Wel et al. 2010)

As mentioned above, Postman & Geller (1984) extended the work of Dressler (1980) to groups regime. Using the data from the CfA survey they found that the MDR extends over six orders of magnitude in the space density and moreover the MDR of groups in the general field matches perfectly the one derived only for clusters. In other words they found a continuum of the MDR among environment that probe different densities.

In this thesis we will characterize the environment in terms of groups, i.e., structures,

rather than focusing on densities, therefore here we list current evidences that support the evolution of galaxies in these structures:

- Red/Passive fraction at fixed stellar mass is higher in groups and clusters when compared to the general field at low redshift (Weinmann et al. 2006; Baldry et al. 2006; Kimm et al. 2009). These trends continues at higher redshift,(Gerke et al. 2007; Balogh et al. 2009; Iovino et al. 2010; McGee et al. 2011a);
- Red/Passive/Early-Type fraction in groups at low redshift seem to be at an intermediate level between field and clusters, (Hansen et al. 2009; Kimm et al. 2009). Since clusters are built from groups, this has arisen the issue of galaxy *pre-processing* in groups before falling into clusters (McGee et al. 2009).

Different physical mechanisms have been invoked to explain the environmental trends listed above. In the next Section I will overview the most important processes that can be active in the group/cluster environment.

1.4 Processes active in groups/clusters

The group/cluster environment is composed by three main elements: DM, galaxies and gas. There are many physical mechanisms that can originate and describe the mutual interaction among these elements. In the following I will summarize the main processes that can take place in the group/cluster environment:

- **DYNAMICAL FRICTION:** the deceleration of an orbiting point mass 'satellite' due to dynamical friction on a uniform background mass distribution was originally formulated by Chandrasekhar (1943) regarding stars:

$$\frac{d}{dt}\mathbf{v}_{orb} = -4\pi G^2 \ln(\Lambda) M_{sat} \rho_{host}(< v_{orb}) \frac{\mathbf{v}_{orb}}{v_{orb}^3} \quad (1.2)$$

where $\rho_{host}(< v_{orb})$ is the density of background particles with velocities less than the orbital velocity, v_{orb} of the satellite, M_{sat} is the mass of the satellite and Λ is the Coulomb Logarithm. In our case the background is composed of DM particles and the satellite is a massive galaxy sinking in the group DMH. In this process the galaxy will spiral towards the group center and finally merge with the central galaxy. We can estimate the time-scale of dynamical friction as $\tau_{dyn} = \mathbf{v}_{orb} / \frac{d}{dt}\mathbf{v}_{orb}$. The above estimate shows that a massive galaxy would spiral towards the cluster center in a few Gyr time-scale: $3 < \tau_{dyn} < 10$ depending on the physical properties of the group/cluster.

1 Introduction

- **GALAXY MERGING:** the interaction between a couple of galaxies can strongly affect the morphology, kinematics, and other properties of the involved galaxies. Toomre & Toomre (1972) first show the dramatic effects of this kind of interaction: tails, rings, bridges. If the galaxies eventually merge into a single object, this can show a completely different morphology. The relative velocity between the two galaxies is the most important parameter in this process: it should be similar to that of the galaxy rotation in order for the encounter to produce significant effects. Both groups and clusters have high density and therefore the probability of interaction between galaxies is higher than in the field, but clusters have too high velocity dispersion. On the contrary groups are favoured environments for galaxy encounters due to their low velocity dispersion and high density. The typical time-scale of this process, τ_{merg} , is of the order of Gyrs.
- **GALAXY HARASSMENT:** In groups and clusters, each galaxy experiences a high-speed close encounters with the other members (Moore et al. 1996). 'Close' means within 50 kpc, that is, enough to perturbate the properties of the galaxy but too far to end in a direct merger. After several strong encounters, the loss of angular momentum combined with impulsive heating leads to a change in morphology and eventually to a compact object. The typical time-scale of this process, τ_{har} , is about 3 Gyrs.
- **RAM PRESSURE STRIPPING:** A galaxy moving through the diffuse gaseous intracluster/intragroup medium (ICM/IGM) experiences a wind: the rapid motion of the galaxy causes a large pressure front to build-up in front of the galaxy (Gunn & Gott 1972; Abadi et al. 1999). Depending on the binding energy of the galaxy's own interstellar medium (ISM), the ICM will either be forced to flow around the galaxy or will blow through the galaxy removing some or all the diffuse ISM. The ISM will be removed if the ram pressure of the ICM is greater than the restoring gravitational force per unit area provided by the disc of the galaxy:

$$\frac{\partial}{\partial z}\phi(R, z)\sigma_g(R) < \rho_{ICM}v^2 \quad (1.3)$$

Where v is the velocity of the galaxy with respect to the ICM and ρ_{ICM} is the gas density of the ICM. Clearly ρ_{ICM} has a key role: the denser is the ICM, the more effective is ram pressure. In other words ram pressure stripping is an effective mechanism at depleting gas from galaxies in the core of clusters, but it is less common in groups due to their lower IGM density. The time-scales

for gas to be removed (and therefore to quench the star formation) is very short $\tau_{ram} \sim 10^7$ yrs, a fraction of the crossing time and smaller than the one of galaxy harassment. Related mechanisms to ram pressure are the thermal evaporation of the ISM and viscous stripping of galaxy disc, these may occur even if ram pressure is not strong enough to directly strip the gas.

- STRANGULATION/SUFFOCATION: this is a softer variant of ram pressure stripping and it removes the thin gaseous halo present around galaxies, so the star formation continues until the remaining disc gas is consumed (Balogh et al. 2000). In other words, this process removes the fuel reservoir while galaxies plunge into the group/cluster potential. The lost of gas reservoir is very attractive and it suggests a gradual decline in the star formation, over time-scale of few Gyrs: $1 < \tau_{strang} < 3$ Gyrs.

All these processes can change galaxy properties, especially concerning colors and morphology. In particular group environment is suspected of being important for galaxy mergers and strangulation due to the high density and rather low velocity dispersion. As a consequence groups are considered excellent physical laboratories and, given the high percentage of galaxies residing in groups, they have become subject of many recent works.

1.5 Segregation effects in groups

Among the observable effects of the processes listed in Sect .1.4 there are segregation phenomena, that is not only differences between group and field galaxy properties, but also radial trends of galaxy properties (e.g., colors, morphologies ...) as a function of distance from the group/cluster center. Assuming a simple model, a galaxy infalls radially onto a group/cluster. During this journey, from the outskirts to the core, it is affected by different mechanisms at different group/cluster-centric distances. Infact each of the processes listed in Sect. 1.4 has a specific sphere of influence depending on the group/cluster mass distribution and gas distribution. Fig. 1.4 shows a nice sketch of the region where key physical mechanisms are likely to operate for the specific case of the cluster CL 0024+16 (Treu et al. 2003), both in a 3D and 2D configuration in the top and bottom panel respectively. Red colors refer to mechanisms that could have affected the galaxy in the region, while blue ones indicate processes that are marginally at work. For example ram pressure stripping and starvation are more efficient towards the center due to the higher IGM/ICM density. On the contrary mergers are more likely to happen in the outskirts where galaxies have lower velocities. Each of these

1 Introduction

processes contribute to the gradual change of galaxy properties as a function of the group/cluster-centric distance and therefore producing the segregation effects.

These segregation phenomena have already been well studied in galaxy clusters, where e.g., a strong radial dependence in the star formation rate is observed (Hashimoto & Oemler 1999; Balogh et al. 1999; Lewis et al. 2002; Balogh et al. 2004; Tanaka et al. 2004).

Hashimoto & Oemler (1999) show that the distribution of the concentration index C , which is a good measure of a galaxy's bulge-to-disk ratio, in galaxy populations varies both with local density and with cluster/group membership. The fraction of centrally concentrated galaxies increases with local galaxy density and is higher in clusters than in field. The transition from cluster-like to field-like galaxies is rather smooth at the intermediate density regime. Meanwhile, the star formation rate of galaxies with a given concentration index is sensitive to local galaxy density and shows a continuous correlation with the local density, in such a way that galaxies show higher levels of star formation in lower density environments. The star formation radial trends are consistent with an age sequence, meaning that the last episode of star formation occurred more recently in the farthest galaxies from the cluster center (Balogh et al. 1999). Most of these works hints to the fact that galaxy properties are predominantly influenced by the local density and not by the broader environments characterized by cluster/field memberships. Furthermore the star formation rates in clusters had not yet reached the field value even at $r \sim r_{vir}$: there is quite a sharp transition between galaxies with field-like star formation rates and galaxies with low star formation rates. Lewis et al. (2002) showed that by only plotting galaxies more than 2 virial radii from the cluster centers, the trend hardly changes if compared to the complete cluster diagram. Through this method Lewis et al. (2002) identified the region where galaxy transformation occurs: that is in the infalling filaments, consisting of chains of groups, where galaxies seem to change from star-forming, field-like galaxies to passive, cluster-like objects. It is also possible to show that the groups in the infall regions of clusters show the same pattern as isolated groups. In conclusion the suppression of star formation is mainly a local process.

From these works, it has become clear the need to explore segregation effects in group environment as it seems to be the key environment which shapes galaxy properties. There are indications of earlier-type (brighter) galaxies being more clustered and closer to the group centers, both in position and in velocity, than later-type (fainter) galaxies (Girardi et al. 2003). There is also a significant dependence of the relative fraction of low star formation galaxies on local galaxy density and group-centric radius (Domínguez et al. 2002). These results agree with a continuum of segregation properties of galaxies in systems, from low-mass groups to massive clusters. However

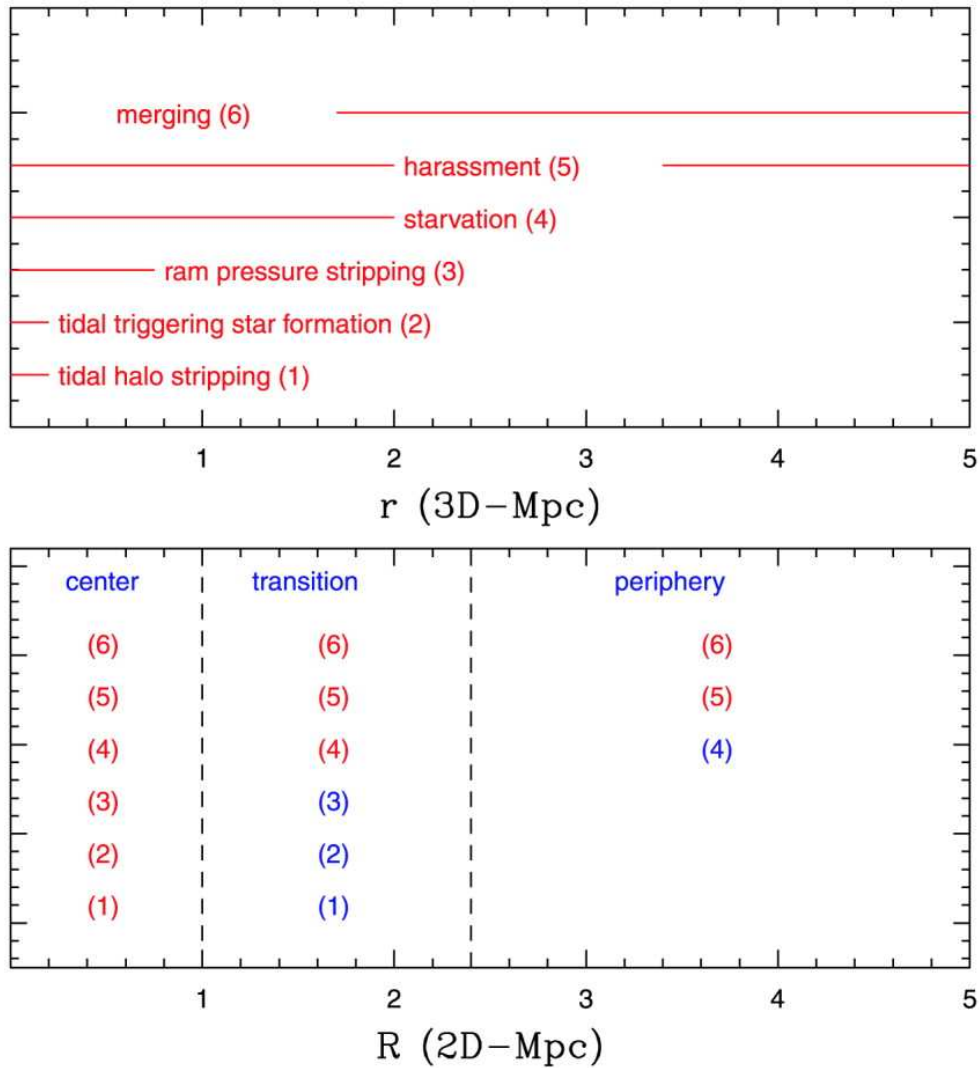


Figure 1.4: Region where key physical mechanisms are likely to operate for the specific case of the cluster CL 0024+16 (Treu et al. 2003), both in a 3D and 2D configuration in the top and bottom panel respectively. Red colors refer to mechanisms that could have affected the galaxy in the region, while blue ones indicate processes that are marginally at work.

even if groups seem to be the key environment to search for *nurture* in action, still the observational evidence for these effects is quite poor and holds mainly for the local universe. (Postman & Geller 1984; Mahdavi et al. 1999; Tran et al. 2001; Carlberg et al. 2001a,b; Girardi et al. 2003; Domínguez et al. 2002; Wilman et al. 2009; Bai et al. 2010; Ribeiro et al. 2010).

1.6 Outline of the Thesis

The goal of this thesis is to search for *nurture* in action by studying segregation effects in the group environment, e.g., trends of galaxy properties as a function of group-centric distance, over a wide range in redshift. This will help to shed light on how rapidly and significantly star formation is suppressed in groups and which are the main mechanisms in act among those listed in Sect. 1.4. I will do this using the wealth of data from both COSMOS and zCOSMOS survey (Scoville et al. 2007; Lilly et al. 2007) and building a composite group to overcome the low number statistics of individual groups. Mock simulations were also used to test the reliability of the chosen strategies.

The thesis is organized as follows:

- In Chapt. 2 I will describe the design, the data and the samples from both COSMOS and zCOSMOS surveys.
- Chapt. 3 will briefly explain the construction of realistic galaxy mock catalogs that I used to test the algorithms I developed.
- In Chapt. 4 I will describe the algorithm I developed to enlarge the data set at our disposal and the centering technique to build a composite group. The first one comprises the adopted strategy to incorporate the COSMOS data to the zCOSMOS spectroscopic ones for those galaxies missing a reliable spectroscopic redshift. This enable us to increase the completeness and the statistic of our data set. The second one was optimize to define the group centers in the most reliable way in order to properly rescale the spatial information for each galaxy. This work has been published in Presotto et al. (2012).
- In Chapt. 5 I will discuss the construction of the composite group, i.e., the selection of the sample, the adopted rescaling method. This strategy enables to establish a statistically reliable sample and to reveal trends of galaxy properties as a function of the group-centric distance and of varying galaxy stellar masses and group richnesses. I will also provide an overview of the properties of the groups that form the ensemble systems.

- Chapt. 6 is dedicated to the study of mass and colors segregation effects in our group sample over a wide redshift/galaxy stellar mass ranges. The joint study of both colors and mass segregation allow us to isolate the true environmental effect: the analysis is performed in narrow galaxy stellar mass bins, this way we disentangle environmental effects from indirect environmental trends. We have been able to isolate the regime of galaxy stellar masses and group richness that hold the smoking gun of environmental effects in action superimposed on galaxy secular evolution and group dynamical evolution. This work has been published in Presotto et al. (2012).
- In Chapt. 7 I present a detailed analysis of composite spectra and morphologies that further investigate the scenario proposed in Chapt. 6. I describe the procedure to co-add spectra from group member galaxies and the strategy to measure spectral indices. This provided us a plenty of information about the star formation history of group member galaxies. We join this information to that from morphologies and we study spectral and morphological segregation effects in our group sample.
- In Chapt. 8 I provide an overall summary of my findings and propose further studies for the future.

2 The zCOSMOS survey and its data set

The Cosmological Evolution Survey (COSMOS) is a large Hubble Space Telescope (HST-ACS) survey, with I-band exposures down to $I_{AB} = 28$ on a field of 2 deg^2 (Scoville et al. 2007). The COSMOS field has been the object of an extensive multi-wavelength ground- and space-based observations spanning the entire spectrum: X-ray, UV, optical/IR, mid-infrared, mm/submillimeter and radio, providing fluxes measured over 30 bands (Hasinger et al. 2007; Taniguchi et al. 2007; Capak et al. 2007b; Lilly et al. 2007; Sanders et al. 2007; Bertoldi et al. 2007; Schinnerer et al. 2007).

The zCOSMOS survey (Lilly et al. 2007) was planned to provide the crucial high-quality spectroscopic redshift information to the COSMOS field. It benefitted of ~ 600 hrs of observations using the VIisible MultiObject Spectrograph (VIMOS) at the Very Large Telescope (VLT) and it consists of two parts: zCOSMOS-bright and zCOSMOS-deep.

In this chapter, I will introduce the zCOSMOS-bright survey, i.e., the main data set of my analysis, and I will describe its outcomes, i.e., the group and field catalogs. As we planned to use also part of the COSMOS photometric redshifts, I will summarize their main properties.

2.1 Survey description

2.1.1 zCOSMOS survey

The zCOSMOS survey is a complementary survey of the COSMOS one: it provides spectroscopic redshift for ~ 30000 sources in the COSMOS field up to $z \sim 3$ (Lilly et al. 2007). Spectroscopic redshifts (alternatively stated as spec-z) provide a wealth of information both on small and large scale. On one hand they are more precise than the corresponding photometric redshifts (alternatively stated as photo-z) and they can be used to map the large-scale structure in the universe and to quantify the density field. On the other hand they can be used to characterize galaxy properties such as

star formation rates, active galactic nucleus (AGN) classification, metallicities etc.

The main goal of zCOSMOS is thus to explore and characterize the galaxy environments throughout the COSMOS volume and over a wide redshift range, as well as enabling studies of the variation of galaxy properties with local density. Among all the environments explored in this survey, groups are of major interest as they are likely to be relevant for the evolution of member galaxies. Indeed, in the Local Universe galaxies reside mostly in groups rather than at higher redshifts, i.e., $z \sim 1/1.5$ (Huchra & Geller 1982; Eke et al. 2004; Berlind et al. 2006; Knobel et al. 2009), and many physical processes have been invoked to explain how group environment can affect galaxy properties, i.e., interaction with other member galaxies (Moore et al. 1996) or strangulation (Balogh et al. 2000). Furthermore spectroscopic redshifts provide a calibration of photometric-redshift schemes that may then be applied to objects not observed spectroscopically.

The zCOSMOS project is divided into two parts: zCOSMOS-bright, and zCOSMOS-deep. The zCOSMOS-deep targets ~ 10000 galaxies within the central 1 deg^2 of the COSMOS field, selected through color criteria to have $1.4 \leq z \leq 3.0$. The zCOSMOS-bright is purely magnitude limited and it covers the whole area of 1.7 deg^2 of the COSMOS field. It provides redshifts for ~ 20000 galaxies down to $I_{AB} \leq 22.5$ as measured from the HST-ACS imaging (Koekemoer et al. 2007). The bright part is now finished, having observed almost 17000 galaxies. This thesis is based on the bright part of the survey and from now onwards I will focus on this part only.

2.1.2 zCOSMOS bright: design and data reduction

Observations were carried out with the VIMOS spectrograph (Le Fèvre et al. 2005) mounted on the VLT telescope. The spectrograph was used in the Medium Resolution (MR) option with 1.0 arcsec slits. The spectral resolution is $R \sim 600$ at $2.5 \text{ \AA} \text{ pixel}^{-1}$ over the spectral range $5550\text{-}9450 \text{ \AA}$. VIMOS is a multislit spectrograph composed of four quadrants covering approximately $7 \times 8 \text{ arcmin}^2$ and separated by a 2 arcmin wide cross-shape. Each pointing was shifted by about 2 arcmin to compensate the gaps between the quadrants and consequently to cover the corresponding area nearly homogeneously. This pattern of pointings ensured eight opportunities to each target, in a large rectangular region, i.e., about 1 square degree , to be selected for observation.

The input catalog for zCOSMOS-bright is based primarily on total F814W magnitudes derived from the 0.1 arcsec resolution HST images (Koekemoer et al. 2007) in the range $15.0 < I_{AB} < 22.5$, totaling 52,792 objects. About 19% of objects, suspected of being galactic stars based on both an unresolved HST image and a UBVRIKZ spectral energy distribution that is better matched by a stellar template, were not targeted

Table 2.1: zCOSMOS classification scheme of confidence classes as in Lilly et al. (2009).

Class	Integer Confidence Classes
4	Very secure redshift exhibiting a quality spectrum
3	Very secure redshift
2	Likely redshift with some doubt
9	Securely detected line, either [OII] λ 3727 or H α λ 6563
1	Insecure redshift
0	No redshift measurement
+10	As above but for broad line AGN, with 18 instead of 9
+20 or +200	As above but for a target only observed as a secondary target
Decimal place modifiers	
.5	Spec-z and photo-z are consistent to within $0.08(1+z)$
.4	No available photometric redshift
.3	Spec-z consistent with photo-z after changing to the alternate redshift (For Class 9 and 18)
.1	Spec-z and photo-z differ by more than $0.08(1+z)$

for spectroscopic observation. Among all objects, some got a higher observing priority (compulsory target), such as X-ray and radio sources, however they represent only 1% of the set.

The slit masks were prepared using the Slit Positioning Optimization Code (SPOC) (Bottini et al. 2005). This software maximizes the number of slits to put in the area of each quadrant. Slits are first placed as much as possible over of the compulsory targets. Then, in a second pass, slits are placed over as many of the random targets as possible.

Data reduction and redshift measurements were carried out independently in two different institutes using the VIPGI software (Scodreggio et al. 2005) and the EZ software (Scaramella et al. in prep.) respectively. Data reduction was mainly automatic, there were only few steps that required manual intervention, e.g., checks in lambda calibration and atmospheric correction. To further reduce human mistakes, each independent redshift measurement was later reconciled by visual inspection at face-to-face meetings between representatives of the two institutes, meetings that I attended. The reliability of redshift measurements is quantified by a confidence class flag that is assigned to each redshift. The classification runs from 0 (no redshift) to a maximum of 4 (most secure, and with a textbook spectrum) with an additional Class 9 for one-line redshifts where the line is expected to be either [OII] λ 3727 or H α , i.e., where an identification with H β or the [OIII] λ λ 4959,5007 doublet can be rejected. Additional integer or decimal classifications modifiers refer to spectrum features, e.g., the presence of broad features adds +10 or +20 to the confidence class flag, or to consistency between spectroscopic and photometric redshifts, e.g., agreement between spec-z and photo-z adds +.5 to the confidence class flag, see Tab. 2.1 for details.

In the final data set there are some repeated observations, these can be used to establish the reliability of redshift measurements and to determine the redshift accuracy. The success rate in redshift measurements is very high, 95% in the redshift range $0.5 < z < 0.8$, and the velocity accuracy is $\sim 100 \text{ km s}^{-1}$ (Lilly et al. 2009). This accuracy is sufficient for the resolution of galaxy groups. Classes 3.x, 4.x redshifts, plus the Classes 1.5, 2.4, 2.5, 9.3, and 9.5 are considered a secure set, with an overall reliability of 99%, (see Lilly et al. 2009, for details).

2.1.3 The final sample: 20K galaxy catalog and its properties

The work of this thesis is based on the the zCOSMOS-bright survey final release: the so called 20K sample (simply 20K from now onwards) and the corresponding group catalog (see Sect. 2.1.4 for details). The 20K totals 16623 galaxies with $z \leq 2$ and secure redshifts according to the above flag classification (18206 objects in total,

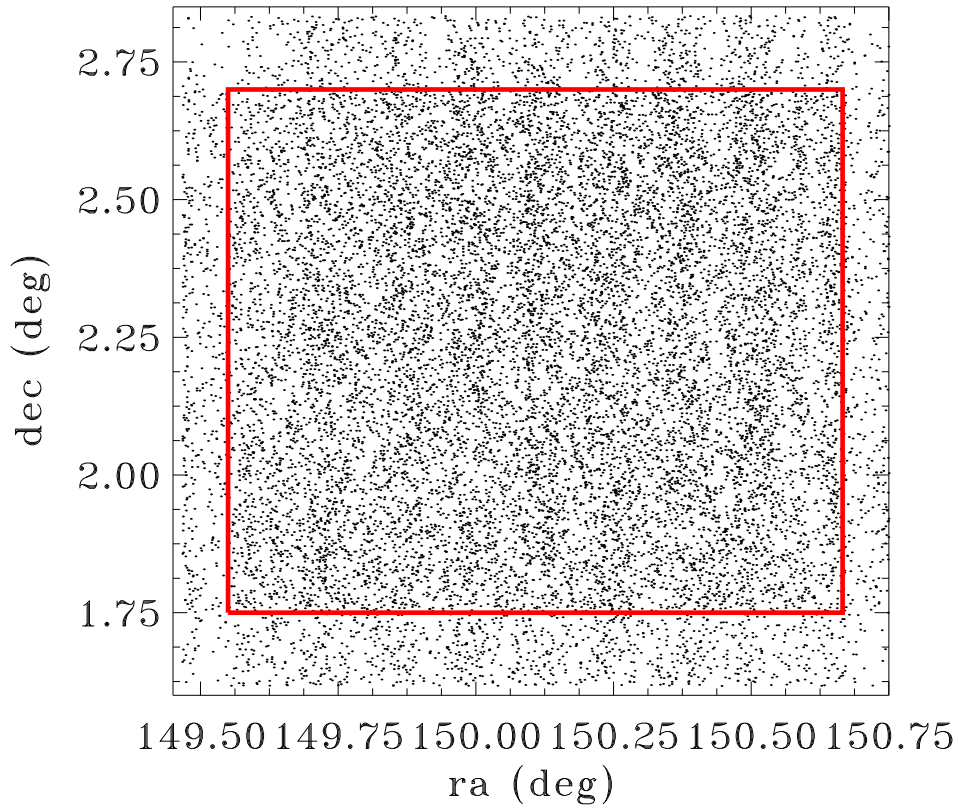


Figure 2.1: Ra-Dec distribution of the 16623 zCOSMOS-bright galaxies with secure redshift $z \leq 2$ (the so-called 20K sample). The area within the red box ($149.55 \leq ra \leq 150.67$ and $1.75 \leq dec \leq 2.70$) has a nearly uniform sampling rate of $\sim 62\%$.

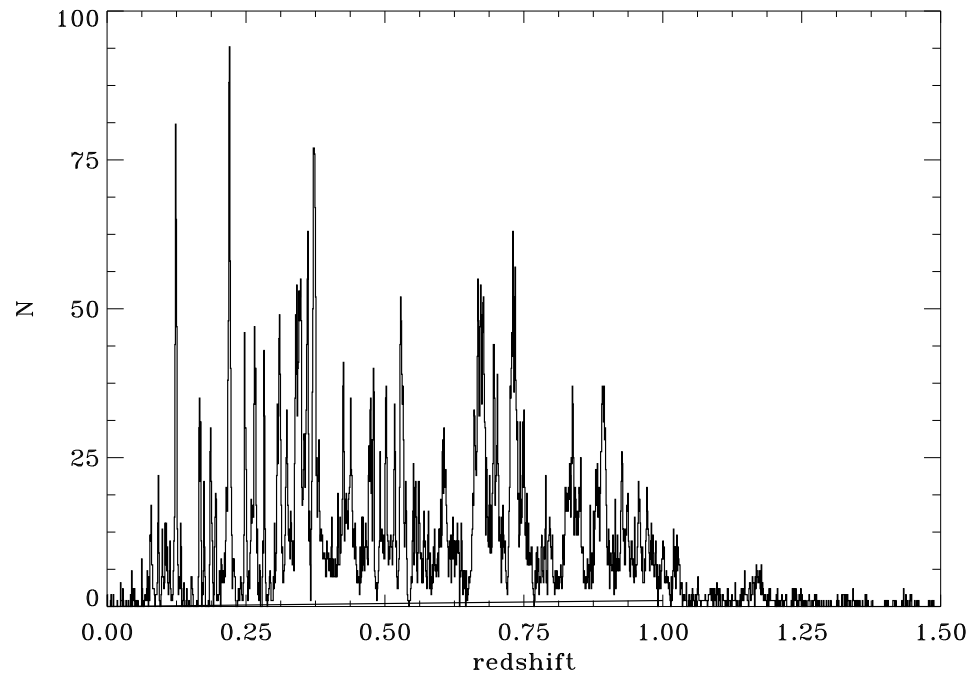


Figure 2.2: Redshift distribution of of the 13619 zCOSMOS-bright galaxies with secure redshift $z \leq 2$ (the so-called 20K sample), within the red box area and binned in intervals $\Delta z = 0.001$. The redshift distribution shows structure on a large range of scales.

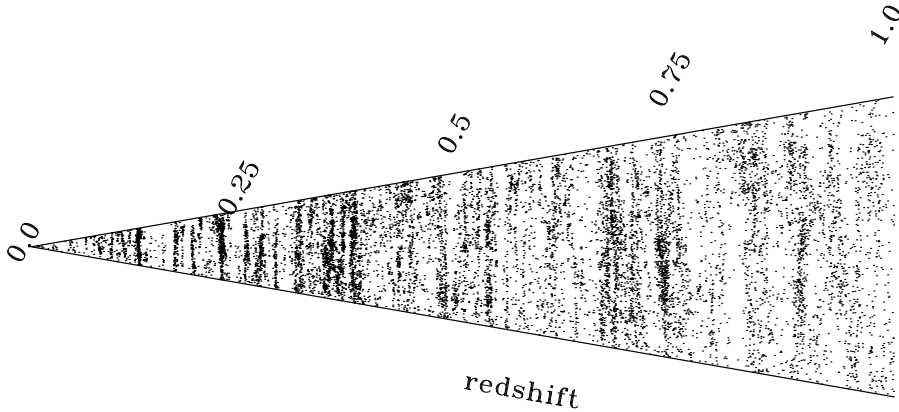


Figure 2.3: Distribution along the line of sight of the of the 20K galaxies within the red box area introduced in Sect. 2.1.3.

irrespective of redshift and including stars).

Fig. 2.1 shows the spatial distribution of the 20K galaxies. The red square corresponds to the region with the highest sampling rate, approximately $\sim 62\%$, its boundaries are $149.55 \leq ra \leq 150.67$ and $1.75 \leq dec \leq 2.70$. The number of galaxies within this region, with secure redshift and $z \leq 1$ is 13619 (15730 objects in total, irrespective of redshift and including stars) and their sky distribution is remarkably uniform.

Fig. 2.2 shows the redshift distribution of the 13619 zCOSMOS-bright galaxies with secure redshift $z \leq 2$, within the red box area and binned in intervals $\Delta z = 0.001$. The redshift distribution shows structures on a large range of scales, the most prominent being at $z \sim 0.3$ and $z \sim 0.73$. Fig. 2.3 shows the distribution along the line of sight of the same galaxies, highlighting the presence of these structures. They encompass a wide range of environments: from less dense regions, and filaments to groups, and richer/denser structures, enabling a detailed study of galaxy properties over different

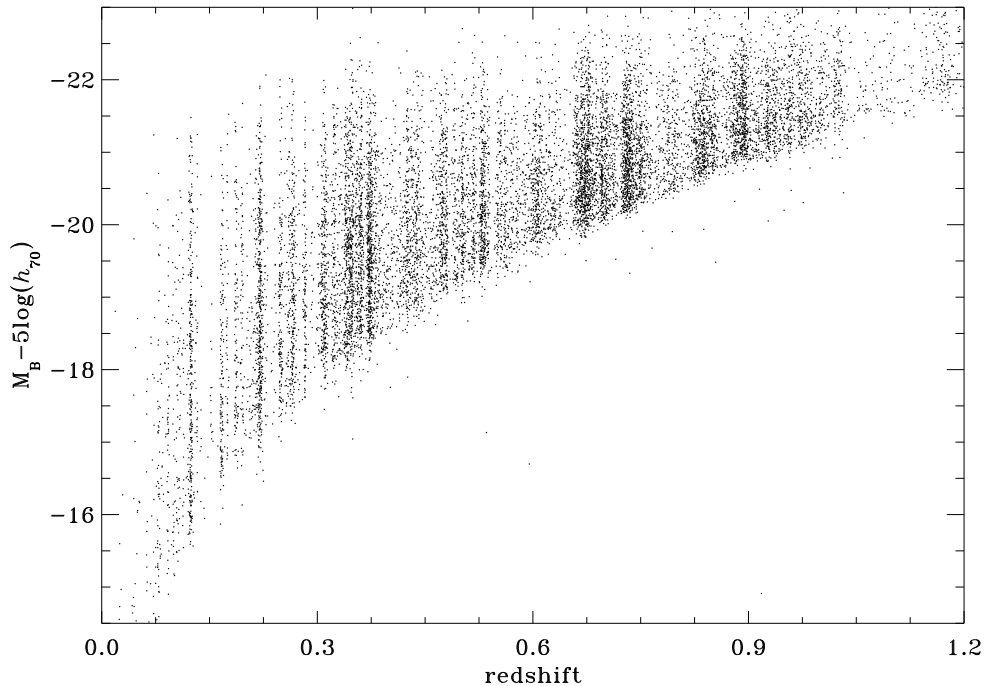


Figure 2.4: Absolute magnitudes in the rest-frame B band of the 20K galaxies within the red box area introduced in Sect. 2.1.3 as a function of redshift.

environments.

For all galaxies, absolute rest-frame magnitudes and stellar masses were obtained using standard multi-color spectral energy distribution (SED) fitting techniques. Rest-frame absolute magnitudes were obtained using the ZEBRA code, (see Feldmann et al. 2006, for the details of the code), while stellar masses were obtained using the Hyperzmass code (Pozzetti et al. 2010; Bolzonella et al. 2010) that yields a typical error for the stellar mass estimates of about 0.2 dex. Among the available stellar population synthesis libraries we chose to adopt the Bruzual & Charlot (2003) ones, assuming a Chabrier initial mass function (Chabrier 2003).

In Fig. 2.4 we show the absolute rest frame magnitude M_B versus redshift distribution of the total galaxy sample introduced in Sect. 2.1.3. This plot clearly shows the restriction of a flux limited survey: the range of observable luminosities varies with redshift. As a consequence, to study the same galaxies at all redshifts, one needs to construct volume limited samples. To this aim one should also take into account the

observed luminosity evolution in the rest-frame B band: the global B band Luminosity Function (LF) shows a brightening of ~ 0.7 mag in M^* from $z \sim 0.2$ to $z \sim 0.9$ (see Zucca et al. 2009, and references therein). An evolving absolute rest-frame magnitude cut-off is therefore more appropriate, see Sect. 5.2 for further details.

A further complication is that a flux-limited survey can target blue star-forming galaxies at lower masses than for red quiescent ones. As a consequence, B-band rest-frame selection is biased towards blue, low mass galaxies, while it misses the corresponding red, equally low mass ones. This can be seen in Fig. 2.5 where we plot $(U - B)$ rest-frame color versus stellar masses in bins of redshift $\Delta z = 0.1$ for the 20K galaxies within the red box area introduced in Sect. 2.1.3. This gives a rough indication of the mass completeness of the sample as a function of redshift and rest-frame $(U - B)$ color. As we can see, the mass limit at which the sample is complete, even for the reddest galaxy, shifts towards more massive galaxies with increasing redshift. We will discuss later on, e.g., Sect. 5.2, the importance of defining a mass-complete sample for our analysis.

2.1.4 Spectroscopic group catalog

The excellent accuracy of zCOSMOS redshifts enabled us to extract a group catalog from the 20K sample (Knobel et al. 2009, 2011). This catalog has a major importance in this study as we used groups as tracers of the environment. In this section I will briefly summarize the adopted group-finding algorithm and the properties of the extracted groups.

As defined in Sect. 1.1 a group is composed by those galaxies that occupy the same DM halo, therefore by definition, group numerosity, N , range is $N \geq 2$. Those galaxies that reside alone in a DM halo are called field galaxies. In spectroscopic redshift surveys, such as zCOSMOS, groups are identified as overdensities in redshift space without recourse to additional color information. However the peculiar velocities of galaxies may cause group members to merge with other nearby field galaxies, i.e., interloper. Furthermore the decrease of the mean density of galaxies with redshift and different selection effects may cause difficulties in group identification. The perfect group catalog should have 100% completeness, (i.e., fraction of real detected groups) and 100% purity (i.e., fraction of non-spurious groups). The former definition of the perfect group catalog is on group-group basis, but one should obtain 100% completeness and 100% purity also on galaxy-group basis, i.e., fraction of reconstructed group galaxy members and fraction of non-interloper galaxies respectively. Naturally the best achievable group catalog is the one with the best balance of completeness and purity.

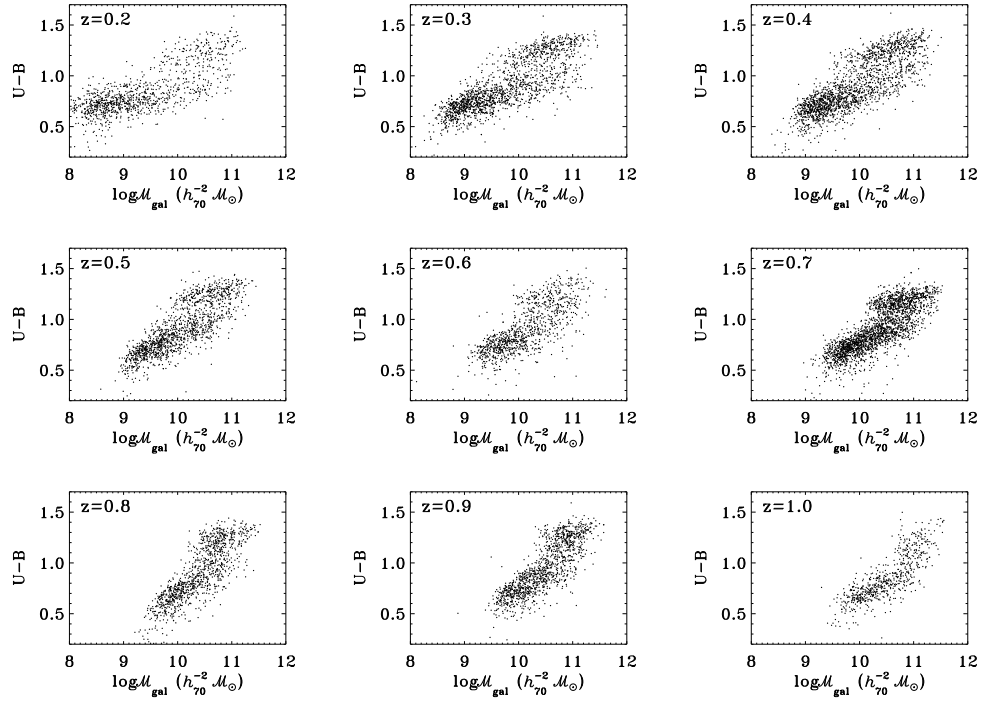


Figure 2.5: $(U - B)$ rest-frame color versus stellar masses in bins of redshift $\Delta z = 0.1$ for the 20K galaxies within the red box area introduced in Sect. 2.1.3.

The most widely used group-finding algorithms are: the Friends-of-Friends (FOF) algorithm (Huchra & Geller 1982; Eke et al. 2004; Berlind et al. 2006) and the Voronoi-Delaunay Method (VDM) (Marinoni et al. 2002; Gerke et al. 2005, 2007). Both these methods are characterized by a set of parameters that can be adjusted so that the resulting group catalog has the best balance of completeness and purity. Knobel et al. (2011) uses a "multi-pass procedure" both with FOF and VDM to achieve an impressive quality in group reconstruction, as tested using realistic mock catalogs, (see also Knobel et al. 2009, concerning a previous version of the algorithm). Knobel et al. (2009) showed that the concurrent optimization of completeness and purity is a function of the group numerosity. Therefore they developed the following "multi-pass procedure":

1. The parameter-set is optimized for the range $N > 6$, the group-finder is run, and only those groups that are in this numerosity range are kept in the group catalog.
2. The parameter-set is then optimized for groups with $N = 5$, the group-finder is run again, and only groups with $N = 5$, which are not yet detected in the first step, are added to the group catalog.
3. Repeat the previous step for $N = 4, 3, 2$.

Each step accepts only those groups which have not been found in a previous step. This method, when combined with the standard FOF algorithm, yields, for the resulting group catalog, values of completeness and purity that are extremely good and stable as a function of both redshift and number of members observed in the reconstructed groups.

Fig. 2.6, taken from Knobel et al. (2009), summarizes the results of the "multi-pass procedure" when applied to the FOF algorithm (blue solid line) as tested on mock catalogs, see Chapt. 3 for mocks details. The upper left panel exhibits completeness and the upper right panel purity on group-group basis. The lower right panel shows the galaxy success rate S_{gal} and the lower left panel the interloper fraction \mathcal{PI} , i.e., completeness and purity on galaxy-group basis. Usual values of completeness and purity, for groups reconstructed with more than five spectroscopic observed members, are around $\sim 85\%$ at all redshifts and do not decrease substantially for groups with lower number of observed members. The interloper fraction, remains constantly below $\sim 20\%$ at all redshifts for groups reconstructed with more than five spectroscopic observed members, except a slight increase for groups with lower number of observed members.

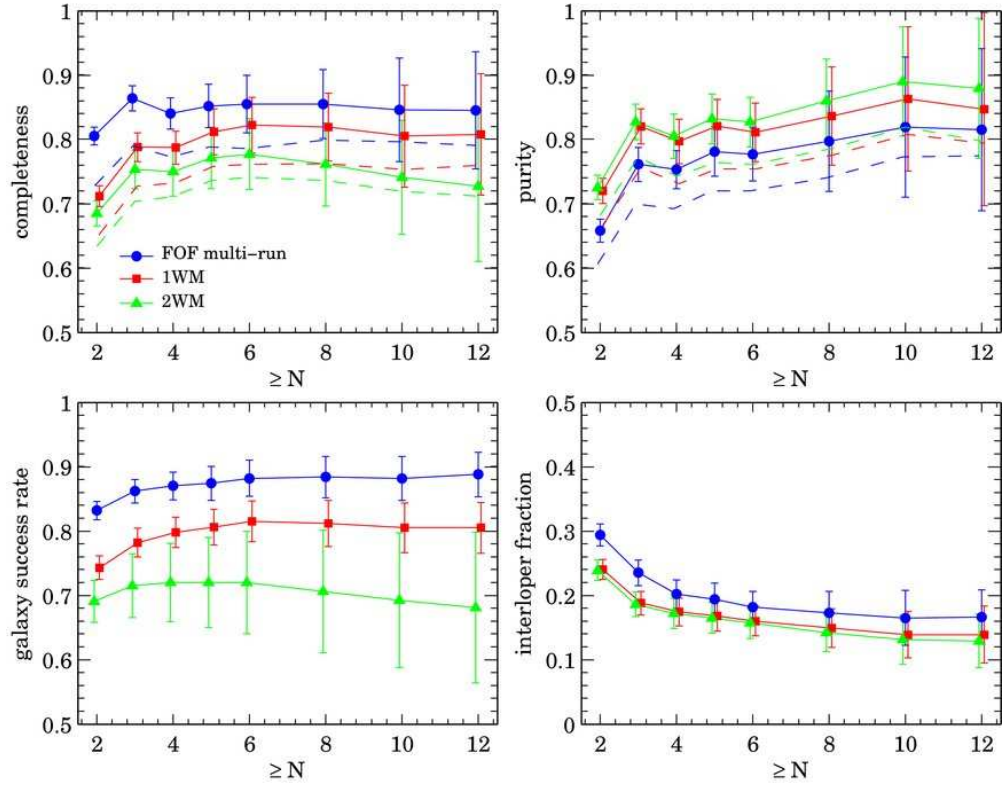


Figure 2.6: Statistics of the "multi-pass" FOF (blue solid line) as a function of numerosity N (other lines refer to specific subcatalogs not used in this thesis). The error bars show the scatter among the 24 mocks. The upper left panel exhibits completeness and the upper right panel purity on group-group basis. The lower right panel shows the galaxy success rate S_{gal} and the lower left panel the interloper fraction \mathcal{PI} , i.e., completeness and purity on galaxy-group basis. Taken from Knobel et al. (2009).

2.1 Survey description

The group catalog provides also the physical properties of each group, e.g., the halo mass, and the virial radius. Knobel et al. (2009) showed that at each redshift z , the observed richness N , corrected for sampling and redshift success rate, is a good proxy for the group halo mass and, by calibrating it with the mock catalogs, it works rather well. In general a certain property of groups, Q , that exhibits a correlation with the number of members in a group, can be estimated and calibrated using the mock catalogs with eq. 2.1:

$$Q_{fudge} = \langle Q_{mock}(\tilde{N}, z) \rangle \quad (2.1)$$

where $Q_{mock}(\tilde{N}, z)$ denotes the quantity Q of a halo at redshift z containing \tilde{N} galaxies (corrected for sampling and redshift success rate) in the mock catalogs, and the angle brackets correspond to the average over the halos among the mock catalogs. In this work we will use the group halo fudge mass, \mathcal{M}_{fudge} , i.e., an estimate of the dynamical mass of the group, and the group fudge radius, R_{fudge} , i.e., an estimate of the group virial radius. The $20K$ group catalog is more than 90% complete for $\mathcal{M}_{fudge} > 10^{13.5} \mathcal{M}_{\odot}$ up to redshift $z \sim 0.8$, while for lower masses the completeness decreases linearly with redshift.

This "multi-pass procedure" has been applied to the $20K$ sample and the resulting $20K$ group catalog consists of 1496 groups with at least 2 spectroscopic member galaxies and 188 groups with at least 5 spectroscopic members. In this thesis the analysis is restricted to groups with at least 5 spectroscopically observed members and within the high sampling rate box introduced in Fig. 2.1. This allows to work with groups for which the finding algorithm of Knobel et al. (2011) reaches the best results for purity and interlopers fraction. Moreover the minimum of five spectroscopic members ensures a reliable first guess of both group center and radius. These two parameters are crucial for the algorithm we used to retrieve group members missing secure spectroscopic redshift information and to build the **SG**, see Chapt. 4.

From now onwards we will call this sample the spectroscopic group catalog: it totals 178 groups and 1437 group member galaxies at $z \leq 1$.

2.1.5 Spectroscopic field sample

To build the field galaxy sample we started by selecting $20K$ galaxies located within the high sampling rate box and outside *any* of the reconstructed groups of Knobel et al. (2011). We therefore discarded from this sample also galaxies located in pairs, triplets and quadruplets, i.e., members of the poorest groups not considered in our science analysis.

To perform the fairest comparison between group and field samples we carefully took into account the possibility of spurious trend introduced by residual group contamination or by the different redshift ranges covered by the group/field galaxy samples that have to be carefully avoided. On one hand galaxies lying in the close proximity of groups could be contaminated by spectroscopic group members missed by the group-finding algorithm. In addition, the fraction of blue galaxies in field evolves with redshift (Iovino et al. 2010, and references therein) while the redshift distribution of the spectroscopic groups catalog is far from being uniform, displaying prominent peaks (especially at low redshift where the 20K field of view limits the cosmic volume explored). To take into account these two factors we further restricted the field sample to galaxies located within redshift distances $2000 \leq |\Delta v| \leq 5000 \text{ km s}^{-1}$ from our selected groups sample and with radial projected distances $R_{field} > 4 \times R_{fudge}$ from any group of 20K group catalog. From now onwards we will call this set of galaxies the *field sample*, totalling 6556 galaxies at $z \leq 1$.

We also introduced a complementary set of field galaxies, that we shall call *near-field*. These are 20K galaxies within the high sampling rate box, that do not belong to *any* of the reconstructed groups of Knobel et al. (2011), but with Δv within $\pm 2000 \text{ km s}^{-1}$ and $R_{field} \leq 4 \times R_{fudge}$ from at least one group of the spectroscopic group sample used in our analysis. The *near-field* sample so defined totals 1694 galaxies at $z \leq 1$ and contains, by definition, galaxies located in the close proximity of the spectroscopic group sample. We will use this sample to check for possible environmental effects extending outside group radii, e.g., color differences of *near-field* population with respect to the field sample as defined above.

2.2 Photometric redshifts

Overall, as compared to previous surveys, the zCOSMOS-bright survey has a high and uniform sampling rate, and offers an unique opportunity to explore the presence/evolution of environmental trends in a wide range of cosmic time. Nevertheless, the spectroscopic sampling rate is $\sim 62\%$, therefore it would be useful to incorporate those galaxies brighter than $I_{AB} = 22.5$ and missing secure spectroscopic redshift in the data set, to get as close as possible to the ideal 100% sampling rate.

The wealth of ancillary photometric data provided by the COSMOS survey ensures good quality photometric redshifts: based on the comparison, between photo-z and spec-z for the 20K galaxies with $17.5 \leq I_{AB} \leq 22.5$ Ilbert et al. (2009) estimates an accuracy of the photo-z of $\sigma_{z_{phot}} = 0.007 \cdot (1 + z_s)$. Similar accuracy is obtained by Oesch (2011) when applying the ZEBRA code to the same 30 bands (pri-

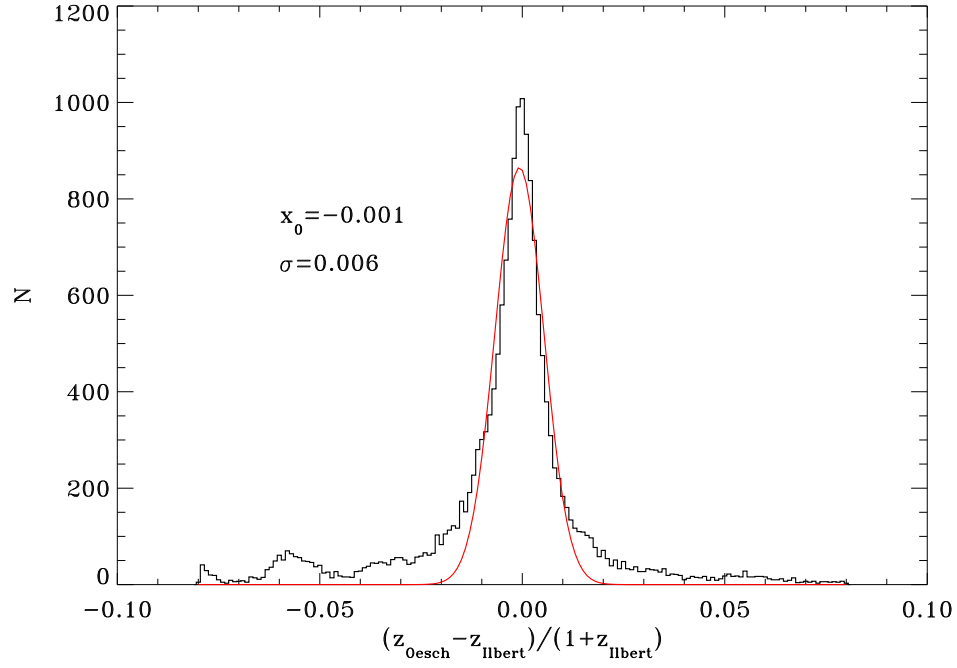


Figure 2.7: Comparison between photo- z from Ilbert et al. (2009) and Oesch (2011). The black solid line shows the distribution of $z_{\text{Oesch}} - z_{\text{Ilbert}} / (1 + z_{\text{Ilbert}})$ for galaxies having $0.25 \leq z_{\text{phot}} \leq 1.1$ and brighter than $I_{\text{AB}} = 22.5$. The red solid line is the fitted Gaussian distribution with $\sigma_{\text{cfr}} = 0.006$.

vate communication). Fig. 2.7 shows the good agreement between Ilbert et al. (2009) and Oesch (2011) photo-z estimates. The black solid line shows the distribution of $(z_{Oesch} - z_{Ilbert})/(1 + z_{Ilbert})$ for galaxies having $0.25 \leq z_{phot} \leq 1.1$ and brighter than $I_{AB} = 22.5$. The red solid line is the fitted Gaussian distribution with $\sigma_{cfr} = 0.006$. The value of σ_{cfr} is even smaller than expected, i.e., $\sim \sqrt{2} \cdot \sigma_{zphot}$, confirming the excellent quality of COSMOS photometric data.

We will use the phot-z values from Oesch (2011) in our analysis (see Chap. 4 for the adopted method to incorporate photo-zs). Rest-frame absolute magnitudes are directly provided by the ZEBRA code, while once again stellar masses are obtained by SED fitting using the code Hyperzmass. Here we report the tests we performed to assess the reliability of Oesch (2011) photo-z.

Left panel of Fig. 2.8 shows the comparison between photo-z and spec-z for the subset of the 20K galaxies with confidence flag 4.x or 3.x. The red solid line corresponds to the linear fit of the dataset. The slope of the fit is 0.980 ± 0.002 suggesting a good agreement between photo-z and spec-z estimates. We checked the accuracy of photo-zs estimates by fitting a Gaussian distribution to the $\Delta z/(1 + zs)$ distribution. Right panel of Fig. 2.8 shows the $\Delta z/(1 + zs)$ distribution, the red solid line is the fitted Gaussian distribution with $\sigma = 0.006$. We also checked the presence of catastrophic failures in estimating photo-z, i.e., the excess of galaxies with errors larger than $3\sigma_{zphot}$ with respect to the simple gaussian distribution. We estimated such percentage as $\sim 7-8\%$ as reported in the top-left corner of the plot.

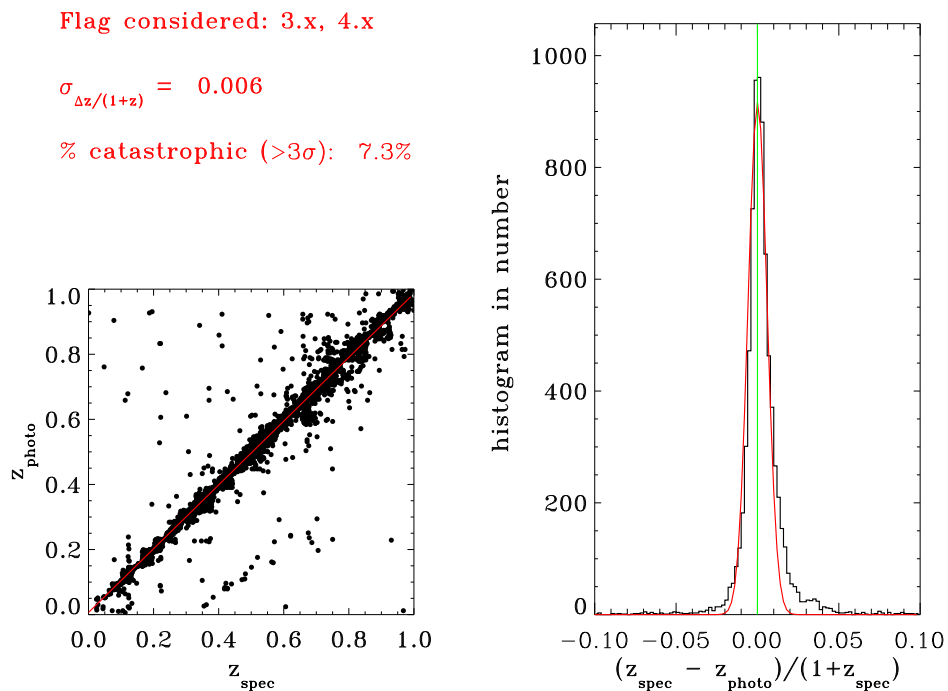


Figure 2.8: Left panel: comparison between photo-z and spec-z for the subset of the $20K$ galaxies with confidence flag 4.x or 3.x. The solid line corresponds to the linear fit of the dataset. Right panel: $\Delta z/(1+z_s)$ distribution. The red solid line is the fitted Gaussian distribution with $\sigma_{z_{\text{phot}}} = 0.006$. The fraction of catastrophic failures, i.e., photo-zs with $\Delta z/(1+z_s) > 3\sigma_{z_{\text{phot}}}$ corresponds to 7-8%, as listed in the top-left corner of the plot.

3 Mock catalogs construction

The use of realistic mock galaxy catalogues is important to assess the reliability of the algorithm we adopted to produce the spec+photo-z group catalog and to validate the procedures we choose to define group centers and richnesses (see Chapt. 4).

We took advantage of the 24 COSMOS mock light-cones, provided by Kitzbichler & White (2007), each covering an area of $1.4deg \times 1.4deg$ with an apparent magnitude limit of $r \sim 26$ and galaxies in the redshift range up to $z \sim 7$. These mock light-cones are based on the Millennium DM N-body simulations of (Springel 2005) and use semi-analytic recipes of Croton et al. (2006) as updated by De Lucia & Blaizot (2007) for populating the simulations volume with galaxies.

From each of these 24 light-cones we extracted four different types of mock catalogs:

1. The 40K mock catalogs: 100% complete to $I_{AB} = 22.5$. In these catalogs all galaxies brighter than $I_{AB} = 22.5$ are supposed to be spectroscopically observed with 100% success rate. We added a redshift error of 100 km s^{-1} to account for typical zCOSMOS spectroscopic redshift error as estimated from observations (see Lilly et al. 2009);
2. The 20K mock catalogs: mimicking the 20K zCOSMOS spectroscopic sample. We applied the same observational strategy adopted to select the spectroscopic zCOSMOS targets: using the slit positioning algorithm SPOC, see Bottini et al. (2005), on the 40K catalogs and accounting for the spectroscopic redshift failures by including the same redshift success rate as the real data.
3. The 20K+photo-zs mock catalogs: mimicking the total set of data we used in our analysis. The spectroscopic galaxies are those listed in the 20K mock catalogs, while a photometric redshift is provided for the remaining galaxies of the 40K mock catalogs. We reproduced both the photometric redshift error and the catastrophic errors expected for the galaxies with photometric redshift. The former error is the quoted error value for $\sigma_{z_{\text{phot}}}$, while the latter error we choose a rather conservative approach and we considered in the 20K+photo-zs mock catalogs also a 10% of catastrophic errors, by randomly permuting for 10% of

3 Mock catalogs construction

the galaxies their photometric redshifts while keeping fixed galaxy ra-dec coordinates.

4. fl.< $I_{AB,max}$ >: 100% complete to $I_{AB,max} = 23.0, 23.5, 24.0, 26.0$. These catalogs are constructed in a similar way as the 20K+photo-zs mock catalogs. The difference regards galaxies fainter than $I_{AB} = 22.5$. For these galaxies the photometric redshift error, σ_{zphot} , is magnitude-dependent. Ilbert et al. (2009) showed that at fainter magnitudes $I_{AB} < 24$ and $z < 1.25$, the accuracy is $\sigma_{\Delta z}/(1 + z_{spec}) = 0.012$. The magnitude-dependent error is than obtained by linearly interpolating the quoted error values for $I_{AB} = 22.5$ and $I_{AB} = 24$ as in eq. 3.1:

$$\sigma_{zphot}(I_{AB}) = \left(\frac{1}{300} \cdot I_{AB} - 0.068\right) \cdot (1 + z). \quad (for\ I_{AB} > 22.5) \quad (3.1)$$

Catastrophic errors are always obtained by randomly permuting for 10% of the galaxies their photometric redshifts while keeping fixed galaxy ra-dec coordinates.

We applied to the 20K mock catalogs the same group finding algorithm used for the 20K sample (see Knobel et al. 2009). We then selected groups with at least five spectroscopic members located within the high sampling rate box introduced in Fig. 2.1 and applied to the 20K+photo-zs and fl.< $I_{AB,max}$ > mock catalogs the algorithm described in Chapt. 4.

The COSMOS mock light-cones provide dark matter halos IDs that can easily be used to identify *real* groups and *real* group members, i.e., the set of galaxies located within the same dark matter halo in each of the above mock catalogues (see also Knobel et al. (2009)).

4 The Algorithm

The aim of this thesis is to explore if and how galaxy properties, e.g., colors, masses, morphologies, star formation rates etc., vary as a function of the group-centric distance. Given our data set, this kind of study has two major complications. On one hand the scarcity of individual group members inhibits a detailed analysis of each group and as a consequence, to explore galaxy properties as a function of the distance from the center of the group, we need to build ensemble systems. On the other hand the number of available member galaxies down to $I_{AB} = 22.5$ for each group of our spectroscopic group sample is limited by the incomplete sampling rate of the *20K*. In other words we need to increase the order of magnitude of the available sample. In order to increase the number of galaxies at our disposal we decided to take advantage of the excellent quality of the photometric redshifts in the COSMOS field, and to incorporate into our analysis photometric redshifts for galaxies brighter than $I_{AB} = 22.5$ and missing reliable spectroscopic data. A higher number of group member galaxies enables to improve, for each group, both centering and richness estimate, two quantities crucial to properly center and rescale distinct groups to build a composite one (see e.g., Carlberg et al. 1997). For this aim, I developed an algorithm in IDL language to recover group members that were not spectroscopically observed. I also defined a new strategy to center each group. In this section I will illustrate in detail the algorithm and centering strategy and the tests I performed on the mock catalogs to assess their reliability.

4.1 Adding photo-zs to the spectroscopic group catalog

4.1.1 Strategy

In this Section I present the details of the algorithm to add photometric candidate group members to the spectroscopic ones. Given a group with N observed members in the *20K* mock catalog, we defined its 3D position by: its position on the sky, ra_{gr} and dec_{gr} center and its redshift position, z_{group} , all these quantities are defined as the mean of member galaxy coordinates and redshifts, as defined in the *20K* spectroscopic

4 The Algorithm

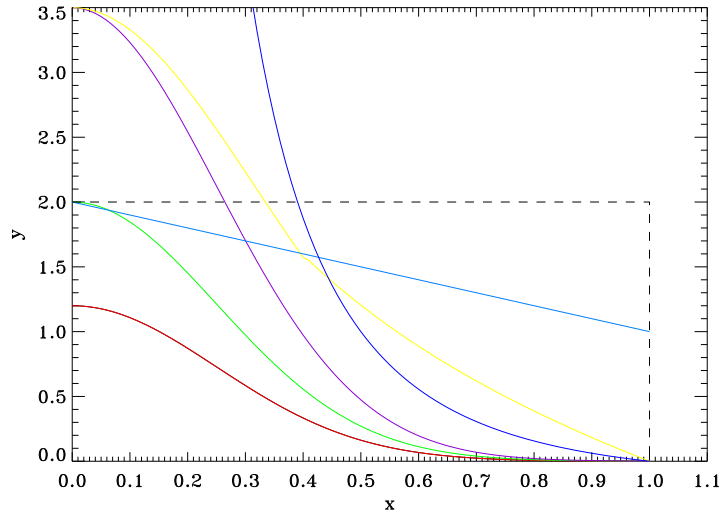


Figure 4.1: Different selection functions for photo-zs candidate members in the plane xy , i.e., the normalized projected radial distance and redshift distance respectively, see text for details. Among exponential (blue), Gaussian (green, red, magenta), Gaussian+logarithmic (yellow) and linear (cyan) profiles we adopted the linear function. The black dashed line highlights the final allowed area in the xy plane to search for photometric putative members.

catalog (see Knobel et al. 2011).

We then defined some useful quantities to characterize each group and its members:

- R_{gr} , the minimum radius of a circle centered on (ra_{gr}, dec_{gr}) and that contains all the spectroscopic confirmed members.
- R_{gal} , the radial projected distance of each galaxy with a photometric redshift to the center of the group;
- $\Delta z = z_{gal} - z_{group}$, the distance in redshift space of each galaxy with a photometric redshift, z_{gal} , to the group;
- $x = R_{gal}/R_{gr}$, the normalized projected radial distance;
- $y = \Delta z / \sigma_{zphot}$, the normalized distance in redshift space, where $\sigma_{zphot} = 0.007 \cdot (1 + z_s)$ is the photometric redshifts accuracy as estimated in Sect. 2.2.

4.1 Adding photo-zs to the spectroscopic group catalog

We decided to use a selection function, $F(x)$, which modulates the acceptable photo-z galaxies depending on their distance both in angular and redshift space normalized to R_{gr} and σ_{zphot} respectively. The accepted photo-zs with (x_i, y_i) must satisfy $y_i \leq F(x_i)$ and $I_{AB} \leq 22.5$.

When choosing the formula of $F(x)$, one should always aim at obtaining the best balance of completeness and purity on galaxy-group base. Furthermore, given the goal of this work, i.e., studying radial trends, we carefully chose the selection function not only to keep the fraction of interlopers as low as possible, but also to avoid introducing any radial dependency of the interlopers fraction.

We tried different selection functions as shown in Fig. 4.1. The colors refer to different $F(x)$: with an exponential (blue), Gaussian (green, red, magenta), Gaussian+logarithmic (yellow) and linear (cyan) profile. The black dashed line highlights the final allowed area in the xy plane to search for photometric putative members. All the functions we tried follow this simple idea: the closer the photo-z galaxy lies in projected radial distance, the wider is the acceptable distance in redshift space.

The exponential, Gaussian and logarithmic profiles provide an intrinsic scale factor where the function decreases towards low values. Unfortunately this drop is quite sharp and the outcome is the nearly absence of photo-z interlopers at the expenses of a small gain in terms of real members. Since one of our most important goal is to recover the real richness of the groups, we excluded these selection functions. On the other hand a linear profile has a smoother decrease at large radii and it allows us to recover a higher fraction of missing real members while keeping small the fraction of interlopers.

The final adopted selection function is $F(x) = 2 - x$, i.e., the maximum acceptable normalized redshift distance is $y = \Delta z / \sigma_{zphot} = 2$ in the center of the group, and it linearly decreases the acceptable distance in redshift space as we go away from the center up to R_{gr} , i.e., the maximum acceptable normalized projected distance is $x=1$. We applied this selection function to all the candidates photometric redshifts within a cylinder of $\pm 2 \cdot \sigma_{zphot}$ depth and within a region of inner radius R_i and an outer radius $R_i + 0.2 \cdot R_{gr}$, increasing R_i iteratively in step of $0.2 \cdot R_{gr}$ from zero up to R_{gr} .

Here we anticipate some of the results of the tests we performed on the mocks in order explain our constrains/choices for the parameter set-up, while we refer the reader to Sect. 4.1.2 for the results concerning the reliability and efficiency of our algorithm.

We computed the normalized distances (x,y) to each group for each galaxy with photometric redshift and $I_{AB} \leq 22.5$ in the 20K+photo-zs mock catalog in each region. We noted that the 95% of the missing real members are always confined within $\pm 2 \cdot \sigma_{zphot}$, while the interlopers are spread all over the range $\pm 4 \cdot \sigma_{zphot}$. This is the reason

4 The Algorithm

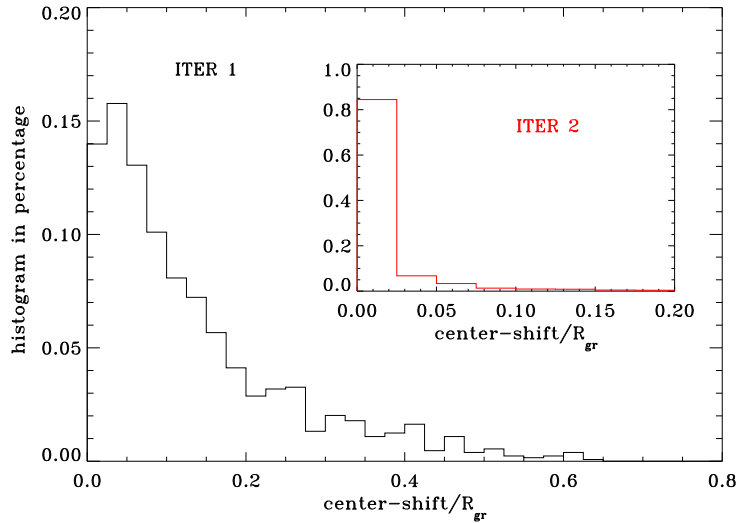


Figure 4.2: Distribution of the center-shift after iter 0 (black) and iter 1 (red) in the inset.

why we constrained the maximum redshift depth to $\pm 2 \cdot \sigma_{z_{\text{phot}}}$. Furthermore in the inner regions the number of real missing members is always higher than the one of interlopers, while as we go far away from the center the ratio reverses. Note that we computed the normalized distances for all the photometric targets in each group region, i.e., an interloper in the outer regions could be a real members of another group in an inner group region. This explains our choice to run the algorithm in concentric annuli: assigning the candidate members this way reduces the number of possible interlopers from other groups rather than adding blindly group members over the whole group radius.

At the end of each run of the algorithm a new catalog of 20K+photo-z member galaxies is produced. If there is any multiple assignment for a single photo-z we used a check function, F_{check} , to univocally assign it to a group. The check function uses both the phot-z information and the more reliable spatial information. It is defined as: $F_{\text{check}}(x, y) = x^2 \cdot y$, so that the photo-z galaxy is assigned to the group with the minimum $F_{\text{check}}(x, y)$. Tests on simulations showed that this check function is able to recover the real membership for 74% of photo-z with multiple assignments to different groups. This way we have dealt with the problem of treating multiple associations.

Once we reached R_{gr} in our search, a new catalog of groups was created and we

4.1 Adding photo-zs to the spectroscopic group catalog

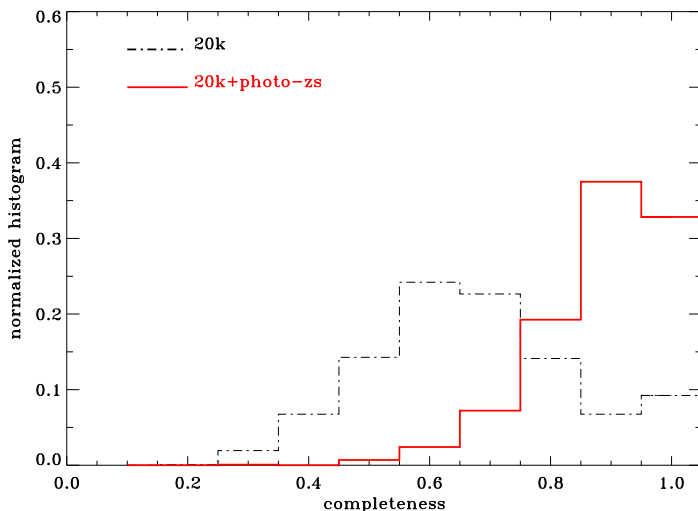


Figure 4.3: Distribution of the completeness for the 20K and for the 20K+photo-zs mock groups: black dot-dashed line corresponds to the 20K mock catalog while red solid line to the 20K+photo-zs mock catalog after running our algorithm to add photo-zs.

determined the new center, as defined in equation 4.2 (see later on Sect. 4.2.1), and the new R_{gr} for each group using both spectroscopic and photometric members.

The whole algorithm is iterative: the j^{th} iteration uses the center and radius of the $(j-1)^{th}$ iteration to search for photo-z member galaxies. We defined the center-shift as the distance between the j^{th} center and the $(j-1)^{th}$ one. In Fig. 4.2 we show the distribution of the center-shift normalized to R_{gr}^{j-1} , the radius R_{gr} of the $(j-1)^{th}$ iteration, after iter 1 (black) in the main panel and iter 2 (red) in the inset.

After two iterations, the center shift is less than 5% of R_{gr}^{j-1} for 90% of the groups, which means that the centering for these groups has converged. The third iteration is enough for the centering to converge also for the remaining 10% of the groups.

4.1.2 Tests on the mocks

To test the reliability of the developed algorithm we applied it to the 20K+photo-zs mocks and we checked our ability to reconstruct the real group membership, i.e. the completeness, the effect of interlopers contamination, and the richness estimates.

4 The Algorithm

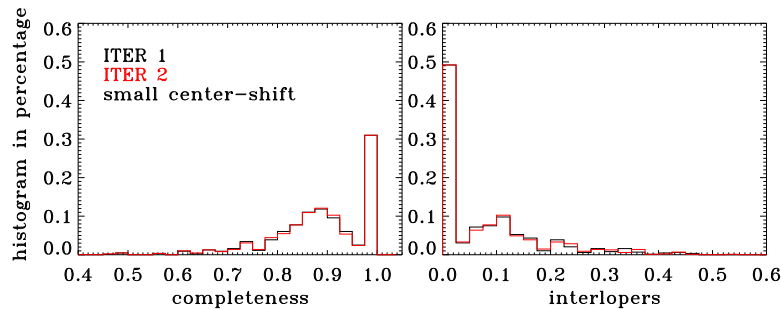


Figure 4.4: *Left panel:* distribution of the completeness after iter 1 (black) and iter 2 (red) for groups with a center-shift $< 15\%$ of R_{gr} . *Right panel:* distribution of the fraction of photo-z interlopers after iter 1 (black) and iter 2 (red) for groups with a center-shift $< 15\%$ of R_{gr} .

We run the algorithm over all the groups with $N_{20k} \geq 5$ within the high sampling rate box introduced in Fig. 2.1 ($149.55 \leq ra \leq 150.666$ and $1.75 \leq dec \leq 2.7$).

The COSMOS mock light-cones provide dark matter halos IDs which can easily be used to identify *real* groups and *real* group members, i.e., the set of galaxies located within the same dark matter halo in each of the mock catalogues introduced in Chapt. 3 (see also Knobel et al. 2009). If we define completeness as the ratio of the reconstructed group members in the 20K/20K+photo-zs mock catalogs to the total number of real group members in the 40K mock catalogs, the improvement introduced by our algorithm is shown in Fig. 4.3. In this plot we show the distribution of the completeness for all the groups of the 20K mocks and for those obtained after applying our algorithm to the 20K+photo-zs mocks (black dot-dashed line and red-solid line respectively). We were able to improve the median completeness from 67% of the 20K mock catalog up to 90% of the 20K+photo-zs mocks: the number of groups 100% complete is three times larger than using only the 20K mocks.

Part of this improvement comes from the auto-recentering and iteration of the algorithm. After each iteration, we can divide the groups into two classes: those with a small center-shift, i.e., less than 15% of R_{gr} , and those with a big center-shift, i.e., $\geq 15\%$ of R_{gr} . In other words, the former subset of groups has already a well defined central peak since the previous iteration, whereas the new added photo-z galaxies have refined the centering for the latter groups. In the case of a big center-shift the next iteration will search for photo-z putative members in an area closer to the real overdensity peak and in a region otherwise left unexplored. This produces a higher probability of retrieving other photo-z candidate members.

4.1 Adding photo-zs to the spectroscopic group catalog

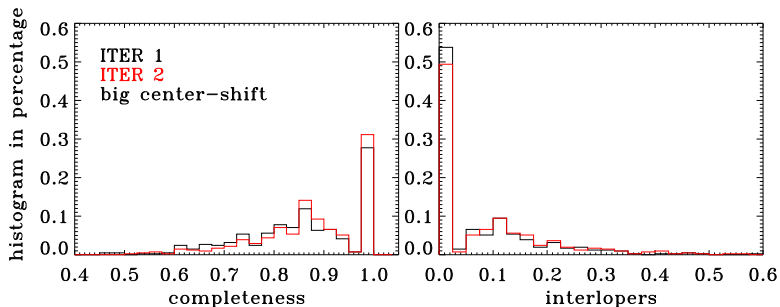


Figure 4.5: *Left panel:* distribution of the completeness after iter 1 (black) and iter 2 (red) for groups with a center-shift $\geq 15\%$ of R_{gr} . *Right panel:* distribution of the fraction of photo-z interlopers after iter 1 (black) and iter 2 (red) for groups with a center-shift $\geq 15\%$ of R_{gr} .

Fig. 4.4 shows the distribution of the completeness (left panels), and the distribution of the fraction of photo-z interlopers (right panel), i.e., photo-z galaxies not sharing the same dark matter halo in the 40K mock catalogs, for the small center-shift groups. In each panel the red solid line refers to the iteration $j=2$, while the black solid line refers to the previous iteration, i.e., $j=1$. Fig. 4.5 is the same as Fig. 4.4, but for the big center-shift groups.

We note that in the case of a small center-shift the completeness and the fraction of photo-z interlopers are similar in iter $j=1$ and in iter $j=2$: in both panels histograms nearly overlap. On the contrary, there is an improvement in completeness in the case of a big center-shift. Fig. 4.5 shows that after iter $j=2$ the distribution of the completeness is shifted towards higher values while the algorithm adds only a small percentage of photo-z interlopers. For example, if the center-shift is 30-40% of R_{gr} , the completeness increases from $\sim 78\%$ to $\sim 90\%$ by adding only $\sim 3\%$ of interlopers. For greater center-shifts, the completeness reaches values of $\sim 100\%$ at the expenses of $\sim 10\%$ interlopers. This means that by adding photo-zs and re-setting the group center for the next iteration, we are retrieving the real overdensity peak, especially for those cases when the 20k sampling was unlucky targeting the outskirts of a group rather than the inner region. Since groups with a big center-shift represent nearly 30% of the cases in iteration $j=1$, the re-centering and iteration strategy is fundamental and very effective.

As a consequence, of the overall completeness improvement, also the group richness, defined as the number of members brighter than an adopted rest-frame absolute magnitude cut-off, is easier to recover in a reliable way. We applied a rest-frame ab-

4 The Algorithm

solute magnitude cut-off $M_{B\text{ cut}} = -20.3 - z_{\text{gal}} + 0.8$ for all the member galaxies of the reconstructed groups in the 20K+photo-zs and 40K mocks with $z_{\text{gr}} \leq 0.8$, i.e., the same cut-off we applied in our analysis of the real 20K+photo-zs sample as explained in Sect. 5.2. We studied the ratio $q_{\mathcal{N}} = \mathcal{N}_{20K+\text{photo-zs}}/\mathcal{N}_{40K}$ between the richness of reconstructed groups in the 20K+photo-zs mocks, $\mathcal{N}_{20K+\text{photo-zs}}$, and their real richness in the 40K mocks, \mathcal{N}_{40K} . For more than 50% of the cases $q_{\mathcal{N}} = 1$, i.e., the richness as measured for reconstructed groups in the 20K+photo-zs mocks equals the same quantity as obtained from the 40K mock catalogs.

Our algorithm achieves this noticeable results while adding a negligible fraction of interlopers, i.e., galaxies not sharing the same dark matter halo in the 40K mock catalogs. For 50% of the groups we add less than 3% of new interlopers with respect to the total members in the 20K+photo-zs catalog, therefore leaving unaltered the interlopers fraction of the spectroscopic group catalog.

We also checked for any dependence of the interloper fraction from the group-centric distance by dividing each group into a central part and two concentric intermediate and external rings. This separation is the same as the adopted one in our analysis of the segregation effects in Chaps. 6 and 7. We also used exactly the same mass and redshift limits later adopted in our analysis, see Sect. 5.2 for precise definition of redshift limits and corresponding mass limits for the low- and high-z bins.

In Fig. 4.6 we show the fraction of interlopers in each of these three regions for the 20K/20K+photo-zs mock groups (black stars and red triangles respectively), as obtained using the low-z, mass-limited, mock group samples. Notice that the trend introduced by the group-finding algorithm in the 20K mock reconstructed groups is not modified by our algorithm adding photo-zs members. In the same panel the orange squares display the fraction of interlopers in the 20K sample spectroscopic group catalog, estimated using the probabilities, $p_{in,i}$, associated to each observed group spectroscopic member:

$$\mathcal{P}I = 1 - \sum_{i=1}^{N_{tot,obs}} p_{in,i}/N_{tot,obs} \quad (4.1)$$

as provided by Knobel et al. (2011). In Knobel et al. (2011) the association probabilities, $p_{in,i}$, of spectroscopic members is determined only by the distance from the group center and it has been calibrated using simulations. As a consequence, they are by construction in good agreement with the interlopers fraction as estimated from 20K mock groups. In turn, as adding phot-z members does not alter significantly the trends, these values are in good agreement with the interlopers fraction for the 20K+photo-zs mock groups. The picture does not change when plotting same quanti-

4.1 Adding photo-zs to the spectroscopic group catalog

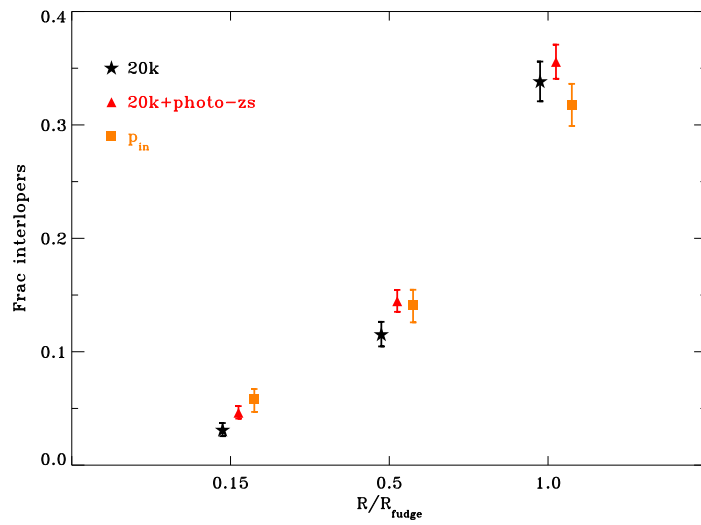


Figure 4.6: Fraction of interlopers in each group region for the 20K/20K+photo-zs mock with black stars and red triangles respectively. Orange squares refer to the fraction of interlopers, \mathcal{P}_{in} , for the real data, see text for details.

ties but for the high- z , mass-limited, mock group samples, nor when selecting subsets of groups according e.g., to their richness. Therefore we will always use \mathcal{PI} to estimate the interlopers' contamination as a function of the distance from the group center for our spec+photo- z group catalog, see Chaps. 6 and 7.

As a check, we tried to vary the limiting values of the parameter set in our algorithm, namely the maximum x , y , and the limiting magnitude of photo- z galaxies. We allowed the maximum x to range between 1.0 and 1.6 and the maximum y to range between 2.0 and 3.0. Increasing the maximum x at fixed y does not turn into a significant gain in terms of completeness (from $\sim 90\%$ to $\sim 93\%$) but it adds a significant percentage of photo- z interlopers (from $\sim 3\%$ to $\sim 10\%$). The same holds when increasing the maximum y at fixed x value or when attempting to reach fainter magnitudes, i.e., $I_{AB} = 23.0$.

Since the interlopers may have a significant impact in our analysis, we decided to constrain the maximum x and y to be 1.0 and 2.0 respectively. Furthermore as we will explain in Sect. 4.2.2, a complete sample down to $I_{AB} = 22.5$ is deep enough to retrieve the correct center of the groups.

4.2 Defining the group centers

4.2.1 Strategy

A good group center definition is essential to our science analysis, as we will be searching for radial trends that can be easily erased by errors on the computed group centers. Typical numerosities of our groups are in the range of 5-50 members, but the numerosity distribution peaks at small numerosities, i.e., 7-9. As a consequence, simple methods of estimating groups center, such as the median of members coordinates, provide only rough estimates of the group center, especially for the numerically poorer groups, and it would not satisfy our needs. We therefore tried alternative strategies, taking into account also sky projected group galaxy densities. Using as proxy for density measurement the 2D-Voronoi areas, we defined two types of group center:

- the *Voronoi-Weighted center* (VW center from now onwards),
- the *Reconstructed Central Galaxy* (RCG from now onwards).

The VW center is defined as:

$$\text{ravw} = \frac{\sum_{i=1}^N \text{ra}_i / A_{V,i}}{\sum_{i=1}^N 1 / A_{V,i}}, \quad \text{decvw} = \frac{\sum_{i=1}^N \text{dec}_i / A_{V,i}}{\sum_{i=1}^N 1 / A_{V,i}}. \quad (4.2)$$

4.2 Defining the group centers

where $A_{V,i}$ is the 2D-Voronoi area associated to the i -th galaxy member, that is the projected area containing all points closer to the i -th galaxy than to any other member galaxy. We used the field galaxies that lie outside $3 \cdot R_{gr}$ and within $1 \cdot \sigma_{zphot}$ to bind the $A_{V,i}$ of those member galaxies at the boundaries of the group to prevent infinite values for their areas.

In Fig. 4.7 we show two examples of the Voronoi Tessellation for two reconstructed groups in the 20K+photo-zs mocks. Red triangles refer to group member galaxies, whereas cyan circles refer to field galaxies. Black solid lines connect the vertices that form the Voronoi Tessellation and provide the 2D-Voronoi area. The Voronoi Tessellation was computed using the IDL version of the algorithm *qhull*.

Clearly galaxies that are located in a high projected concentration of galaxies, i.e., towards the center of the group, have a smaller $A_{V,i}$ and they will weight more in eq. 4.2, while those that are in less dense regions will affect less the center determination. The groups in Fig. 4.7 have different numerosities, nevertheless the 2D-Voronoi areas well correlate with the region of highest projected density in both cases. In other words, the Voronoi-Weighted center provides a center for the group which is located by definition in the area of greatest galaxy over-density, and is not affected by the details of the spatial distribution of galaxies at the outskirts. For a similar approach see Diaz et al. (2005).

We then defined the RCG as the group member galaxy having the maximum specific density, $\delta_{M_*,A_{V,i}}$, where:

$$\delta_{M_*,A_{V,i}} = \frac{M_{*,i}}{A_{V,i}} \quad (4.3)$$

where $M_{*,i}$ is the stellar mass of the i^{th} galaxy. This definition is a direct consequence of the so called central galaxy paradigm (CGP). The CGP assumes the central galaxy, i.e., the galaxy with the lowest specific potential energy, to be the most luminous/most massive galaxy in a DMH, and that it resides at rest at the center of the halo potential well. In the weighting scheme of eq. 4.3 the $A_{V,i}$ takes into account the latter property of the CGP, if we assume that galaxies trace the group halo potential well, while $M_{*,i}$ accounts for the former one.

4.2.2 Tests on the mocks

We used our set of mock catalogs to test the reliability and the advantages of our VW center definition with respect to simpler ones, like the median of the member galaxies coordinates (Median center). We also tested our ability to retrieve the correct central galaxy using our RCG definition. In mock catalogs the center of the DMH, i.e., the

4 The Algorithm

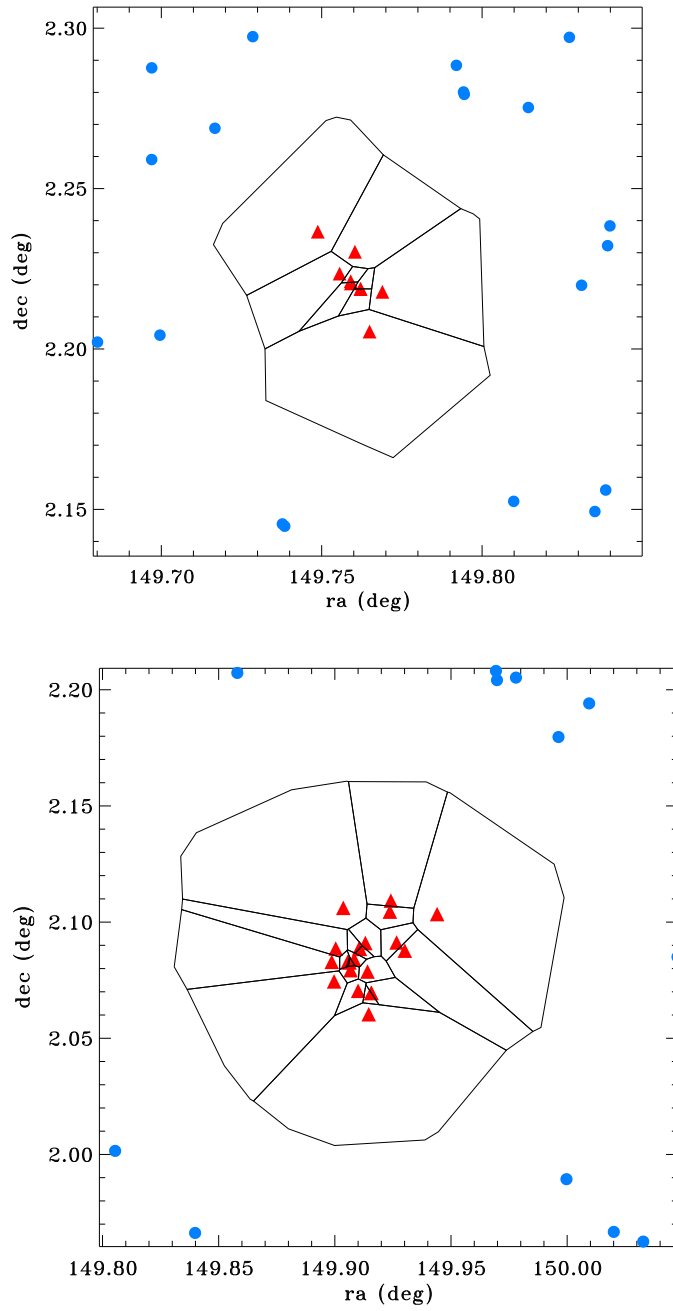


Figure 4.7: Example of Voronoi Tessellation for two groups in the 20K+photo-zs mocks. Red triangles refer to group member galaxies, whereas cyan circles refer to field galaxies. Black solid lines connect the vertices that form the Voronoi Tessellation and provide the 2D-Voronoi area.

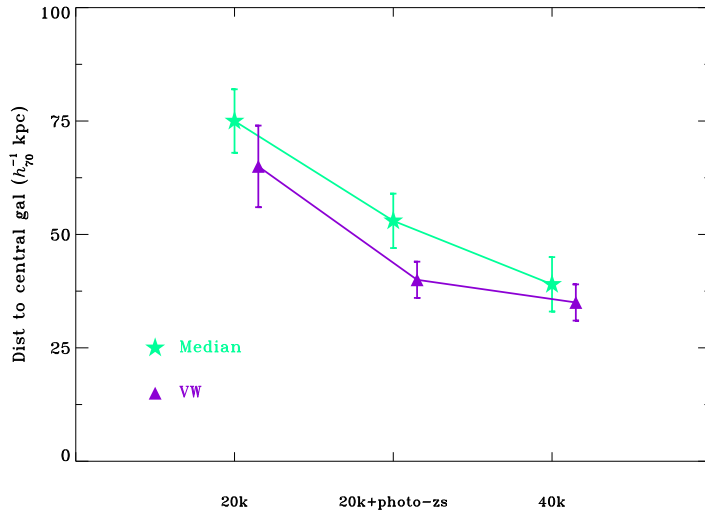


Figure 4.8: Median distance to the central galaxy of the VW center (violet triangles) and the Median center (cyan stars) as a function of the analyzed mock catalog.

position with the deepest potential well, corresponds with the position of the central galaxy within the halo. Therefore we assumed as fiducial center for each reconstructed mock group the position of its central galaxy, as provided by the mocks.

We first focus on the VW center: in Fig. 4.8 we show the median distance of the VW center (violet triangles) and that of the Median center (cyan stars) for the 20K, 20K+photo-zs mocks, and 40K mock catalogs defined in Chapt. 3. Error bars are the rms among mock catalogs extracted from the different 24 light-cones. We note that the VW center provides a better estimate of the center with respect to the Median center. Furthermore the VW center, when applied to the groups where the photo-zs have been added according to our algorithm are nearly indistinguishable from those obtained when all members down to $I_{AB} = 22.5$ possess spectroscopic redshift. The median value of the distance of the VW centers from the group central galaxy is $40 h_{70}^{-1} Kpc$ for 20K+photo-zs mocks, with an improvement of nearly 40% in centering with respect to the 20K mocks.

In Fig. 4.9 we show the histogram of the distance of the VW center to the central galaxy position for the reconstructed groups in the 20K mocks in black dot-dashed line and for those in the 20K+photoz mocks in red solid line. The improvement in group centering obtained when adding photo-zs members is quite obvious. We note that the

4 The Algorithm

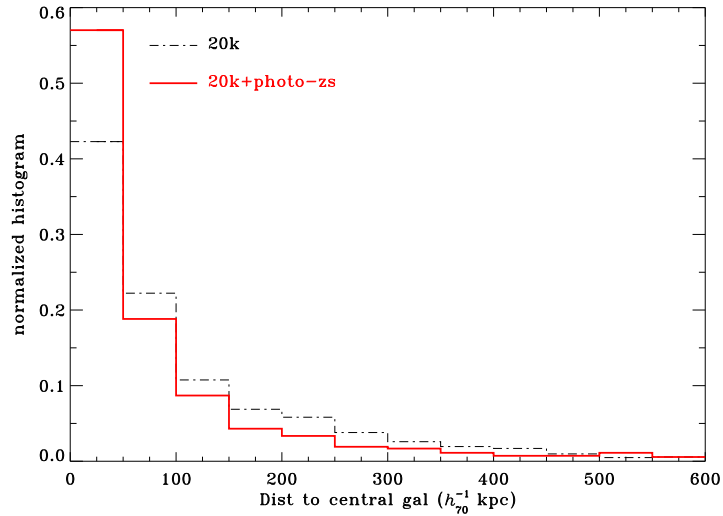


Figure 4.9: Distribution of the distance of the VW center to the central galaxy position for the 20K mocks and for the 20K+photo-zs mocks. Black dot-dashed line corresponds to the 20K mock catalog while red solid line to the 20K+photo-zs mock catalog after running our algorithm to add photo-zs.

improvement regards mainly those groups that in the 20K had a big offset, 100-250 kpc, and that in the 20K+photo-zs fill the first bin of the distribution.

In Tab. 4.1 we report the estimates of the median distance of the VW center and of the Median center to the fiducial center for each of the mock catalogs introduced in Chapt. 3. In this table we list the distances also for the mocks 100% complete down to $I_{AB} = 23.0, 23.5, 24.0, 26.0$. We note that in these catalogs the offsets of both the VW center and of the Median center are almost fixed at $\sim 30-35 h_{70}^{-1} Kpc$, suggesting that the overdensity peak has already been recovered at $I_{AB} = 22.5$.

We now test our definition of the RCG when compared to the real central galaxy of a reconstructed mock group. One could argue that, assuming the CGP to be correct, we do not need any particular strategy to retrieve the central galaxy of a group since it will be the most massive galaxy of the group. Nevertheless, in the ideal case of the 40K mock catalog, the central galaxy of a group is also the most massive one only in $\sim 80\%$ of the cases.

Therefore trusting the CGP is not always correct. Moreover, in the real case, we should take into account two further complications.

Table 4.1: Median distance of the VW center and of the Median center to the fiducial center for each of the mock catalogs introduced in Chapt. 3.

Cat	Med vs Central (kpc)	VW vs Central (kpc)
20K	75 ± 7	65 ± 9
20K+photo-zs	53 ± 6	40 ± 4
40K	39 ± 6	35 ± 4
fl_23.0	40 ± 4	33 ± 4
fl_23.5	35 ± 4	32 ± 4
fl_24.0	34 ± 3	32 ± 2
fl_26.0	33 ± 2	32 ± 2

First of all due to the SPOC random targetting we expect that at least half of the central galaxies have a spectroscopic redshift and therefore they should be part of the 20K mocks. The other half will have a photometric redshift and therefore will be present only in the 20K+photo-zs mocks. As a consequence our ability of retrieving the correct central galaxy depends on the performances of the algorithm to add the photo-z, i.e., we are limited by the 90% completeness reached with our algorithm.

We checked that the central galaxy of a group was already sampled for 53% of the reconstructed groups of the 20K mocks, applying our algorithm we are able to recover another 36% of the central galaxies, while the remaining 11% is lost.

Secondly galaxy stellar masses estimates have a typical error of 0.25 dex. This is crucial given that the typical mass difference between the most massive and the second massive galaxy of a group is of the same order. The joint effect of these two complications makes even more unreliable the choice of the most massive galaxy as the central galaxy of a group. To account for the stellar mass uncertainty we perturbed the stellar mass of each member galaxy of a mock group with an error of 0.25 dex normally distributed.

In the end, choosing the most massive galaxy as the central one in the 20K+photo-zs mocks turned out to be correct only in 48% of the cases. On the contrary the definition of the RCG recovers the real central galaxy in 60% of the cases.

We assigned a probability to each RCG to be the real central galaxy. We perturbed the galaxy stellar masses of each galaxy for 1000 times, each time generating the errors

4 The Algorithm

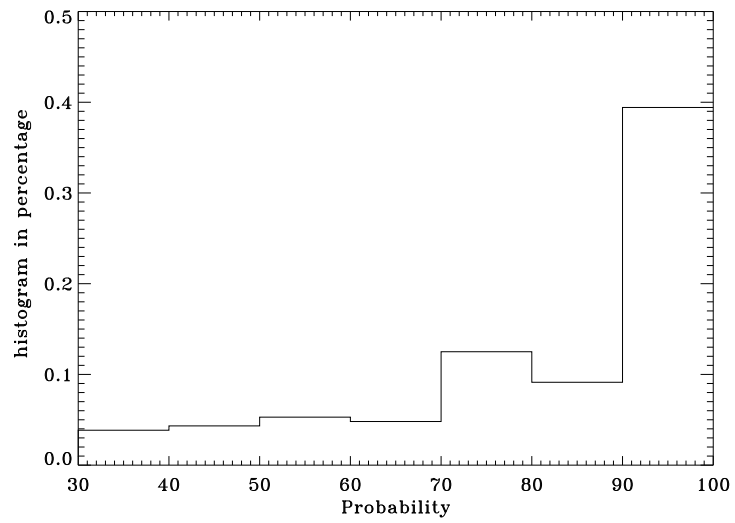


Figure 4.10: Distribution of the probability assigned to each RCG of the reconstructed 20K+photo-zs mock groups of being the correct central galaxy. This probability is never less than 30%.

4.2 Defining the group centers

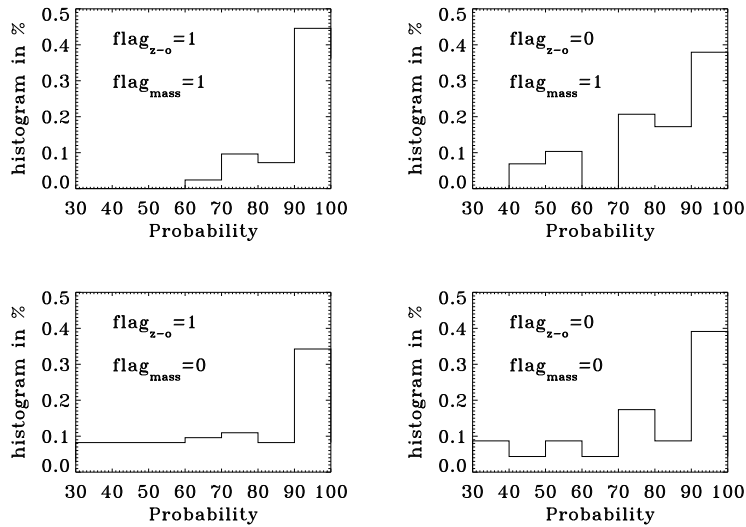


Figure 4.11: Same as Fig. 4.10 for different combinations of flag_{mass} and flag_{z-o} , see text for a detailed explanation of the meaning of each flag. *Top Left panel:* the case of a centered and most massive RCG. *Top Right panel:* the case of an offset and most massive RCG. *Bottom Left panel:* the case of a centered and not most massive RCG. *Bottom Right panel:* the case of an offset and not most massive RCG.

from a different seed. Each time we determined the new RCG and the probability of the RCG is then the percentage of times that we retrieved the same RCG among the 1000 cycles. Fig. 4.10 shows the distribution of the probability assigned to each RCG of the reconstructed 20K+photo-zs mock groups. The median probability is $\sim 90\%$ and it is never less than 30%.

We also study the properties of the RCG with respect to the global properties of the group. First of all we assigned a flag, flag_{mass} , to indicate whether the RCG is the most massive of the group, $\text{flag}_{mass} = 1$, or not, $\text{flag}_{mass} = 0$. Then we estimated R_{RCG} , i.e., the projected radial distance of the RCG to the VW center, and we normalized it to R_{gr} , $\mathcal{R}_{RCG} = R_{RCG}/R_{gr}$. We also provided a flag, flag_{z-o} , that indicates whether the central galaxy is offset with respect to the VW center: $\text{flag}_{z-o} = 1$ if $\mathcal{R}_{RCG} < 0.3$, whereas $\text{flag}_{z-o} = 0$ if $\mathcal{R}_{RCG} \geq 0.3$,

In Fig. 4.11 we show the distribution of the probability assigned to each RCG of the reconstructed groups in the 20K+photo-zs mock for different combinations of flag_{mass} and flag_{z-o} . Top left panel shows the cases of a centered and most massive RCG,

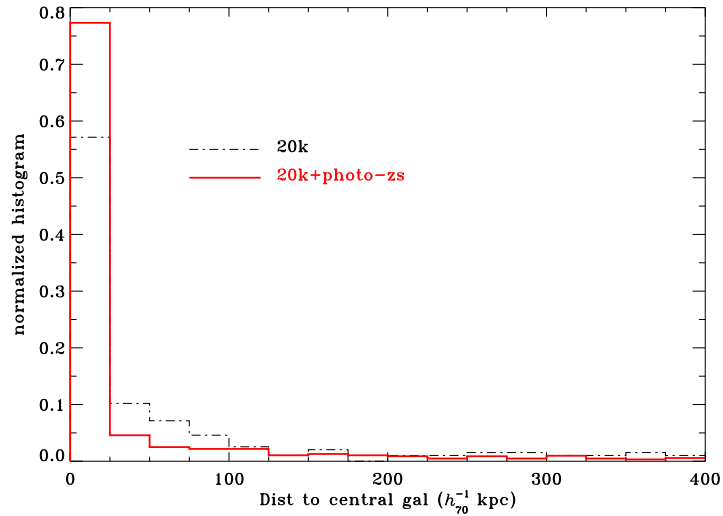


Figure 4.12: Distribution of the RCG distance to the central galaxy for all reconstructed groups. We compare the distribution of the 20k, black, and that of the 20k+photo-z, red.

this is the most common configuration and it comprises nearly 44% of the cases. In this case the probability is always larger than 60% and the distribution peaks towards 100%. On the contrary the bottom right panel shows the cases of an offset and not most massive RCG. This is the less common combination, as it makes up to only 12% of the cases. Moreover the distribution covers the whole range of probabilities, from 30% to 100%.

Furthermore, we might think of the RCG as a mass-density weighted center. In Fig. 4.12 we show the distribution of the distance of the RCG to the real central galaxy for all the reconstructed groups. The black solid line refers to the 20k, while the red one refers to the 20k+photo-z. The higher quartile of the 20K+photo-zs distribution is $16 h_{70}^{-1} Kpc$. Whenever the RCG chose the wrong central galaxy, the average distance to the real central galaxy is $55 h_{70}^{-1} Kpc$.

4.3 Conclusions

In this chapter, I described the algorithm I have developed to incorporate into groups those galaxies brighter than $I_{AB} = 22.5$ and missing the spectroscopic redshift in-

formation. This enabled us to increase the galaxy population of zCOSMOS groups down to $I_{AB} = 22.5$ providing a statistically reliable sample to study galaxy evolution in group environment. Using mock catalogs I tested the reliability of the algorithm and found that it works very well as the final completeness is $\sim 90\%$ while introducing a small percentage of interlopers, $\sim 3\%$. Furthermore this code do not introduce any significant radial trend of the contamination from interlopers, thus providing a reliable sample to study the variation of group member galaxies as a function of the group-centric distance.

I have also developed a new strategy to determine the group center: the VW center. This new definition enabled us to get as close as $40 h_{70}^{-1} Kpc$ to the real center of the groups, as tested on the mocks. This definition works always better than simpler definitions, i.e., the Median center, and when it is joint with the photo-zs information provides centers that are virtually indistinguishable from those that could be obtain in a 100% complete spectroscopic sample.

Finally I have defined a new estimator to retrieve the central galaxy of a group: the RCG. Using this definition we are able to recover the correct central galaxy of a group in 60% of the cases. Furthermore we can use the RCG as the center of the group, this way the overall median distance of the RCG to the group center is $16 h_{70}^{-1} Kpc$.

Both the VW center and the RCG provide a good centering for our groups, however the RCG center is biased towards most massive galaxies. As we planned to study also mass segregation effects (see Sect. 6.5), choosing the RCG as the center of our groups would have introduced artificial trends in the distribution of masses as a function of the group-centric distance. We therefore adopted the VW center as the center of each group of our sample, see Sect. 5.3.

Part of this work has been published in Presotto et al. (2012)

5 The Stacked Group

In this Chapter I will introduce the final data set I will work with, i.e., the spectroscopic and photometric group member galaxies obtained after running our algorithm on the 20K final sample and the photo-zs sample from Oesch et al. (2010). I will explain the construction of volume and mass limited samples, which we will use to perform a fair analysis, i.e., free from selection biases due to the well-known correlation between galaxy properties and its stellar mass. I will describe the method we adopted to build the ensemble systems and I will summarize the properties of the stacked groups.

5.1 Applying the algorithm to the 20K final sample

Our algorithm adds further 684 member galaxies with photometric redshifts to the already existing 1437 spectroscopic groups member galaxies, and from now onwards this is the groups sample we will use. Reassuringly the ratio of the number of spectroscopic redshift members to the total number of members (i.e., including member galaxies with photometric redshift only) is in good agreement with the median sampling rate within the central area ($\sim 62\%$ as quoted in Sect. 2.1.3) once our completeness of $\sim 90\%$ - as tested from simulations - is taken into account (see Sect. 4.1.2).

The final number of groups with more than 10(/15) members after applying our algorithm is twice(/three times) that in the spectroscopic group catalog, i.e., there are 78(/41) groups instead of the original 39(/14) groups. The number of groups with more than 20 members is six times the original one: 25 groups instead of the original 4 groups.

In 19% of the cases the algorithm does not add any photo-z galaxy to the group. We explored the properties of these groups to search for any peculiarity which can be responsible of their photo-zs deficiency. They are smaller in projected size with respect to the whole group sample, i.e., they have $R_{\text{gr}} \sim 340 h_{70}^{-1} Kpc$ to be compared to $R_{\text{gr}} \sim 500 h_{70}^{-1} Kpc$ for the whole sample. However, they share the same redshift distribution as the whole sample, as confirmed with more than 99% confidence level by a KS test. Therefore their smaller sizes are not a reflection of a higher redshift distribution and can be considered a peculiar property of these groups. These are also

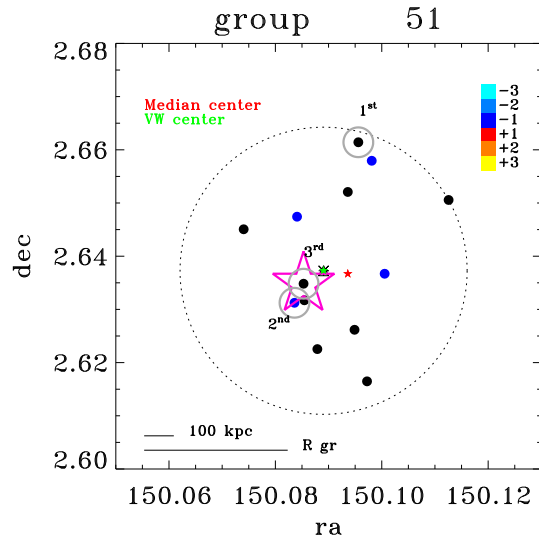


Figure 5.1: Distribution on the sky of spec-z (black circles) and photo-z (blue circles) galaxies which are members of group 51. Grey circles highlight the three most massive galaxies of the group, while red and green filled stars correspond to the Median and VW center respectively. The dotted line draws the circles centered on (ra_{gr}, dec_{gr}) and with radius R_{gr} . As a reference we draw a bar corresponding to $100h_{70}^{-1} Kpc$ at the redshift of the group with a solid line.

groups with small numerosity, i.e., 5-6 members. We checked that the mocks have a similar behaviour: in 13% of the cases our procedure does not add any photo-z to the reconstructed groups in the 20K+photo-zs mocks. The reconstructed mock groups are also smaller and poorer than the whole sample as we observed in the 20K.

We did not investigate this point any further, but it could be interesting to explore the density field these groups live in and whether they have a genuine compact configuration.

In Fig.5.1 we show the distribution on the sky of spec-z (black circles) and photo-z (blue circles) galaxies which are members of one of our groups. Grey circles highlight the three most massive galaxies of the group, while red and green filled stars correspond to the Median and VW center respectively. The pink star is centered on the RCG of the group. The dotted line draws the circles centered on (ra_{gr}, dec_{gr}) and with radius R_{gr} . As a reference we draw a bar corresponding to $100 h_{70}^{-1} Kpc$ at the redshift of the group with a black solid line.

5.1 Applying the algorithm to the 20K final sample

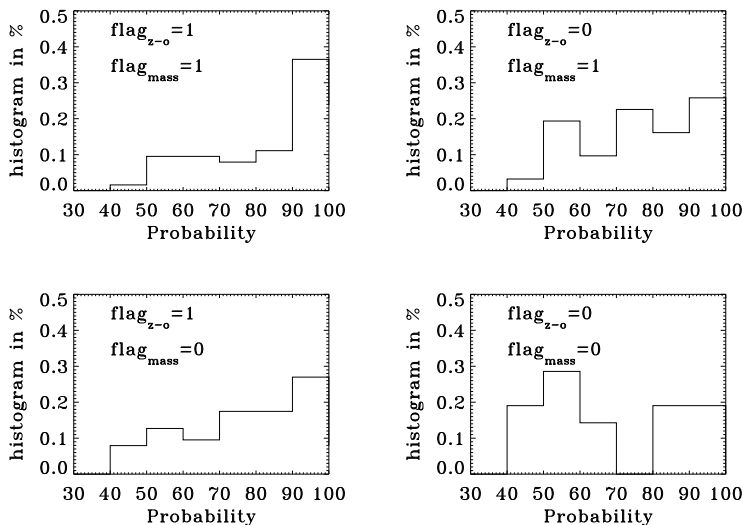


Figure 5.2: Same as Fig. 4.11 for the 20K. *Top Left panel*: the case of a centered and most massive RCG. *Top Right panel*: the case of an offset and most massive RCG. *Bottom Left panel*: the case of a centered and not most massive RCG. *Bottom Right panel*: the case of an offset and not most massive RCG.

This group is a nice example that summarizes the strength of our algorithm: here we added four new photo-z members to the pre-existing 9 spec-z members, the VW center is closer to the overdensity peak than the Median center and the RCG lies in the overdensity peak. Note that the RCG is the third massive galaxy of the group, while choosing the most massive one would have meant selecting one of the outermost galaxy.

As already done in Sect. 4.2.2, we flagged each RCG of our groups depending on both its mass and its position with respect to the VW center, i.e., using flag_{mass} and flag_{z-o} as defined in Sect. 4.2.2. In Fig.5.2 we show the probability distribution of the observed 20K RCG for different combinations of flag_{mass} and flag_{z-o} . The properties of the observed RCG are in good agreement with those of mock RCG: the case of a centered and most massive RCG is the most common configuration also among the observed RCG and it comprises nearly 35% of the cases. The cases of an offset and not most massive RCG make up to only 13% of the groups. We note that for the real 20K the probability distribution are somewhat more spread among the full range, though the general trend is consistent with that of Fig. 4.11.

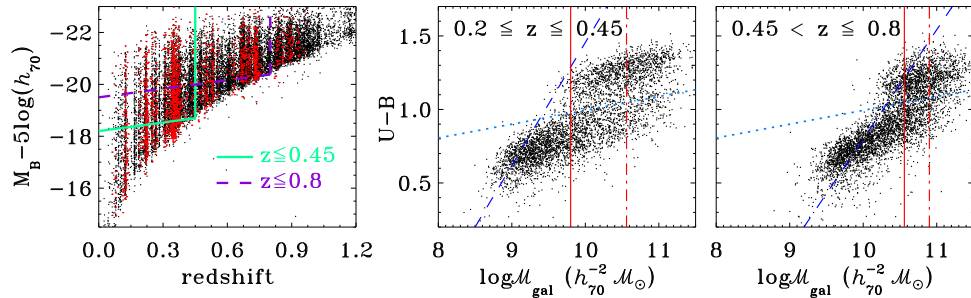


Figure 5.3: *Left panel:* redshift distribution of the zCOSMOS-Bright galaxies (black). Red points represent group member galaxies with both spectroscopic and photometric redshifts as obtained from our algorithm. The cyan solid line and the violet dashed line correspond to the two different magnitude cut-offs adopted to define the volume-limited samples of the low and high redshift bin respectively, see text for details. *Central and right panel:* $(U - B)$ rest-frame color versus mass for the lowest and the highest redshift bin respectively. The blue dashed line corresponds to the color dependent $\mathcal{M}_{\text{cut-off}}$, while the red solid line corresponds to the fixed $\mathcal{M}_{\text{cut-off}}$ for our mass volume-limited sample. The red dot-dashed lines highlight the mass ranges adopted in the mass-segregation analysis, see Sect. 6.5 for details. The cyan dotted line corresponds to the separation between red and blue galaxies (see text for its precise definition).

5.2 Volume-mass limited samples

We focused our analysis into two redshift bins: $0.2 \leq z \leq 0.45$ and $0.45 < z \leq 0.8$, where we defined the classical volume limited samples taking into account the luminosity evolution of individual galaxies. Following Zucca et al. (2009), we adopted a linear evolution with redshift: $M_{B_{\text{ev}}}^* = -20.3 - 5 \log h_{70} - 1.1 z$ to parametrize the evolution of M_B^* of the luminosity function. The corresponding evolving cut-off magnitudes are: $M_{\text{cut-off}} = M_{B_{\text{ev}}}^* + 2.1(/ + 0.8)$ for the low(/high) redshift bin respectively. For $0.2 \leq z \leq 0.45$ the volume-limited sample consists of 829 out of 1128 total galaxies, belonging to 79 groups. For $0.45 < z \leq 0.8$ it consists of 510 out of 660 total galaxies, belonging to 64 groups (see Tab. 5.1). The total volume limited field sample consists of 1869(/2893) galaxies, while the *near-field* volume limited sample consists of 683(/612) galaxies, for the low(/high) redshift bin respectively. In the left panel of Fig. 5.3 we show the M_B^* versus redshift distribution of the total galaxy sample (black points) and that of both spectroscopic and photometric redshift group member galaxies (red points). The cyan solid line and the violet dashed line correspond to the

magnitude cut-offs defining the low and high redshift volume-limited samples. From now onwards, group richness \mathcal{N} for each group is defined as the number of (phot+spec-z) member galaxies surviving to the more conservative absolute rest-frame magnitude cut-off: $M_{B_{\text{ev}}}^* + 0.8$, unless explicitly stated. This quantity correlates, albeit with a large scatter, with the mass of the halo where the group resides and therefore is a good proxy for it (see Knobel et al. 2009).

The flux limited target definition of zCOSMOS-bright, $I_{\text{AB}} \leq 22.5$, translates into a B-band rest-frame selection at $z \sim 0.8$. Therefore the 20K galaxy sample, when rest-frame B-band selection is adopted, is free from significant color-dependent incompleteness in $(U - B)$ rest-frame colors up to $z \sim 1$. However $(U - B)$ rest-frame color completeness in B-band rest frame selection does not imply completeness in mass selection: B-band rest-frame selection is biased towards blue, low mass galaxies, while missing the corresponding red, equally low mass ones. Environmental trends observed in samples selected using rest-frame B-band magnitudes could therefore be simply the results of such incompleteness coupled with different galaxy mass distributions in different environments (Bolzonella et al. 2010).

To disentangle true environmental effects from mass-driven ones, we used in our analysis mass volume-limited samples, that is samples complete down to a fixed galaxy mass cut-off. To obtain them we followed the same approach as in Iovino et al. (2010). In brief we first calculated the limiting stellar mass for each galaxy in the 20K sample, i.e., the stellar mass it would have, at its spectroscopic redshift, if its apparent magnitude was equal to the limiting magnitude of our survey: $\log(\mathcal{M}_{\text{lim}}(z_{\text{gal}})) = \log(\mathcal{M}_{\text{gal}}) + 0.4(I_{\text{AB}} - 22.5)$. We then used these estimated limiting masses to define, in bins of $(U - B)$ rest-frame colors for each redshift bin, the mass $\mathcal{M}_{\text{cut-off}}$ below which 85% of galaxies of that color lie. We fitted $\mathcal{M}_{\text{cut-off}}$ to obtain a color dependent mass limit cut off. The value of $\mathcal{M}_{\text{cut-off}}$ for the reddest galaxies in each redshift bin is the one that we use as the limiting mass for that bin.

In the central and right panel of Fig. 5.3 we show the $(U - B)$ rest-frame color versus the stellar mass for the lowest and highest redshift bin respectively. The blue dashed line shows the color dependent $\mathcal{M}_{\text{cut-off}}$, while the red solid line shows the value chosen to define mass-limited samples: $\log(\mathcal{M}_{\text{gal}}/\mathcal{M}_{\odot}) \geq \mathcal{M}_{\text{cut-off}} = 9.8$ and $\log(\mathcal{M}_{\text{gal}}/\mathcal{M}_{\odot}) \geq \mathcal{M}_{\text{cut-off}} = 10.56$ for the lowest and highest redshift bins respectively.

To define the mass dependent color cut separating the blue and red galaxies, we performed a robust fit of the red sequence as a function of the galaxy stellar mass in the high-z bin, where the large number of observed galaxies displays a prominent and well defined red sequence. The separation between red and blue galaxies is then obtain

5 The Stacked Group

Table 5.1: Number of volume-limited and mass-volume-limited (spec+phot-z) group member galaxies. In brackets we report the number of spectroscopic-only group members. The number of groups containing these galaxies is listed in the last column.

Redshift	Vol-lim N_{gals}	Vol-Mass-lim N_{gals}	N_{gr}
$0.2 \leq z \leq 0.45$	829 (570)	571 (410)	79
$0.45 < z \leq 0.8$	510 (391)	265 (200)	64

by shifting the fitting line by $2 \cdot rms_{red}$, where $rms_{red} \sim 0.08$ is the dispersion of the red galaxies along the red sequence. We adopted the same color cut for the low-z bin. Numerically, the stellar mass dependent color cut in the low and high redshift bin is:

$$(U - B) = 0.094 \cdot \log(\mathcal{M}_{gal}/M_{\odot}) + 0.05 \quad (5.1)$$

and it is shown by the cyan dotted line in Fig. 5.3. We tested that our results do not change if we apply a constant color cut as $(U - B) = 1$ to separate red and blue galaxies, a simpler definition that also corresponds quite well to the dip of the bimodal distribution.

For the lowest redshift bin the final group mass-complete sample contains 571 galaxies while for the highest redshift bin it contains 265 galaxies. The mass-complete field samples consist of 743(/728) galaxies for the lowest(/highest) redshift bin respectively, while the *near-field* samples consist of 293(/211) galaxies for the lowest(/highest) redshift bin respectively.

5.3 Group rescaling

The procedure of stacking groups of different sizes and masses into an ensemble system requires that individual galaxy center distances are properly scaled. In studies of galaxy clusters, projected cluster-centric-distances R are generally rescaled with R_{vir} or R_{200} , whose estimate is proportional to σ_v , that is a proxy of cluster mass (Carlberg et al. 1997; Biviano et al. 2002; Katgert et al. 2004). However, the issue is not trivial when dealing with galaxy groups. In this case there are larger uncertainties in the estimate of velocity dispersions, masses, size and the group dynamical state in general, due to the small number of group members.

In the literature there are different approaches in rescaling R for groups using: 1) the virial radius R_{vir} or R_{200} , 2) an estimate of the rms of the position of member galaxies

R_H , and 3) sometimes radial distances are not rescaled at all (see Girardi et al. 2003, for a detailed review).

Our groups span a wide range of sizes, and therefore a rescaling of physical distances seemed unavoidable. We decided to use as the scaling factor R_{fudge} , provided by Knobel et al. (2011). This *fudge* quantity, as many other ones correlating with the observed group richness, is estimated and calibrated using our realistic mock catalogs, as explained in Sect. 2.1.4. Here we briefly remind that, given an observed group at redshift z with richness \mathcal{N} , its R_{fudge} corresponds to the mean R_{vir} among all reconstructed mock groups having the same \mathcal{N} and redshift (see Knobel et al. 2011, for more details on how this quantity is calculated). The quantity R_{fudge} well correlates with $M_{\text{halofudge}}$, an estimate of the mass of the group as defined in Knobel et al. (2009), further supporting its relevance for our analysis.

As our goal is to distinguish properties of galaxies located in regions with different physical properties, e.g., the central virialized regions and the outskirts, rescaling by a quantity related to the R_{vir} as R_{fudge} well suits our needs. In fact the virial radius is a scaling factor for many timescales of different processes such as the crossing time, the relaxation time or the merging time (Boselli & Gavazzi 2006; Weinmann et al. 2006). All the galaxies that are inside the virial radius are experiencing the group potential effects either for the first time or more times. On the contrary those galaxies that are outside the virial radius are a mixed population of both in-falling galaxies and galaxies that once passed through the virial radius but now are in the outskirts, the so called back-splash population (Gill et al. 2005).

As discussed in Sect. 4.2.2, both the VW center and the RCG provide a good centering for our groups, however the RCG center is biased towards most massive galaxies. Since we planned to study also mass segregation effects, choosing the RCG as the center of our groups would have introduced artificial trends in the distribution of masses as a function of the group-centric distance. We therefore adopted the VW center as the center of each group of our sample. Before stacking groups we rescaled each member galaxy distance to the VW center, R_{gal} , with the corresponding R_{fudge} of its group. Hereafter we will use only scaled distances, \mathcal{R} , unless otherwise specified.

We remark also a final caveat: when discussing our results we should take into account projection effects. We observe the 2-D projection of a 3-D distribution of member galaxies. Assuming a spherical distribution, this implies that e.g., the inner observed region includes galaxies located in the outer group shells and located along the line of sight of the group central part. Hence a fraction of galaxies observed in the projected inner region actually belongs to the outskirts. These projection effects will tend to smooth the radial trends we are looking for, so that any observed trend

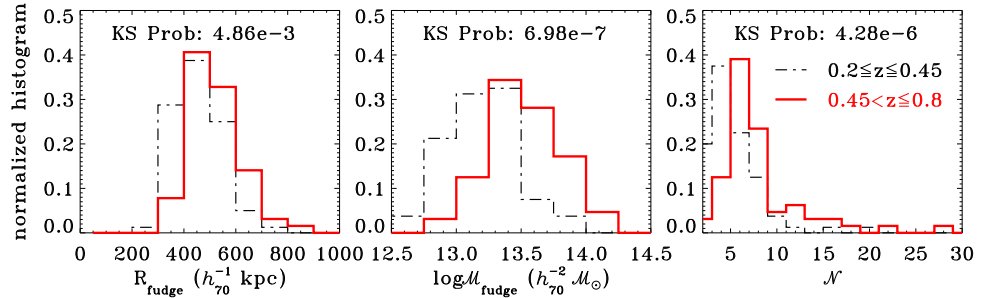


Figure 5.4: Comparison of the global properties of groups in the $0.2 \leq z \leq 0.45$ (black dot-dashed line) and $0.45 < z \leq 0.8$ (red solid line) redshift bin. From left to right we compare R_{fudge} (the estimate of the virial radius), $\log \mathcal{M}_{fudge}$ (the estimate of the mass of the group), both fudge quantities are calibrated with the mocks as defined in Knobel et al. (2009)), and \mathcal{N} , as defined in Sect. 5.2.

is a lower limit for the real trend present in 3-D. Viceversa in the external regions of groups, the contamination by field galaxies, on the mean bluer and less-massive than group galaxies, will tend to introduce spurious segregation trends, and we need to account carefully for them.

5.4 Low-z and High-z Stacked-Groups

For each of the two redshift bins defined in Sect. 5.2, $0.2 \leq z \leq 0.45$ and $0.45 < z \leq 0.8$, we proceeded to build the corresponding SG. Notice that while for centering purposes we used all spec-z and phot-z galaxies available in our group catalog, irrespective of their mass and B-band rest-frame luminosity, for our analysis we will use only galaxies within the mass volume-limited samples as defined in Tab. 5.1.

Before moving to a detailed study of the group member galaxies properties, it is interesting to compare the global properties of groups in low and high redshift bins, to highlight any redshift dependent trend in the groups sample we will use in our science analysis.

In Fig. 5.4 we compare, from left to right, R_{fudge} - the virial radius estimate (Knobel et al. 2011), \mathcal{M}_{fudge} - the mass of the group calibrated with the mocks as in Knobel et al. (2009), and the group richness, \mathcal{N} , as defined in Sect. 5.2, for low (black dot-dashed line) and high (red solid line) redshift galaxy groups. The KS test always rejects, with more than 99.99% confidence, the hypothesis that properties of low and

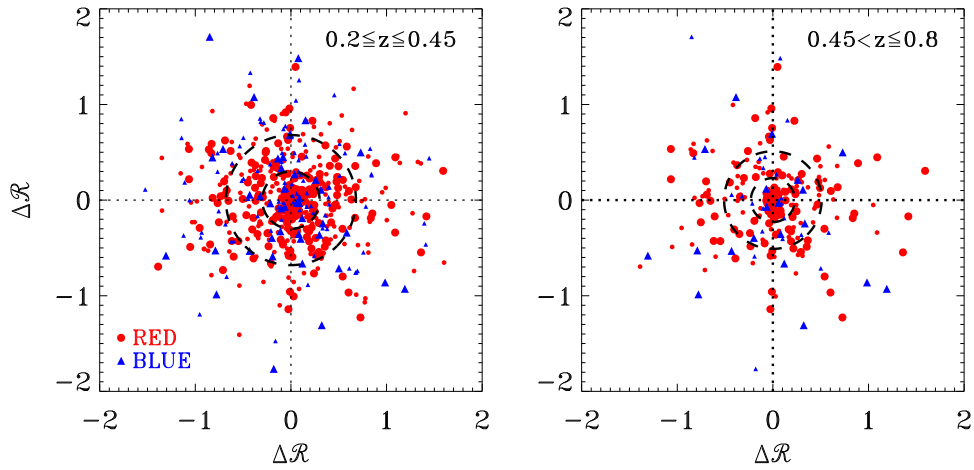


Figure 5.5: Sky distribution of the galaxies belonging to the low-z (left) and high-z (right) composite group. Ra-dec positions are expressed in terms of the rescaled distances \mathcal{R} . Points are colored according to the $(U - B)$ colors of the galaxies, while points dimensions are scaled according to the masses of the galaxies. As a reference we draw dashed circles corresponding to the different central/intermediate/external region limits in each composite group.

5 The Stacked Group

Table 5.2: Radial range explored in the three **SG** regions. All distances \mathcal{R} are normalized to R_{fudge} .

Redshift	1 st region		2 nd region		3 rd region	
	range	\mathcal{R}_{median}	range	\mathcal{R}_{median}	range	\mathcal{R}_{median}
$0.2 \leq z \leq 0.45$	$\mathcal{R} \leq 0.30$	0.15	$0.30 < \mathcal{R} \leq 0.68$	0.47	$\mathcal{R} > 0.68$	0.94
$0.45 < z \leq 0.8$	$\mathcal{R} \leq 0.23$	0.13	$0.23 < \mathcal{R} \leq 0.51$	0.37	$\mathcal{R} > 0.51$	0.74

high redshift groups are drawn from the same distribution. In the low redshift bin on the mean we deal with smaller, less massive and poorer groups than those in the highest redshift bin. This is not an unexpected result given that zCOSMOS is a flux limited survey and therefore the observed population of both galaxies and groups varies with increasing redshift. As a consequence the group detection works only on progressively brighter/more massive galaxies moving to higher redshifts. We shall need to take into account these differences when discussing our results. We define a subset of richer groups for the low redshift bin using richness \mathcal{N} , defined for this bin as the number of member galaxies surviving the evolving magnitude cut off: $M_{cut-off} = M_{Bev}^* + 2.1$ (see Sect. left panel of Fig. 5.3). We adopted a separation of $\mathcal{N} \leq (/ >)12$ to distinguish between poor(/rich) groups, a value roughly corresponding to $M_{fudge} \leq (/ >)13.3$, so that rich low- z groups are virtually indistinguishable in mass distribution from the high redshift sample. In fact while a KS test comparing the distributions of M_{fudge} of poor and rich groups defined this way rejects with more than 99.99% confidence the hypothesis that they are drawn from the same distribution, the KS test comparing distributions of M_{fudge} of rich low- z groups and of high- z groups does not reveal, on the contrary, any significant difference between the two.

To explore how galaxy population properties change as a function of group-centric distance we first sorted **SG** galaxies into increasing scaled distances from **SG** center and then divided their distribution into three equipopulated bins corresponding to inner, intermediate, and peripheral **SG** regions.

In Tab. 5.2 we list the exact radial ranges of each of these three regions, all values are normalized to R_{fudge} . The corresponding three median distances are $\mathcal{R} \sim 0.15$, $\mathcal{R} \sim 0.4$ and $\mathcal{R} \sim 0.85$ respectively, therefore these regions can be thought as the group inner core, intermediate, and more external/in-fall region.

Given that the median R_{fudge} is $\sim 500 h_{70}^{-1} Kpc$ in both redshift bins, the inner region extends typically up to $\sim 150 h_{70}^{-1} Kpc$. Since the VW center is on the average only $\sim 40 h_{70}^{-1} Kpc$ away from the group fiducial center (see Sect. 4.2.2), our error in centering is negligible with respect to the median inner region size, and should

not have a significant impact when exploring the group-centric dependence of galaxy properties.

The sky distribution of galaxies belonging to the low- z (left) and high- z (right) composite group is shown in Fig. 5.5. Points are coded according to the $(U - B)$ colors of the galaxies, while points dimensions are scaled according to galaxy masses. As a reference we draw dashed circles corresponding to the division between the different regions in each composite group. We note that the overall shape of the composite group has a well defined peak corresponding to the center, while the projected density decreases as we move from the center to the outskirts. A visual inspection of the galaxies sky distribution already shows rough differences in masses and colors depending on the area we explore. In the next Section we proceed to extensively analyze these trends and their dependence on intrinsic galaxy/group properties, properly accounting for possible field contamination effects.

5.5 Conclusions

In this chapter, I described the results obtained after applying to the $20K$ the algorithms I developed. The improvement in terms of group membership are in good agreement with the expectations from the tests I made on mock catalogs. I compared the global properties e.g., the position and the mass rank, of the $20K$ RCGs and of the RCGs from simulations. I highlighted the presence of a significant percentage of RCG that are not the most massive and that are not centered. This is in agreement with values provided by simulations only after taking into account the errors in the galaxy stellar mass estimates.

I explained the construction of a volume-mass limited sample which is unavoidable in order to correctly study color trends. This kind of sample enable us to disentangle true environmental effects from mass-driven ones and I will use it in our analysis in Chapt. 6 and 7

I explicated the adopted method to build two stacked groups: one at low redshift ($0.2 \leq z \leq 0.45$) and the other at high redshift ($0.45 < z \leq 0.8$). I compared the global properties of the two stacked groups and I selected a subset of groups which show the same global properties across the whole redshift range. This way I obtained a sample which enable a fair comparison of the results of our analysis, see Chapt. 6.

6 Segregation effects in the zCOSMOS 20k groups: colors and masses

In this Chapter I will present the new results I have obtained exploring the group-centric dependence of galaxy colors and masses, i.e., the segregation effects in the zCOSMOS 20k group catalog. I will start the analysis by exploring how galaxy colors are affected by group environment, irrespective of galaxy position within the group (see Sect. 6.1). I will then move to investigate the presence of color segregation within group environment (Sect. 6.2), and if the effect of the group environment extends to scales somewhat larger than those of the group size itself (see Sect. 6.3). Thank to the high statistic of the 20K I will also be able to investigate if and how observed trends depend on both group richness and on galaxy stellar mass (see Sect. 6.4). Finally I will search for evidence of mass segregation inside groups and how it might depend on group richness and affect observed mass trends (see Sect. 6.5).

6.1 F_{blue} and galaxy stellar masses in groups vs field

The cumulative galaxy stellar mass distributions of the mass-complete group and field samples are shown in top panels of Fig. 6.1, red solid and cyan dot-dashed lines respectively, left(/right) panels refers to the low(/high) redshift bin. The KS test rejects the hypothesis that group and field galaxy mass distributions are drawn from the same population with more than 99.99% confidence for both the redshift bins. Group environment hosts preferentially more massive galaxies than the field one, confirming well known literature results (Iovino et al. 2010; Kovač et al. 2010b; Bolzonella et al. 2010).

As a consequence, to explore the presence of color trends as a function of environment we need to separate the joint effect of mass and environment and to perform the analysis in narrow mass bins of galaxy stellar mass. We adopted a galaxy stellar mass bin of 0.4 dex, that is approximately twice our error in estimating galaxy stellar masses

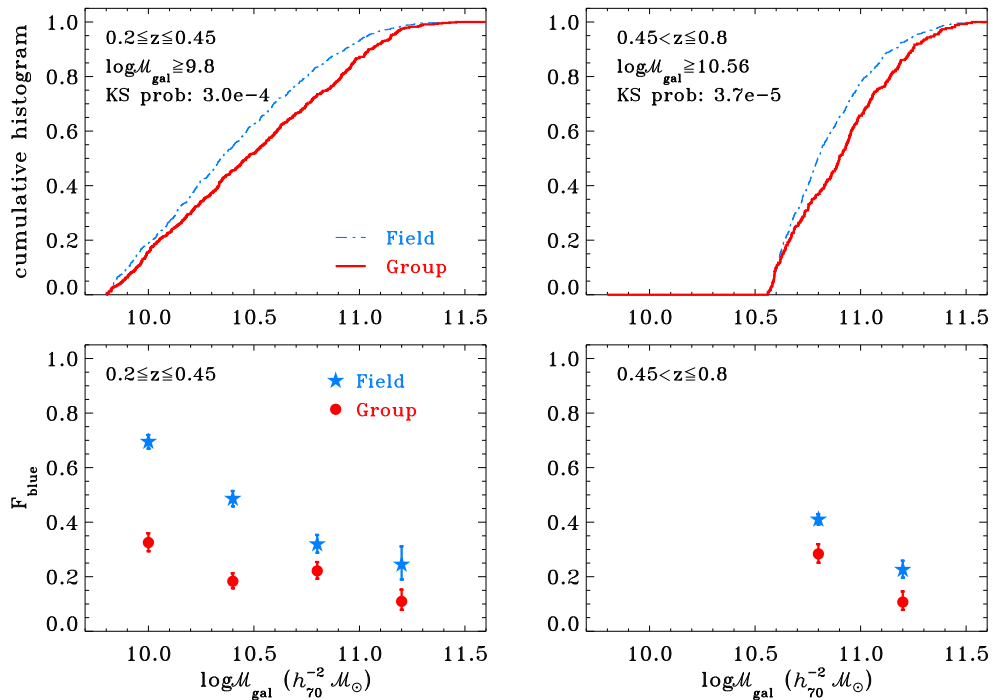


Figure 6.1: *Top panels:* cumulative galaxy stellar mass distribution of the mass-complete group and field samples in red and cyan colors respectively. *Bottom panels:* F_{blue} at fixed galaxy mass in both groups (red circles) and field (cyan stars). *Left panels* always refer to the low redshift bin, while *right panels* refer to the high redshift one. We used galaxy mass bins 0.4 dex wide.

(Pozzetti et al. 2010). Bottom panels of Fig. 6.1 show F_{blue} at fixed galaxy stellar mass in groups (red circles) and field (cyan stars), while Tab. 6.1 lists in detail the F_{blue} values and their errors. Both at high and low redshift, the blue fraction increases when moving towards less massive galaxies. F_{blue} is always higher in field than in group, a difference that decreases moving to more massive galaxies. The most massive galaxies ($\log(\mathcal{M}_{\text{gal}}/\mathcal{M}_{\odot}) > 11.0$) do not show any significant F_{blue} evolution with redshift within the error bars. For the galaxies with $10.6 \leq \log(\mathcal{M}_{\text{gal}}/\mathcal{M}_{\odot}) \leq 11.0$, F_{blue} decreases for both group and field environment when moving from high to low redshift,

Notice that, on average, groups in the low- z bin are poorer than those in the high- z bin. As we will show later on, see Sect. 6.4, F_{blue} depends on the group richness, F_{blue} being lower in richer groups. As a consequence the decrease of F_{blue} across the explored

6.1 F_{blue} and galaxy stellar masses in groups vs field

redshift range for the sample of group galaxies should be even more significant.

Table 6.1: Observed blue fractions in groups and field for different galaxy stellar mass bins.

Sample $0.2 \leq z \leq 0.45$	group	field
$9.8 \leq \log(\mathcal{M}_{gal}/\mathcal{M}_{\odot}) \leq 10.2$	$0.33_{-0.03}^{+0.03}$	$0.70_{-0.03}^{+0.03}$
$10.2 \leq \log(\mathcal{M}_{gal}/\mathcal{M}_{\odot}) \leq 10.6$	$0.18_{-0.03}^{+0.03}$	$0.49_{-0.03}^{+0.03}$
$10.6 \leq \log(\mathcal{M}_{gal}/\mathcal{M}_{\odot}) \leq 11.0$	$0.22_{-0.03}^{+0.03}$	$0.32_{-0.03}^{+0.03}$
$11.0 \leq \log(\mathcal{M}_{gal}/\mathcal{M}_{\odot}) \leq 11.4$	$0.11_{-0.03}^{+0.04}$	$0.25_{-0.06}^{+0.07}$
Sample $0.45 < z \leq 0.8$	group	field
$10.6 \leq \log(\mathcal{M}_{gal}/\mathcal{M}_{\odot}) \leq 11.0$	$0.28_{-0.03}^{+0.04}$	$0.41_{-0.02}^{+0.02}$
$11.0 \leq \log(\mathcal{M}_{gal}/\mathcal{M}_{\odot}) \leq 11.4$	$0.11_{-0.03}^{+0.04}$	$0.23_{-0.03}^{+0.03}$

At fixed galaxy stellar mass, the migration to the red sequence happens earlier in the groups and later in the field, suggesting the presence of physical mechanisms able to remove gas causing the earlier quenching of galaxies in groups. We remind the reader that any contamination of the group sample by field galaxies and viceversa, for which we are not applying any correction, will only render less prominent the observed trends. The real, corrected, trends therefore would be even more significant. This result is in excellent agreement with our previous zCOSMOS results on groups (Iovino et al. 2010; Bolzonella et al. 2010; Peng et al. 2010).

The questions we will address in the following sections are: do the group member galaxies all share the same F_{blue} value irrespective of their position within the group? Do the galaxies located in the central region of groups share the same mass distribution than the galaxies located in the groups outskirts? Ideally the first question is better addressed in narrow bins of galaxy stellar mass, to avoid the mass-color degeneracy. However, even with such a data set as the 20K, we are still limited by small number statistic when splitting our sample according to distances from group center and therefore in the next section we will start our analysis working in cumulative mass

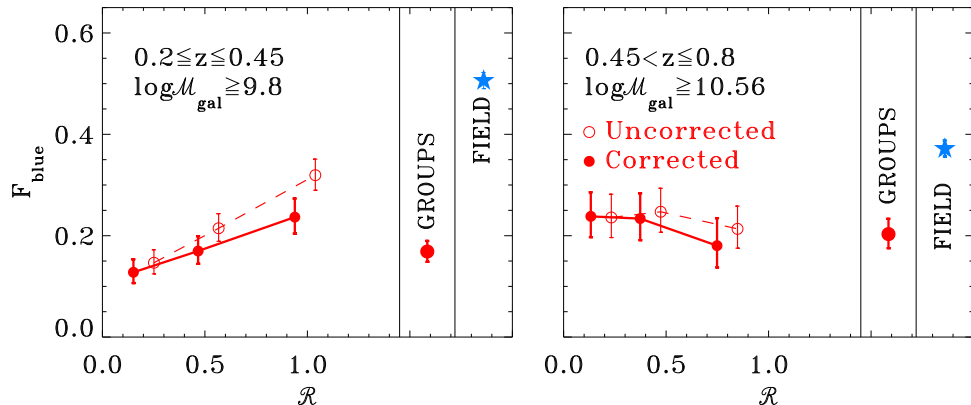


Figure 6.2: SG blue fraction as a function of the group-centric distance. Left/(right) panels refer to the low/(high) redshift bin and mass limits are $\mathcal{M}_{\text{cut-off}} = 9.8/(\mathcal{M}_{\text{cut-off}} = 10.56)$. Open circles refer to observed F_{blue} while filled ones to corrected F_{blue} , i.e., taking into account interlopers contamination (see text for details). The points refer to the three regions: inner core, intermediate, and more external/infall region. Corrected blue fractions values are displayed at the median distance of each region, while observed blue fractions are offset for clarity’s sake. As a reference we plot the fraction of the blue field galaxies (cyan star) and the mean corrected blue fraction in groups (big red circle).

ranges.

6.2 Color segregation: F_{blue} as a function of the group-centric distance

To explore color segregation we measured $F_{\text{blue},\text{obs}}^{\text{GR}}$, the observed fraction of blue group member galaxies, in each of the three SG regions defined in Sect. 5.4. We used the formula:

$$F_{\text{blue},\text{obs}}^{\text{GR}} = \frac{N_{\text{blue},\text{obs}}^{\text{GR}}}{N_{\text{tot},\text{obs}}^{\text{GR}}} \quad (6.1)$$

where the index GR refers to group galaxies. However in order to establish the reliability of any observed changing mix of galaxy colors at different radial distances from the group center, it is essential to properly account for the presence of field galaxy

6.2 Color segregation: F_{blue} as a function of the group-centric distance

contaminants and their (changing) relative contribution at different distances from the group center, as the field population has a higher F_{blue} than the group one. We thus need to estimate the corrected group fraction of blue galaxies, F_{blue}^{GR} :

$$F_{\text{blue}}^{GR} = \frac{N_{\text{blue}}^{GR}}{N_{\text{tot}}^{GR}} = \frac{N_{\text{blue},\text{obs}}^{GR} - N_{\text{blue}}^{INT}}{N_{\text{tot},\text{obs}}^{GR} - N_{\text{tot}}^{INT}} \quad (6.2)$$

that is the corrected ratio of the blue member galaxies to the total number of member galaxies, after excluding the percentage of interlopers - indicated by the index INT - entering in the observed list of group members because of group detection algorithm failures.

If \mathcal{PI} is the estimated percentage of interlopers defined in Sect. 4.1.2, we can obtain N_{tot}^{INT} for each group region by $N_{\text{tot}}^{INT} = \mathcal{PI} \times N_{\text{tot},\text{obs}}^{GR} = \mathcal{PI} \times (N_{\text{tot}}^{GR} + N_{\text{tot}}^{INT})$. The value of N_{blue}^{INT} can simply be estimated as $N_{\text{blue}}^{INT} = F_{\text{blue}}^{FIELD} \times N_{\text{tot}}^{INT}$, where F_{blue}^{FIELD} is the known blue fraction of the field galaxies. This way we take into account the radial trend of interlopers contamination and have all the ingredients to retrieve the corrected values of F_{blue}^{GR} from equation 6.2.

In Fig. 6.2 the left/(right) panel shows the blue fraction as a function of the group-centric distance in the **SG** for the low/(high) redshift bin in the mass-complete sample down to $\mathcal{M}_{\text{cut-off}} = 9.8/(\mathcal{M}_{\text{cut-off}} = 10.56)$. Uncorrected and corrected blue fraction values are indicated with open and filled circles respectively. Corrected blue fractions are displayed at the median normalized \mathcal{R} distance of galaxies in each region, while uncorrected blue fractions are slightly offset for clarity's sake. As a reference we plot the fraction of blue field galaxies (cyan stars) and of the whole group (big red filled circle, corrected values only). Error bars are estimated using the approximate analytical formulas for a binomial distribution provided by Gehrels (1986). In Tab. 6.2 we list the values of observed and corrected F_{blue} for each region and sample considered.

In the low redshift bin, the observed F_{blue}^{GR} raises as the distance from the group center increases (left panel of Fig. 6.2). Though becoming less prominent, this color segregation holds even when correcting for interlopers contamination. Considering the field point, we can see a trend of increasing F_{blue} moving from the inner core of groups to their outskirts and further away to the field.

The difference between F_{blue}^{GR} in the inner core and that in the outskirts is $1.7\sigma_{1st-3nd}$, where $\sigma_{1st-3nd}$ is the sum in quadrature of σ_{1st} and σ_{3rd} , the error of the fraction of blue galaxies in the inner core and outskirts respectively. The difference between F_{blue}^{GR} in the outskirts and F_{blue}^{FIELD} is $7\sigma_{3nd-field}$. Entering the group potential well has a significant influence in changing galaxy colors, but the most relevant difference is

Table 6.2: Blue fractions in groups, observed and corrected for field contamination. Last two columns list total group and field values.

Sample $0.2 \leq z \leq 0.45$	1 st region		2 nd region		3 rd region		group	field
	obs	corr	obs	corr	obs	corr	corr	
$\log(\mathcal{M}_{gal}/\mathcal{M}_{\odot}) \geq 9.8$	$0.15^{+0.03}_{-0.02}$	$0.13^{+0.03}_{-0.02}$	$0.22^{+0.03}_{-0.03}$	$0.17^{+0.03}_{-0.03}$	$0.32^{+0.03}_{-0.03}$	$0.24^{+0.04}_{-0.03}$	$0.17^{+0.02}_{-0.02}$	$0.51^{+0.02}_{-0.02}$
$\log(\mathcal{M}_{gal}/\mathcal{M}_{\odot}) \geq 10.56$	$0.11^{+0.04}_{-0.03}$	$0.10^{+0.04}_{-0.03}$	$0.16^{+0.04}_{-0.03}$	$0.13^{+0.05}_{-0.03}$	$0.25^{+0.05}_{-0.04}$	$0.22^{+0.06}_{-0.05}$	$0.14^{+0.03}_{-0.03}$	$0.30^{+0.03}_{-0.03}$
$\log(\mathcal{M}_{gal}/\mathcal{M}_{\odot}) \geq 9.8$ & $5 \leq \mathcal{N} \leq 12$	$0.18^{+0.04}_{-0.04}$	$0.16^{+0.04}_{-0.04}$	$0.20^{+0.04}_{-0.04}$	$0.15^{+0.04}_{-0.04}$	$0.43^{+0.05}_{-0.05}$	$0.39^{+0.06}_{-0.06}$	$0.22^{+0.03}_{-0.03}$	$0.51^{+0.02}_{-0.02}$
$\log(\mathcal{M}_{gal}/\mathcal{M}_{\odot}) \geq 9.8$ & $\mathcal{N} > 12$	$0.14^{+0.04}_{-0.03}$	$0.13^{+0.04}_{-0.03}$	$0.23^{+0.04}_{-0.04}$	$0.19^{+0.04}_{-0.04}$	$0.28^{+0.05}_{-0.04}$	$0.18^{+0.05}_{-0.04}$	$0.16^{+0.03}_{-0.03}$	$0.51^{+0.02}_{-0.02}$
Sample $0.45 < z \leq 0.8$	1 st region		2 nd region		3 rd region		group	field
	obs	corr	obs	corr	obs	corr		
$\log(\mathcal{M}_{gal}/\mathcal{M}_{\odot}) \geq 10.56$	$0.24^{+0.05}_{-0.04}$	$0.23^{+0.05}_{-0.04}$	$0.25^{+0.05}_{-0.04}$	$0.23^{+0.05}_{-0.04}$	$0.21^{+0.05}_{-0.04}$	$0.18^{+0.05}_{-0.04}$	$0.20^{+0.03}_{-0.03}$	$0.37^{+0.02}_{-0.02}$

between F_{blue}^{GR} in the inner core and F_{blue}^{FIELD} : $11\sigma_{1^{st}-field}$.

Moving to the highest redshift bin, we do not detect any significant color radial trend within the **SG**, while we still detect a significant difference with respect to the field galaxy population (right panel of Fig. 6.2). The group blue fraction is at a constant value of $F_{\text{blue}}^{GR} \sim 0.1$, a value 3.9σ lower than the corresponding blue fraction in the field sample. Both values of F_{blue} for group and field are significantly lower in this redshift bin than those obtained in the low redshift been discussed previously. In order to understand this result we need to remember that we applied a higher galaxy stellar mass cut-off in the high-redshift bin: $\log(\mathcal{M}_{\text{gal}}) \geq 10.56$, thus we are observing galaxies more massive than in the low redshift bin, this being the obvious cause for the global lowering of the values of F_{blue} for the field and the groups population. A further factor to consider is that we are observing groups that are on the mean more massive than their low redshift counterparts (see Fig. 5.4).

Before moving to investigate in detail how our findings depend on group richness and galaxy stellar masses in Sect. 6.4, we will explore in the next Section whether the observed differences between group and field stop at group boundaries, or if there is a continuous trend of increasing F_{blue} in the closest proximity of groups.

6.3 Large scale trend

The physical scale, in terms of density or projected distances, over which environment begins to set up the well known correlations with galaxy star formation rates, colors and morphologies is a question still open (Kauffmann et al. 2004; Balogh et al. 2004; Blanton et al. 2006). We explored the possible presence of large-scale trends of F_{blue}^{FIELD} , with the aim of detecting for the galaxy population located in the closest proximity of our groups e.g., colors redder than those of field sample. As discussed in Sect. 2.1.5 we defined a sample of field galaxies ideally not affected by group environment, and a sample of so called *near-field* galaxies, i.e., galaxies located in the closest proximity of groups.

In the low redshift bin, where the sample size enables us to do such an analysis, we split the *near-field* into subsets of 3 nested rings of increasing projected radial distances from **SG** center and defined as follows: $\mathcal{R} \leq 2.0$, $\mathcal{R} \leq 3.0$ and $\mathcal{R} \leq 4.0$, and measured F_{blue} for each of them. These values are plotted in Fig. 6.3 with empty stars, and display a regular increase moving away from the group center, progressively nearing the value obtained for the field sample. However this apparent continuous trend, extending beyond group size, disappears when excluding from each of the points shown in Fig. 6.3 field galaxies with projected radial distances $\mathcal{R} \leq 2.0$ (filled stars), suggesting

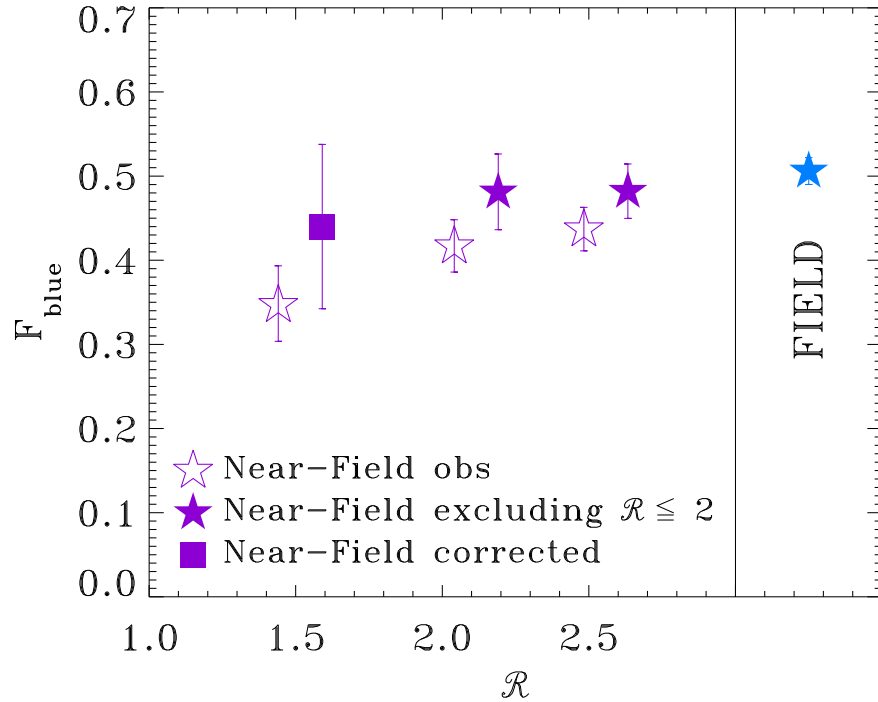


Figure 6.3: F_{blue} of *near-field* (violet empty stars) as a function of increasing projected radial distances from groups in the low redshift bin: $\mathcal{R} \leq 2.0$, $\mathcal{R} \leq 3.0$ and $\mathcal{R} \leq 4.0$. Violet filled stars show F_{blue} of *near field* after excluding *near-field* galaxies with projected radial distances $\mathcal{R} \leq 2.0$. The filled square shows F_{blue} for the first *near-field* annulus, after correcting for the 15% spectroscopic galaxy-group incompleteness, see text for details. Observed F_{blue} values are displayed at the median distance of each *near-field* region, while corrected ones are slightly offset for clarity's sake. As a reference we display the F_{blue} of the field with a cyan star.

that the trend in question is caused by contamination from missed group members, predominantly located in the nearest neighborhood of groups.

The same result can be obtained correcting the values of the first *near-field* ring with a procedure similar to that used for group galaxies. The galaxy success rate of the group finding algorithm turns into a spectroscopic incompleteness on galaxy-group basis of 15%, as estimated in Knobel et al. (2009). Correcting for such a percentage of contamination by group galaxies is enough to raise the observed value of $F_{\text{blue}}^{\text{FIELD}}$ in the first *near-field* annulus to that of the field, as shown by the filled square in Fig. 6.3.

This analysis confirms that the physical scale on which the environment plays its role coincides with the group physical scales, in agreement with Kauffmann et al. (2004); Blanton et al. (2006); Wilman et al. (2010). It therefore suggests that there is no transition region from field to group domain and field galaxies start getting affected by the group environment when they enter it.

Interestingly it also implies that the values we estimated for the incompleteness of our group catalog is realistic, as it produces, once the corresponding correction is applied, values of F_{blue} for the first *near-field* annulus that are in good agreement with field values.

6.4 Galaxy stellar mass and group richness dependence

In Sect. 6.2 we have shown that low and high- z group galaxies display different radial color trends. However we also noticed two important differences: the galaxy stellar mass cut-off adopted ($\log(\mathcal{M}_{\text{gal}}/\mathcal{M}_{\odot}) \geq 9.8$ to be compared to $\log(\mathcal{M}_{\text{gal}}/\mathcal{M}_{\odot}) \geq 10.56$), and the different range in group richness spanned in these two redshift bins. It is therefore interesting to investigate how the observed radial trends of F_{blue} depend on these two quantities. We split the low- z group sample according to richness \mathcal{N} defined as the number of member galaxies surviving after applying the evolving magnitude cut off $M_{\text{cut-off}} = M_{\text{Ev}}^* + 2.1$, adopting a separation of $\mathcal{N} \leq (/ >)12$ to distinguish between poor(/rich) groups. We then split the total galaxy sample for each of the two rich and poor SG into two bins of galaxy stellar mass: galaxies with stellar masses $9.8 \leq \log(\mathcal{M}_{\text{cut-off}}) \leq 10.56$ and $\log(\mathcal{M}_{\text{cut-off}}) \geq 10.56$.

In Fig. 6.4 we show how F_{blue} varies for the sub-samples defined this way (from now onwards we display only corrected values). Poor(/rich) groups are on the left(/right) panel respectively and triangles refer to lower stellar mass bin, squares to higher stellar mass bin, and filled circles to the total mass volume-limited sample. As a reference and with the same symbols for each stellar mass bin, we plot the values of F_{blue} for

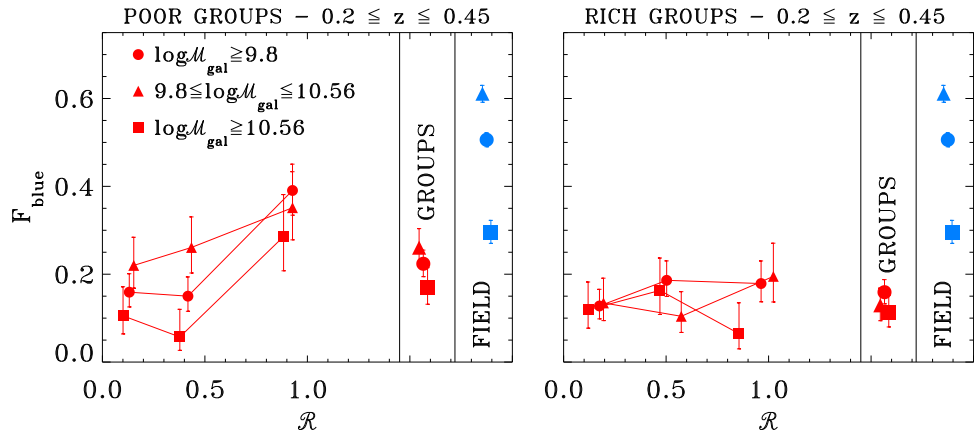


Figure 6.4: Corrected blue fraction as a function of the group-centric distance in the low- z poor groups (left) and rich groups (right). We define poor(/rich) groups as those with number of member galaxies \leq ($>$) 12 after applying the evolving magnitude cut off $M_{\text{cut-off}} = M_{B_{\text{ev}}}^* + 2.1$ (see Fig. 5.3). The mass bins adopted are indicated in the legenda. Corrected blue fractions are displayed at the median of the distances from the center for galaxies in each region. As a reference we also plot the fraction of the blue field galaxies and the mean corrected blue fraction in groups.

field galaxies and those for the total poor and rich group galaxies sample considered.

The value of F_{blue} increases moving from higher to lower galaxy stellar masses, for each environment considered (see also Sect. 6.1). However there is a further trend superimposed to this one: at fixed stellar mass the mean F_{blue} is higher in poor groups than in rich ones, confirming previous tentative results (see Margoniner et al. 2001; Gerke et al. 2007; Iovino et al. 2010, and references therein).

As far as radial trends are concerned Fig. 6.4 shows that only for poor groups bluer galaxies are preferentially located in the group outskirts. No such trend is observed for richer groups. For poor groups, galaxies with lower stellar mass show a continuous trend of increasing F_{blue} , whereas F_{blue} for most massive galaxies increases only in the outermost group region. Rich groups do not show any obvious radial trend.

Thus poor groups display higher F_{blue} values for their member galaxies than richer groups and stronger radial trends at fixed galaxy stellar mass than richer groups. The observed galaxy color radial trends become more evident moving from richer to poorer groups and moving from higher to lower galaxy stellar masses.

We can therefore better explain the observed differences between low and the high- z

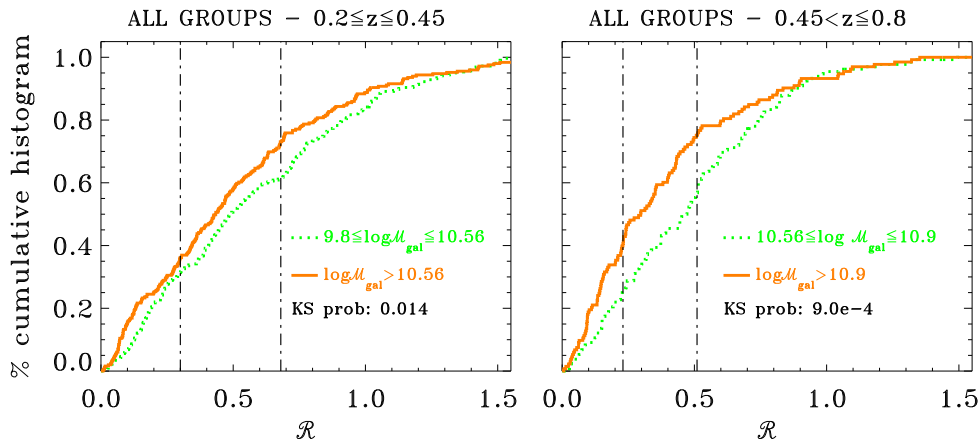


Figure 6.5: Cumulative radial distribution of the galaxies belonging to each mass bin for both the lowest (left) and highest (right) redshift bin. We show the most massive galaxies with orange solid line and the less massive galaxies with green dotted line. As a reference we draw the limits of the 1st and 2nd regions with a dot-dashed black line.

groups trends discussed in Sect. 6.2 as due to the different cut-off in galaxy stellar masses and to the different group richness ranges observed in the two different redshift bins.

It is somewhat expected that at high- z the massive groups we explore do not display any radial trend for the massive galaxies shown in plot Fig. 6.2.

We will now proceed to explore if the differences observed in radial trends between poor groups and rich groups relate to the possible presence of galaxy stellar mass segregation within groups, a factor that could be important in creating and/or enhancing observed color trends.

6.5 Mass segregation

Goal of this Section is to check for the presence of mass segregation within our group sample, to clarify if any of galaxy colors radial trends we observed are simply the reflection of the galaxy colors and stellar mass correlation coupled with varying galaxy stellar mass functions moving from central to peripheral group regions.

We split the mass-complete galaxy sample into two stellar mass bins: at low redshift the stellar mass limits chosen are: $9.8 \leq \log(\mathcal{M}_{gal}/\mathcal{M}_{\odot}) \leq 10.56$ and $\log(\mathcal{M}_{gal}/\mathcal{M}_{\odot}) > 10.56$, with a total of 320/(251) galaxies in the lowest/(highest) mass bin. At high

redshift the stellar mass limits chosen are: $10.56 \leq \log(\mathcal{M}_{gal}/\mathcal{M}_{\odot}) \leq 10.9$ and $\log(\mathcal{M}_{gal}/\mathcal{M}_{\odot}) > 10.9$; in this case there are 132(/133) galaxies in the lowest(/highest) mass bin. In the left(/right) panel of Fig. 6.5 we show the cumulative radial distribution of the galaxies belonging to these bins for the low(/high) redshift SGs. The dotted line always refers to the lowest stellar mass bin, while the solid line refers to the highest stellar mass bin. As a reference a dot-dashed black line indicates the boundaries of the different group regions defined in Sect. 5.4. In both redshift bins the most massive galaxies populate preferentially the innermost regions, while the less massive galaxies prefer the outer ones. A KS test confirms with confidence higher than 98.6%(/99.99%) the existence of a mass segregation for the low(/high) redshift bin.

Also in this case we explored group richness dependency of the mass segregation by repeating the same radial analysis but dividing the low-z bin groups into poor and rich sub-samples (see Sect. 5.4 for definitions). The cumulative radial distributions of galaxies are plotted in Fig. 6.6, for poor, left panel, and rich groups, right panel. In both panels dotted lines refer to galaxies with $9.8 \leq \log(\mathcal{M}_{gal}/\mathcal{M}_{\odot}) \leq 10.56$, while the solid lines to galaxies at $\log(\mathcal{M}_{gal}/\mathcal{M}_{\odot}) > 10.56$. For poor groups there is no significant mass segregation as the KS test results are consistent with the hypothesis that the radial distribution of galaxies from the two mass bins are drawn from the same distribution. Viceversa, galaxies located in rich groups display a significant mass segregation, with most massive galaxies being closer to the SG center than the less massive ones. In this case the KS test rejects with more than 99.3% confidence the hypothesis that the radial distribution of galaxies from the two mass bins are drawn from the same distribution.

We performed KS test comparing the galaxy stellar mass distribution in different SG regions and field galaxies. For low-z rich and high-z groups there is no significant difference between field galaxies and the outermost SG region, while the inner/intermediate regions display a significant difference with respect to the field, in agreement with their observed galaxy stellar mass segregation. For low-z, poor groups the galaxy stellar mass distribution is only marginally different from that of field galaxies (a $\sim 2.5\sigma$ result), and this outcome holds irrespective of group-centric distance, in agreement with the absence of galaxy stellar mass segregation in these groups. In Tab. 6.3 we detail all the numerical results of the various KS tests.

One could argue that the mass segregation we are detecting within rich low-z groups and high-z groups raises from interlopers contamination. On the mean, interlopers would preferentially populate group peripheral regions, where we actually observe a galaxy stellar mass distribution that resembles more that of field galaxies, thus producing the observed stellar galaxy mass distribution radial trends. We used a

Table 6.3: KS test probabilities that the mass distribution of the galaxies in each group region and that of the field sample of galaxies are drawn from the same distribution. Redshift ranges and group richness are indicated in the Sample column.

Sample	1 st gr region vs field	2 nd gr region vs field	3 rd gr region vs field
$0.2 \leq z \leq 0.45 \ \& \ \log(\mathcal{M}_{gal}/\mathcal{M}_{\odot}) \geq 9.8$	5.7×10^{-4}	1.1×10^{-4}	0.176
$0.2 \leq z \leq 0.45 \ \& \ \log(\mathcal{M}_{gal}/\mathcal{M}_{\odot}) \geq 9.8 \ \& \ \mathcal{N} \leq 12$	0.012	0.044	0.067
$0.2 \leq z \leq 0.45 \ \& \ \log(\mathcal{M}_{gal}/\mathcal{M}_{\odot}) \geq 9.8 \ \& \ \mathcal{N} > 12$	9.1×10^{-4}	1.3×10^{-3}	0.425
$0.45 < z \leq 0.8 \ \& \ \log(\mathcal{M}_{gal}/\mathcal{M}_{\odot}) \geq 10.56$	6.8×10^{-9}	0.014	0.841

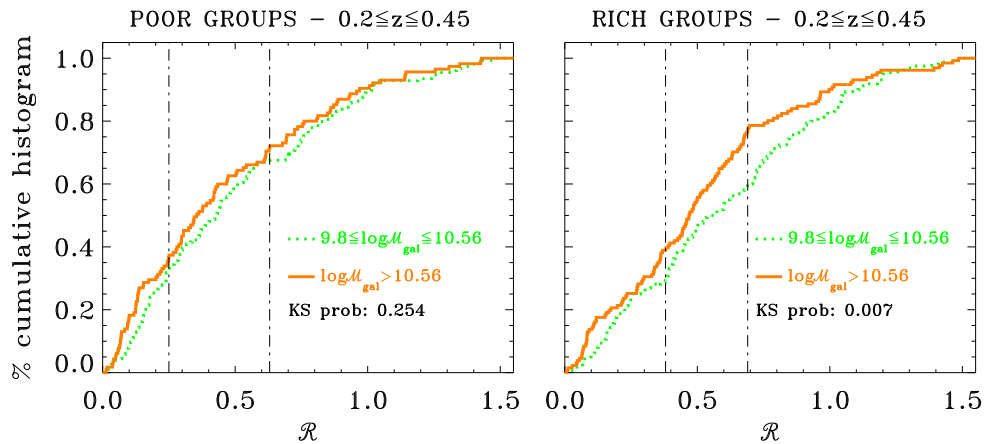


Figure 6.6: Cumulative radial distribution of the galaxies belonging to each mass bin for poor (left) and rich (right) groups in the lowest redshift bin. We show the most massive galaxies with orange solid line and the less massive galaxies with green dotted line. As a reference we draw the limits of the 1st and 2nd regions with a dot-dashed black line.

Monte Carlo technique in order to establish the robustness of our results with respect to such an effect. For each of the two SGs - rich low-z and high-z - we depleted the mass-complete sample of its galaxy members by the estimated interloper fraction in each group region. We used galaxy colors to select the most probable interlopers, so that the galaxies removed had a value of F_{blue} equal to that estimated for field galaxies (see Sect. 6.1). We performed this exercise 1000 times, keeping constant the total number of galaxies (i.e., randomly counting some of the surviving galaxies twice). Each time we estimated the KS test probability that the radial distribution of less and most massive member galaxies were drawn from the same radial distribution.

For rich low-z groups the KS test confirms a mass segregation with a median confidence level of $97.8^{+1.9}_{-5.9}$. For high-z groups, the KS test confirms a mass segregation with a median confidence level of $99.9^{+0.1}_{-1.2}$. In both cases the quoted errors correspond to the lowest and highest quartiles of the KS test probability distribution. We can conclude that at high-z the signal for a genuine and significant radial stellar mass segregation for group galaxies is strong and reliable, while at low-z the observed mass segregation for rich group galaxies is somewhat enhanced by interloper contamination, but, albeit a lower significance, an indication of its existence is still present.

The main result of this Section is therefore that low-z poor groups do not show

significant mass segregation; viceversa low- z rich groups and high- z groups, whose group mass ranges are somewhat similar, display a significant mass segregation in the galaxy stellar mass ranges explored.

As low- z poor groups are those that show a significant color segregation, whereas it is undetected in low- z rich groups and high- z groups (see Sect. 6.4), we conclude that the changing mix of color and masses are unrelated phenomena, possibly originating from different physical mechanisms. In the next Section we will discuss a possible interpretation.

6.6 Migration from blue to red: the effects of group environment

Our analysis has confirmed that stellar mass is an important parameter in the discussion of environmental influence upon galaxy properties and their evolution.

In Sect. 6.1 we have shown that for massive galaxies, $\log(\mathcal{M}_{gal}/\mathcal{M}_{\odot}) \geq 11.0$, the value of F_{blue} does not change moving from field to group galaxies: most massive galaxies are red and *dead* irrespective of the environment they live in, a well known result both at low redshift (see e.g., Hansen et al. 2009; Bamford et al. 2009; Kimm et al. 2009, and references therein) and at intermediate/high redshift (see e.g., Iovino et al. 2010; Kovač et al. 2010b; Peng et al. 2010; McGee et al. 2011b, and references therein).

Below this mass threshold we observe a gradual 'opening up' of the difference between group and field values, so that lower values of F_{blue} are reached earlier in groups than in the field (see Fig. 6.1), confirming results previously obtained using the zCOSMOS 10K sample (see e.g., Iovino et al. 2010; Kovač et al. 2010b; Bolzonella et al. 2010, and references therein) and recent results from the COSMOS survey (George et al. 2011).

In addition to these trends, our analysis has shown that moving to masses below $\log(\mathcal{M}_{gal}/\mathcal{M}_{\odot}) = 11.0$ some subtler differences emerge when observing trends within groups, both as a function of galaxy stellar mass and as a function of group richness. In the following discussion we concentrate on the lower redshift bin of our sample ($0.2 < z < 0.45$), where we were able to study in detail the joined effect of galaxy stellar mass and group richness on galaxy colors. The conclusions we will infer are easy to translate to the higher redshift bin, where we can explore only higher group richnesses and higher galaxy stellar mass ranges (see Sect. 5.4 and 6.4).

For galaxies in the mass range $\log(\mathcal{M}_{gal}/\mathcal{M}_{\odot}) > 10.56$ we do not observe any strong radial trend within groups in the mix of red and blue galaxies (except possibly for

poorer groups of our sample, where the F_{blue} value in the outermost region increases) while we observe a clear difference with respect to F_{blue} for field galaxies.

For galaxies in the lower mass range $9.8 \leq \log(\mathcal{M}_{\text{gal}}/\mathcal{M}_{\odot}) < 10.56$, we observe a significant radial dependence of the mix of red and blue galaxies in poorer groups: red galaxies are preferentially found in the group center. Viceversa for richer group the trend disappears, suggesting that galaxies situated in richer groups (i.e., presumably located in more massive dark matter halos) reach a redder color at earlier redshifts for each fixed galaxy stellar mass.

This picture echoes what is found in the local universe: most massive galaxies do not show a significant color radial trend within groups, while less massive galaxies are those responsible for the progressive blueing of the group member galaxies at intermediate and large group-centric distances. Furthermore these trends are stronger in poorer environments (see e.g., Bamford et al. 2009).

Opposite to this differentiation in terms of a color segregation is the result shown in Fig. 6.6, implying that a significant mass segregation is already set up in rich groups, whereas poor groups display a constant mix of galaxy stellar masses irrespective of the radial distance from group center.

Do these differences provide the mean to better understand how the group environment influences the migration of galaxies from the blue cloud to the red sequence, and to derive estimates for the timescales involved in this process?

In other words does the observed difference in the radial color segregation between richer and poorer groups implies the presence of a different efficiency in the two environments of the mechanisms that cause the transition of a galaxy from the blue cloud to the red sequence? Or could this difference just be due to a different time-scale for the evolution of structures of different mass (different overdensity), such that richer groups formed earlier than poorer ones, so that within them simply there has been more time for environmental effects to act upon group member galaxies?

The observed difference in mass segregation trends provides an important element for us to try and answer this question. It is well known that mass segregation occurs when the exchange of energy among group member galaxies has led most massive galaxies to set in the core of the group while the lighter galaxies, moving at higher velocities, preferentially reside in the outer regions. The setting/absence of mass segregation in a group therefore is a rough indication of the time lapse since group formation and the fact that we do not detect any significant mass segregation in poor groups, suggests that these systems are probably formed later than the richer ones.

In turn this may suggest that the absence of color radial gradient in richer groups at all the masses we explored it is the result of the longer time-scale of these systems, that

is of the longer time available for group environment to influence its member galaxies.

Viceversa poorer groups have not yet been able to set mass segregation, possibly still being in process of forming and accreting field galaxies. Their radial distribution in galaxy stellar masses does therefore not show any strong segregation yet. The radial color trends we observe somewhat bear memory of the still recent accretion history of these groups and suggest that peripheral galaxies have been accreted more recently than those located near the group center.

Interestingly, however, even the galaxies located at the outskirts show redder colors than field galaxies of similar masses. In addition, the simple exercise we performed in Sect. 6.3 shows that there is no continuous trend in color segregation moving from the outskirts of groups towards the nearest field: the physical scale on which the environment plays its role coincides with the group physical scales and the processes that affect galaxy colors starts to operate as soon as galaxies enter the group environment. This result confirms that group environment influences galaxy colors on short time-scales, in agreement with what is suggested by the strong bimodality in color distribution itself: any quenching process that would last more than 1.5-2 Gyrs would erase the observed bimodality of galaxy colors by overpopulating green valley (Balogh et al. 2009; McCarthy et al. 2008; Font et al. 2008).

Our analysis therefore implies that galaxy color transformation and mass segregation originate from different physical processes, whose time-scale, of a few Gyrs, are only slightly different, so that whenever mass segregation is observed, color segregation has been already wiped out and viceversa. Furthermore it suggests that up to a fixed galaxy stellar mass limit, galaxies have already been residing for a longer time within richer groups than poorer groups, while for each group richness considered galaxies of lower masses are presumably those that have more recently entered the group environment (see Fig. 6.4). The physical processes causing the color trends observed in our data could be both starvation and/or galaxy-galaxy collisions/interactions, as both operate with similar time scale. Starvation operates exclusively on the hot-gas reservoir, i.e., there are no indications that it results in an structural transformations (Weinmann et al. 2009).

Viceversa galaxy-galaxy interactions can change morphology, boost specific SFR (sSFR) and quench galaxies, and galaxy-pair fractions are highly environmentally dependent, as denser environments show more pairs (Kampczyk et al. 2011). An analysis including galaxy morphologies and spectral features could help to understand which is the most likely the process between the two, as galaxy-galaxy collisions cause morphological transformations while starvation produces the so called 'strangled' red-spirals population, and we plan to present it in a forthcoming paper.

Our high- z results well fit within the above picture presented for low- z groups. McGee et al. (2009) show that at fixed mass of group/cluster considered the accretion history of member galaxies is remarkably similar and independent of redshift.

Given that the $\mathcal{M}_{\text{fudge}}$ distributions of rich low- z groups and high- z groups do not differ significantly, we would expect a similar behavior in terms of both color and mass segregation.

A KS test shows that the stellar mass distribution of galaxies more massive than $\log(\mathcal{M}_{\text{gal}}/\mathcal{M}_{\odot}) > 10.56$ does not differ significantly for low- z rich groups and high- z groups and in both cases they do not show any color radial trend. Finally both rich low- z groups and high- z groups show evidence of mass segregation, confirming that high- z groups we observed in zCOSMOS do not deviate from the simple picture we proposed.

6.7 Conclusions

In this Chapter I studied in detail how galaxy stellar masses and colors vary as a function of the distance from the group center. The analysis was performed using mass-complete samples to disentangle the obvious galaxy stellar mass/color dependencies.

The main results are:

(i) In the lowest redshift bin explored, the color of most massive galaxies, i.e., $\log(\mathcal{M}_{\text{gal}}/\mathcal{M}_{\odot}) \geq 10.56$, does not display strong group-centric dependence, despite displaying a clear lower blue fraction in groups than in the field. This result holds irrespective of group richness, except possibly for poorer groups of our sample, where however it is driven exclusively by the F_{blue} value in the outermost region. On the contrary for galaxies of lower masses, i.e., $9.8 \leq \log(\mathcal{M}_{\text{gal}}/\mathcal{M}_{\odot}) < 10.56$, there is a radial dependence in the changing mix of red and blue galaxies, red galaxies being found preferentially in the group center. This trend is stronger for poorer groups, while it disappears for richer groups.

(ii) In the highest redshift bin, where only higher galaxy stellar masses and richer groups are available within zCOSMOS survey, the color of observed galaxies, at $\log(\mathcal{M}_{\text{gal}}/\mathcal{M}_{\odot}) \geq 10.56$, does not display strong group-centric dependence, despite still displaying a lower blue fraction in groups than in the field.

(iii) The global F_{blue} for group galaxies shows a clear dependence on group richness: rich group galaxies are redder than poor group galaxies on average;

(iv) Mass segregation shows the opposite behavior with respect to galaxy colors trends: it is visible only in rich groups, while poorer groups have a constant mix of galaxy stellar masses as a function of group-centric distances. Therefore the ob-

served color trends cannot be simply explained as caused from different stellar masses distribution in different group regions.

(v) The physical length-scale on which the environment plays its role coincides with the group physical scales.

The parallel absence(/presence) of color segregation in rich(/poor) groups hints to the fact that nurture effects are still in action in poorer structures, whereas in richer systems have already exhausted their effects, so that all galaxies are uniformly red irrespective of their position within the group (at least down to the galaxy stellar masses we explored). The corresponding presence(/absence) in rich(/poor) groups of mass segregation suggests that richer systems have been in place for time long enough so that more massive galaxies have sank to the group center, something that has yet to happen for the poorer groups, that still keep memory of their more recent growth history.

Both observations suggest a simple scenario where color and mass segregation originates from different physical processes, with similar time-scales, so that whenever mass segregation is observed color segregation has been already wiped out and viceversa.

Lower mass galaxies in poorer groups hold the smoking gun of environmental effects in action superimposed to secular galaxy evolution: these galaxies still display gradually bluer colors moving from group center to more external regions, as a consequence of the still recent accretion history of these groups. Starvation and galaxy-galaxy interactions could both be a reasonable culprit for a mechanism that quenches star formation in groups at a faster rate than in the field. This work has been published in Presotto et al. (2012)

In the next Chapter I will include the preliminary results from galaxy morphologies and composite spectra in order to further investigate the scenario we presented in this Chapter.

7 Segregation effects: further insights from spectra and morphologies

In this Chapter I will further explore the dependence of galaxy properties on group-centric distance by focusing on morphological and spectral segregation effects. This will complete the scenario we proposed in the previous Chapter and it will help us clarify some issues concerning the environmental processes in act. First of all I will briefly describe the morphological classification I adopted, namely the one provided by the ZEST code. For the spectral analysis I will obviously rely only on the galaxies with available spectroscopic redshift of each of the SGs, introduced in Sect. 5.4. To ensure a high statistic and a good signal to noise ratio, I will stack the spectra of galaxies that share the same properties, e.g., spectral type, color, mass, and morphology. I will explain the procedure I developed to stack the spectra, the adopted method to perform template fitting of the stacked spectra, and the measurement of the emission lines. Finally, I will present the preliminary results on morphological and spectral segregation effects in the zCOSMOS group sample.

7.1 Morphologies

As mentioned in Chapt. 2, zCOSMOS is based on HST-ACS observations. ACS imaging enables to derive robust structural parameters and to obtain a reliable morphological classification for all galaxies down to about $I_{AB} = 24$ (well below the flux limit of the $20K$).

Here we used the structural parameters and morphological classification based on the Zurich Estimator of Structural Types (ZEST) and presented in Scarlata et al. (2007). The ZEST classification scheme is based on a principal component analysis of five non-parametric diagnostics of galaxy structure: asymmetry A , concentration C , Gini coefficient G , the second-order moment of the brightest 20% of galaxy pixels $M20$, and the ellipticity (see Scarlata et al. 2007, for details on their definition).

The principal component analysis transform this set of variables into a new set of orthogonal variables, PC_i , where i runs from 1 to 5. The PCs are a linear combination

Table 7.1: The ZEST Classification Scheme as in Scarlata et al. (2007).

Parameter	Type 1 Elliptical Galaxies	Type 2 Disk Galaxies	Type 3 Irregular Galaxies
Bulgeness		From 0 (massive bulge) to 3 (bulgeless disk)	
Elongation	From 0 to 3 (edge on)	From 0 (face on) to 3 (edge on)	
Irregularity	From 0 to 2 (highly irregular)		
Clumpiness	From 0 (smooth) to 3 (very clumpy)	From 0 (smooth) to 3 (very clumpy)	

of the observed variables and they can be ordered depending on their power in retaining the variance present in the original data set. Scarlata et al. (2007) showed that the first three diagnostics can fully describe the key aspects of the galaxy structure, i.e., to calibrate a three-dimensional classification grid of axes PC_1 , PC_2 , and PC_3 . At each point in the three-dimensional eigenvector space, a dominant morphological class is assigned. Then the Sérsic index is used to refine the classification scheme of disk galaxies, by splitting these in four separate bins of a bulgeness parameter.

Galaxies are classified by ZEST into elliptical, disk, and irregular galaxies (TYPE class equal to 1, 2, and 3 respectively). The disk galaxies are further split in bulge-dominated, intermediate-bulge, small-bulge, bulgeless disk galaxies (BULGE type equal to 0, 1, 2, 3 respectively). See Tab. 7.1 for further details on the classification scheme.

From now onwards we will consider all galaxies that are classified by ZEST as either elliptical or bulge-dominated systems, i.e., specifically ZEST Classes 1 and 2.0, as early-type. All other ZEST types are collectively considered to be late-type galaxies. In terms of the conventional Hubble classification scheme, our division would roughly be between Sa and Sb. When considering the whole disk class galaxies, i.e., irrespective of their bulge type, we will alternatively call them 'spirals'.

Tests on a sample of $z=0$ galaxies from Frei et al. (1996) to determine the reliability of ZEST show a perfect agreement between the two classifications. Moreover this classification scheme is very robust: for magnitudes $I_{AB} \leq 22.5$, more than 90% of galaxies do not change morphological class even when degrading the S/N of images down to a level which is comparable with the faintest of our galaxies.

7.2 Spectra

In this section I will explain the technical details of stacking, fitting the spectra and measuring the emission lines.

7.2.1 Co-adding spectra: the procedure

The advantage of stacking spectra is that it increases their S/N, thus enabling us to obtain more accurate measurements of the mean properties of stacked galaxies. This technique has been widely used in recent years to overcome low quality of spectroscopic data set (Francis et al. 1991; Vanden Berk et al. 2001; Eisenstein et al. 2003; Mignoli et al. 2005; Muzzin et al. 2011) When applied to the galaxies belonging to one of the regions introduced in Sect. 5.4, it provides the typical spectrum of a

core/intermediate/outskirt galaxy. This way we are able to study the typical spectral properties of a galaxy as a function of its group-centric distance.

First of all we visually inspected all the galaxy spectra to remove those cases where either the atmospheric correction failed or there was a contamination from the zero order of the spectrum obtained from a close slit containing a bright object or an AGN was present.

Then we developed an IDL procedure to co-add the spectra of a set of objects which were interactively selected depending on their properties, e.g., their redshifts, color, group-centric distance, mass and equivalent width (EW) of a specific emission line, see later on for details, i.e., Sects. 7.2.2 and 7.3.

The procedure follows these steps: each spectrum of the input list is shifted and rebinned to its rest-frame according to its redshift (with a 1 \AA rest-frame bin) and normalized to the mean flux in a specific wavelength range, $range_{norm}$. The normalization range is selected in order to be present in the observed spectroscopic window at each galaxy redshift: $range_{norm} = 5500 - 5600 \text{ \AA}$ for the low-z bin and $range_{norm} = 4150 - 4250 \text{ \AA}$ for the high-z bin. Moreover we chose both ranges to be free of substantial absorption or emission lines and in the meanwhile to be close to the most important feature of each spectrum, e.g., $H\alpha$ and [OII] for the low-z and high-z bin respectively.

After normalization the spectra are co-added into a composite spectrum by deriving both the mean and the median of all the spectra included in the selection. We shall highlight that the rest-frame wavelength coverage depends on the galaxy redshift. To keep a reasonable and fairly uniform S/N in each wavelength range of the composite spectrum we therefore adopted a minimum threshold of 5 spectra for each pixel. As a consequence the blue and red ends of each composite spectrum can be slightly different (and obviously noisier than the central regions). Along with the mean (median) spectrum, the procedure provides also a smoothed version of it (with a 3 \AA Gaussian filter smoothing) and the standard deviation (semi-quartile).

We built a stacked spectrum of each region of the SGs and of the field for different combination of colors, masses, and spectral features. Spectral features, e.g., line fluxes, EWs, of individual galaxy spectrum were available thanks to the automated pipeline *platefit_vimos* (Lamareille et al. 2009), which simultaneously fits all the emission lines with Gaussian functions after removing the stellar continuum. We divided our sample into four classes:

1. the typical galaxy: we co-added all galaxies irrespective of their colors and spectral features, for the whole mass complete sample (galaxies with $\log(\mathcal{M}_{gal}/\mathcal{M}_{\odot}) > \mathcal{M}_{cut-off}$), the low mass bin ($9.8 \leq \log(\mathcal{M}_{gal}/\mathcal{M}_{\odot}) \leq 10.56$) and the high mass

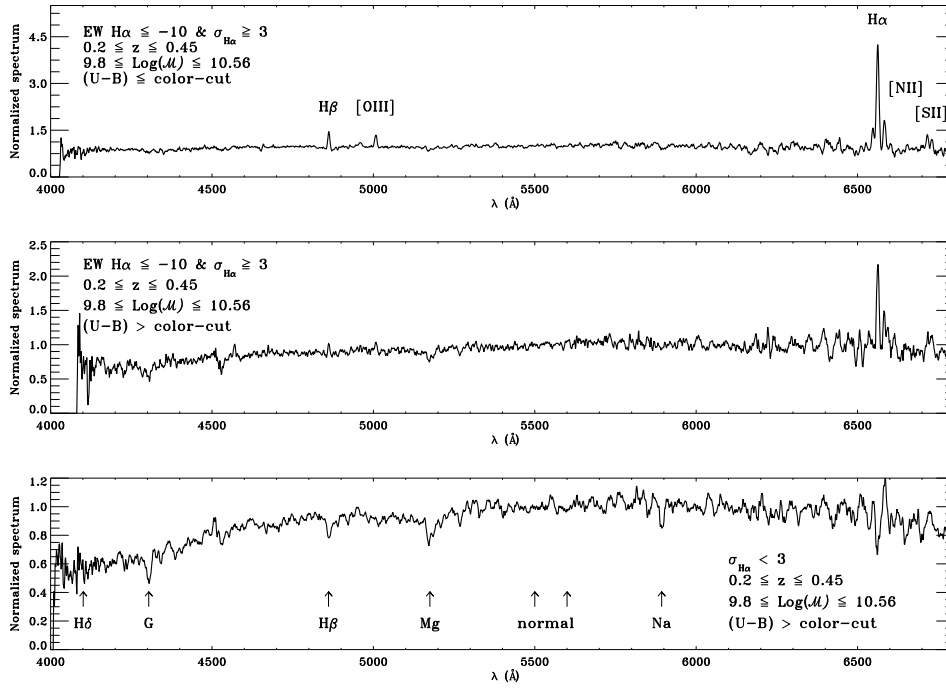


Figure 7.1: Example of the composite spectrum for different galaxy classes: from top to bottom we show the composite spectrum of the blue active galaxy, the red active galaxy, and the red inactive galaxy for the low mass galaxies in the low- z bin. The most important absorption and emission features are identified. The fluxes are per unit wavelength and the normalization is defined by the two arrows labeled *normal*.

7 Segregation effects: further insights from spectra and morphologies

bin ($\log(\mathcal{M}_{gal}/\mathcal{M}_{\odot}) > 10.56$). These spectra reflect the mean mixture of galaxies at fixed mass and/or fixed environment.

2. the blue active galaxy: we co-added all blue galaxies (according to the color cut defined in Sect. 5.2) having the EW of the characteristic emission line larger than an arbitrary cut-off and at least 3σ significance. For the low- z bin we adopted $\text{EW}(\text{H}\alpha) \leq -10$, while $\text{EW}([\text{OII}]) \leq -5$ for the high- z bin. These galaxies are undergoing some level of star formation, as witnessed by the relatively intense emission lines and blue continuum.
3. the red active galaxy: we co-added all red galaxies having the EW of the characteristic emission line larger than the above cut-offs. These galaxies show an antithetical behavior in the stellar/gaseous components and usually present intermediate spectral properties.
4. the red inactive galaxy: we co-added all red galaxies showing no emission line up to 3σ significance. These galaxies are not currently undergoing significant star formation detectable with the typical sensitivity of our spectra.

In Fig. 7.1 we show an example of the composite spectrum of the last three galaxy classes, while we refer the reader to Sect. 7.3.3 for a discussion of the typical galaxy spectrum. From top to bottom we show the composite spectrum of the blue active galaxy, the red active galaxy, and the red inactive galaxy. Fig. 7.1 refers to galaxies with $9.8 \leq \log(\mathcal{M}_{gal}/\mathcal{M}_{\odot}) \leq 10.56$ in the low- z bin and we have highlighted the most important absorption and emission features. The fluxes are per unit wavelength and the normalization is indicated by the arrows *normal*. The range of the y-axis changes to highlight the different features of each spectrum, but here we stress that the continuum of the red active and inactive galaxy are almost indistinguishable. In the red part all the spectra become noisier due to the well-known fringing problems of the old VIMOS CCDs. We are able to detect all the main emission lines that are available at the low- z bin: $\text{H}\beta$, $[\text{OIII}]$, $\text{H}\alpha$, $[\text{NII}]$ and $[\text{SII}]$ ($\text{H}\alpha$ being the most prominent). Among the absorption lines we detect: the G band, $\text{H}\beta$, the Mg triplet and Na.

7.2.2 SSP fitting and line measuring

Our aim is to measure spectral features both in absorption and in emission, and we must take into account the stellar absorption in the measurements of Balmer emission lines. In order to remove the continuum and to account for stellar absorption, we used the software GOSSIP, (Franzetti et al. 2008).

GOSSIP is a tool created to fit the Spectral Energy Distribution (SED) of an object against synthetic models, to find the simulated one that best reproduces the observed data. GOSSIP can combine both the magnitudes from different instruments and the spectrum of a galaxy. In our case we focus on the spectra as we need the best template that reproduces the continuum of the composite spectra, and we added to each composite spectrum an arbitrary magnitude value. This magnitude was assigned to the instrument filter that best matches the normalization wavelength range of the spectrum, i.e., V-subaru and B-COMBO17 for the low-z and high-z bin respectively. We then used the Bruzual & Charlot (2007) models and run GOSSIP to perform the fitting and retrieve the model which best represents the composite spectrum.

In Fig. 7.2 we show the main SED visualization window of GOSSIP with an example of a fit to a spectrum, i.e., that of a typical galaxy of the high-z SG. The blue line corresponds to the observed object, i.e., the stacked spectrum, while the black one refers to the best fit model. Green points represent the rebinned observed spectrum, which was used by GOSSIP to match the resolution of the models. The red dot refers to the arbitrary magnitude value adopted to anchor the model.

Once identified the best fitting model we extracted it from the Bruzual & Charlot (2007) full set. We rebinned both the composite and the model to a resolution of 5\AA px^{-1} and we normalized the composite spectrum to the model. This way we could subtract the stellar continuum and we measure the emission lines corrected flux.

To measure emission lines we used both the IRAF¹ *splot* procedure and the *linebackfit* IDL procedure developed by the SDSSIII group. The results obtained from the two methods are in perfect agreement and from hereafter we will quote only EW measured with the *linebackfit* procedure.

7.3 Morphological and Spectral segregation

In this Section I will present the preliminary results I have obtained exploring the group-centric dependence of galaxy morphologies and spectral features in order to complete the scenario introduced in Sect. 6.7. I will start the analysis by exploring how galaxy morphologies depend on environment, see Sect. 7.3.1. In this context I will highlight once again the importance of lower mass galaxies in revealing the *nurture* effects in act, see Sect. 7.3.2. I will then move to investigate the presence of spectral segregation within group environment by focusing on star forming properties

¹IRAF is distributed by the National Optical Astronomy Observatories, which are operated by the Association of Universities for Research in Astronomy, Inc., under cooperative agreement with the National Science Foundation.

7 Segregation effects: further insights from spectra and morphologies

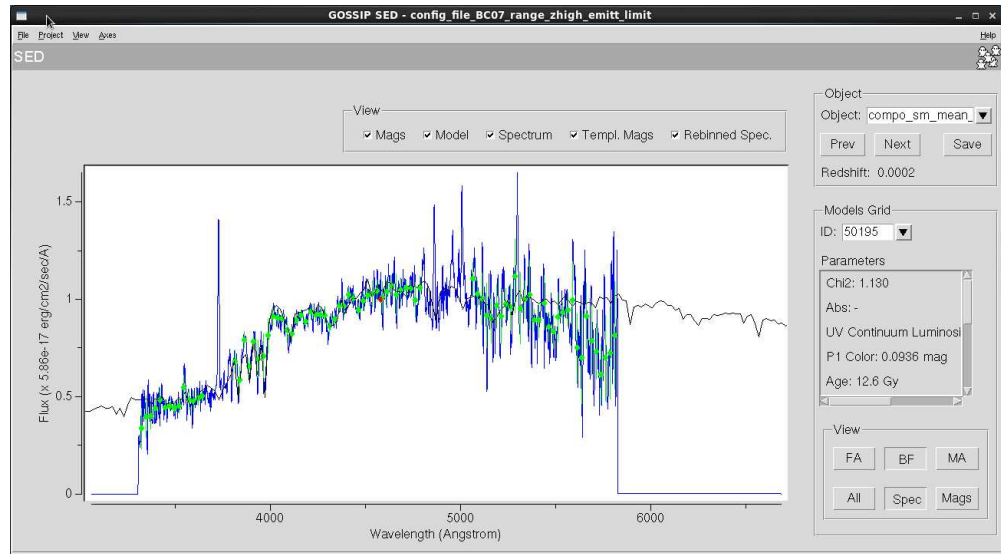


Figure 7.2: Example of SED fitting with GOSSIP: the blue line corresponds to the observed object, while the black one refers to the best fit model. Green points represent the rebinned observed spectrum, which was used by GOSSIP to match the resolution of the models. The red dot refers to the arbitrary magnitude adopted to anchor the model.

7.3 Morphological and Spectral segregation

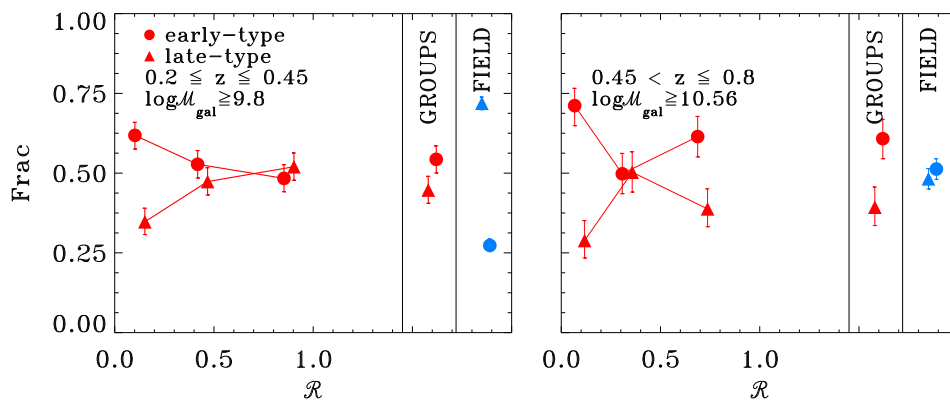


Figure 7.3: left/(right) panel shows F_{late}^{GR} and F_{early}^{GR} , the corrected late-type and early-type fraction, as a function of the group-centric distance in the SG for the low/(high) redshift bin in the mass-complete sample down to $\mathcal{M}_{\text{cut-off}} = 9.8$ ($\mathcal{M}_{\text{cut-off}} = 10.56$). Corrected late/early-type fraction values are indicated with filled triangles and circles respectively. Late-type fractions are displayed at the median normalized \mathcal{R} distance of galaxies in each region, while early-type fractions are slightly offset for clarity's sake. As a reference we plot the fraction of late/early-type field galaxies (cyan symbols) and of the whole group (red symbols).

of group/field galaxies, i.e., exploring the EW changes of both the typical group/field galaxy and the blue active group/field galaxy, see Sect. 7.3.3.

7.3.1 Morphological changes as a function of group-centric distance

To explore morphological segregation we measured $F_{late,obs}^{GR}$ and $F_{early,obs}^{GR}$, the observed fraction of late-type and early-type group member galaxies, in each of the three SG regions defined in Sect. 5.4. As already done in Chapt. 6 (see eq. 6.2) we corrected each fraction using \mathcal{PI} , the estimated percentage of interlopers defined in Sect. 4.1.2, to derive the corrected late-type and early-type fraction, F_{late}^{GR} and F_{early}^{GR} .

In Fig. 7.3 the left/(right) panel shows F_{late}^{GR} and F_{early}^{GR} as a function of the group-centric distance in the SG for the low/(high) redshift bin in the mass-complete sample down to $\mathcal{M}_{cut-off} = 9.8/(\mathcal{M}_{cut-off} = 10.56)$. Corrected late/early-type fraction values are indicated with filled triangles and circles respectively. Late-type fractions are displayed at the median normalized \mathcal{R} distance of galaxies in each region, while early-type fractions are slightly offset for clarity's sake. As a reference we plot the fraction of late/early-type field galaxies (cyan symbols) and of the whole group (red symbols). Error bars are estimated using the approximate analytical formulas for a binomial distribution provided by Gehrels (1986). In Tab. 7.2 we list the values of corrected F_{early}^{GR} for each region and sample considered.

In the low redshift bin, we observe strong morphological segregation for both early and late-type galaxies, the former residing preferentially in the core region, the latter populating mainly the outermost region. Considering the field point, we can see a clear and continuous trend of decreasing/increasing $F_{early}^{GR}/F_{late}^{GR}$ moving from the inner core of groups to their outskirts and further away to the field. The observed morphological segregation is in agreement with previous works (Domínguez et al. 2001; Girardi et al. 2003; Thomas & Katgert 2006; Bamford et al. 2009).

There is a significant difference between $F_{early}^{GR}/F_{late}^{GR}$ in the outskirts and $F_{early}^{FIELD}/F_{late}^{FIELD}$. Therefore entering the group potential well has a significant influence not only in changing galaxy colors, but also in shaping galaxy morphologies. Once again the most relevant difference between group and field is observed in the core where more than 60% of the galaxies have a early-type morphology with respect to 27% in the field.

Globally the field is dominated by late-type galaxies, while in the group environment the ratio reverses and early-type galaxies become more important.

Moving to the highest redshift bin, the morphological segregation trends inside the group environment become noisier, though already in place. The early/late-type segregation is more evident when focusing on the core of groups with respect to the outskirts and, further away, to the field. We shall remind that at high redshift we are studying

Table 7.2: Early/late-type fractions in group regions and corrected for field contamination. Last two columns list total group and field values.

Sample $0.2 \leq z \leq 0.45$	1 st region	2 nd region	3 rd region	group	field
$\log(\mathcal{M}_{gal}/\mathcal{M}_{\odot}) \geq 9.8$	$0.63^{+0.04}_{-0.04}$	$0.53^{+0.04}_{-0.04}$	$0.48^{+0.04}_{-0.04}$	$0.55^{+0.04}_{-0.04}$	$0.27^{+0.02}_{-0.02}$
$\log(\mathcal{M}_{gal}/\mathcal{M}_{\odot}) \geq 10.56$	$0.70^{+0.05}_{-0.06}$	$0.55^{+0.06}_{-0.06}$	$0.52^{+0.05}_{-0.06}$	$0.59^{+0.05}_{-0.05}$	$0.48^{+0.04}_{-0.04}$
$9.8 \leq \log(\mathcal{M}_{gal}/\mathcal{M}_{\odot}) \leq 10.56$	$0.55^{+0.06}_{-0.06}$	$0.48^{+0.06}_{-0.06}$	$0.45^{+0.06}_{-0.06}$	$0.51^{+0.05}_{-0.05}$	$0.18^{+0.02}_{-0.02}$
Sample $0.45 < z \leq 0.8$	1 st region	2 nd region	3 rd region	group	field
$\log(\mathcal{M}_{gal}/\mathcal{M}_{\odot}) \geq 10.56$	$0.71^{+0.06}_{-0.06}$	$0.50^{+0.06}_{-0.06}$	$0.61^{+0.06}_{-0.06}$	$0.61^{+0.06}_{-0.06}$	$0.48^{+0.03}_{-0.03}$

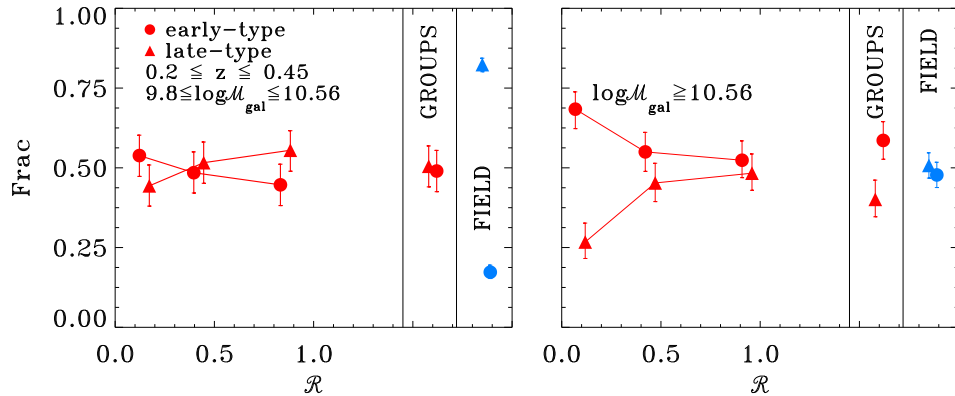


Figure 7.4: Same as Fig. 7.3 for the sub-sample of less massive galaxies (left panel) and for that of most massive galaxies (right panel) at low- z .

the most massive galaxies ($\log(\mathcal{M}_{\text{gal}}) \geq 10.56$), this causes the similar values of $F_{\text{early}}^{\text{GR}}$ and $F_{\text{late}}^{\text{GR}}$ in the field and the smaller difference between group and field $F_{\text{early}}^{\text{GR}}/F_{\text{late}}^{\text{GR}}$ global values.

We now split the low- z sample into the same two stellar mass bins as done in Sect. 6.4, i.e., galaxies with stellar masses $9.8 \leq \log(\mathcal{M}_{\text{gal}}/\mathcal{M}_{\odot}) \leq 10.56$ and $\log(\mathcal{M}_{\text{gal}}/\mathcal{M}_{\odot}) \geq 10.56$. In Fig. 7.4 we show how $F_{\text{early}}^{\text{GR}}/F_{\text{late}}^{\text{GR}}$ varies for the sub-sample of less massive galaxies (left panel) and for that of most massive galaxies (right panel).

We note that for massive galaxies the morphological segregation inside the group environment is mainly driven by the points in the core region that strongly differ from the outskirts. In the outermost region the $F_{\text{early}}^{\text{GR}}/F_{\text{late}}^{\text{GR}}$ are in good agreement with those of the field galaxies.

Less massive galaxies show a mild trend of morphological change from the core to the outskirts of group. Less massive galaxies are almost equally divided into early and late-type galaxies. In this case the strong difference is between the global $F_{\text{early}}^{\text{GR}}/F_{\text{late}}^{\text{GR}}$

group value and that of the field. In the field the less massive galaxies are almost all late-type, while this percentage drops to nearly 50% in the group. This suggests that entering the group environment is much more effective in morphological changes for less massive galaxies.

Fig. 7.4 also shows that there is a strong morphological dependence on stellar masses at fixed environment: The value of $F_{early}^{GR}/F_{late}^{GR}$ increases/decreases moving from lower to higher galaxy stellar masses.

This last analysis has highlighted once again the strong influence of environment on galaxies with $9.8 \leq \log(\mathcal{M}_{gal}/\mathcal{M}_{\odot}) \leq 10.56$. We will further explore this topic in the next section.

7.3.2 The 'strangled' red-spirals population

A clear indication has arisen from the color and morphological segregation analysis: less massive galaxies represent our unique opportunity to witness the *nurture* effects in act. These galaxies show the most striking differences between group and field and we supposed that they have become satellites only recently, therefore they are still suffering from environmental processes. In this section we focus on both the morphology and SFR of these galaxies.

Fig. 7.5 shows the distribution of the Bulge type for spiral galaxies with $9.8 \leq \log(\mathcal{M}_{gal}/\mathcal{M}_{\odot}) \leq 10.56$ and $\log(\mathcal{M}_{gal}/\mathcal{M}_{\odot}) > 10.56$ in the left and right panel respectively. We stress that in this case spirals means all galaxies classified with TYPE class equal to 2, irrespective of their Bulge type. Red solid line refers to the group galaxies, while cyan dashed line refers to the field. The most massive galaxies display the same Bulge type distribution irrespective of the environment they live in. On the contrary a KS test confirms with more than 99.99% confidence that the Bulge distribution of less massive group galaxies is different from that of field galaxies in the same mass bin. In particular we notice that there is an excess of bulge dominated galaxies, i.e., Bulge type < 2 , with low mass in the group environment and a corresponding lack of bulgeless galaxies, i.e., Bulge type ≥ 2 , of the same mass with respect to the field.

As a further step in understanding the effect of environment we now isolate those cases of a late-type galaxy that has been quenched, the so called red passive spirals. By passive we mean galaxies showing $EW(H\alpha) > -10\text{\AA}$ and with a significance less than 3σ . These galaxies are a typical result of environmental processes in act, i.e., starvation removes the gas supply to infalling field-like galaxies, once the remaining gas is consumed these galaxies are red and passive, while showing a late-type morphology (Weinmann et al. 2009).

In Fig. 7.6 we show the fraction of red passive late-type galaxies as a function of

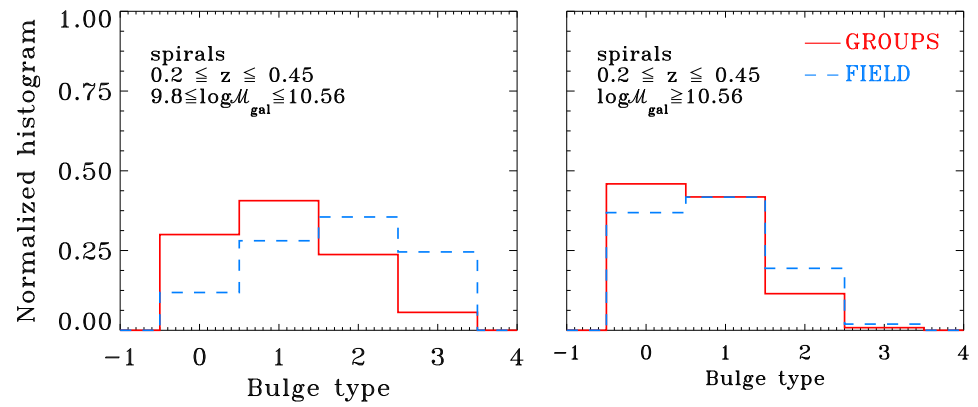


Figure 7.5: Distribution of the Bulge type for less massive (left panel) and most massive (right panel) spiral galaxies. Red solid line refers to the group galaxies, while cyan dashed line refers to the field.

7.3 Morphological and Spectral segregation

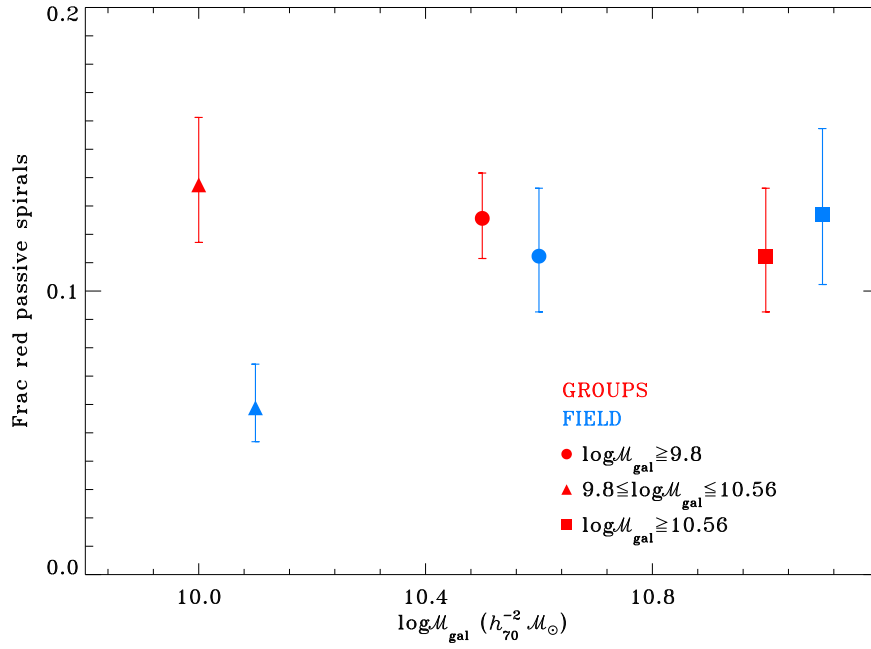


Figure 7.6: Fraction of red passive late-type galaxies as a function of galaxy stellar mass and environment. Triangles refer to galaxies with low mass, squares to galaxies with high mass, and circles to the whole mass complete sample. Red and cyan symbols correspond to group and field fractions respectively.

galaxy stellar mass and environment. Triangles refer to galaxies with $9.8 \leq \log(\mathcal{M}_{\text{gal}}/\mathcal{M}_{\odot}) \leq 10.56$, squares to galaxies with $\log(\mathcal{M}_{\text{gal}}/\mathcal{M}_{\odot}) > 10.56$, and circles to the whole mass complete sample, $\log(\mathcal{M}_{\text{gal}}/\mathcal{M}_{\odot}) > 9.8$. Red and cyan symbols correspond to group and field fractions respectively. There is a higher fraction of red passive spirals with low mass in the group than in the field. This is the only difference we are able to evidence, thus confirming the importance of less massive galaxies as witnesses of the *nurture* effects in act. Figs. 7.5 and 7.6 show that less massive group spirals not only are much more bulge dominated than their counterpart in the field, but also that the few of them showing a late-type morphology are much more quenched than in the field. As a final test we verify whether the red passive spirals with low stellar mass reside in a preferential region of the group in order to understand if the quenching process can be correlated to a specific region of the group. A KS test shows that these peculiar objects share the same projected radial distribution as the whole SG population. Therefore the process seems to be ubiquitous.

7.3.3 Star forming galaxies at fixed environment and stellar mass

We now move to analyze spectral segregation effects by studying the typical galaxy, as defined in Sect. 7.2.1, which resides in different environments. In Fig. 7.7 we show the mean spectrum of the typical galaxy with $\log(\mathcal{M}_{\text{gal}}/\mathcal{M}_{\odot}) > 9.8$ which populates, from top to bottom, the field, the outer, intermediate and the core region of the low-z SG. Each spectrum belonging to a group region is built from nearly 130 spectra, while the field typical spectrum is the mean of about 700 spectra. We have highlighted the most important absorption and emission features. The fluxes are per unit wavelength and the normalization range is indicated by the two arrows *normal*. A visual inspection of the spectra already shows rough differences in the main features of the spectra depending on whether they refer to the field, to group outskirts or to the group core. The intensity of the main emission lines, e.g., $\text{H}\alpha$, $\text{H}\beta$, and $[\text{OIII}]$, gradually fades as we move from the field to the core of the SG. In the core region, $\text{H}\beta$ vanishes in the underlying absorption line. The Mg triplet becomes more defined in the core with respect to the field.

Fig. 7.8 is the same as Fig. 7.7 but for galaxies with $\log(\mathcal{M}_{\text{gal}}/\mathcal{M}_{\odot}) > 10.56$ in the high-z SG. Each spectrum belonging to a group region is built from nearly 60 spectra. In this case there are no obvious differences among the spectra, the only one being the presence of $\text{H}\beta$, and $[\text{OIII}]$ in the field mean composite spectrum, while missing in the group spectra. Nevertheless these features lay in a part of the spectrum which is very close to the fringing and therefore less reliable.

To quantify the differences of the mean spectral properties among the stacked spectra

7.3 Morphological and Spectral segregation

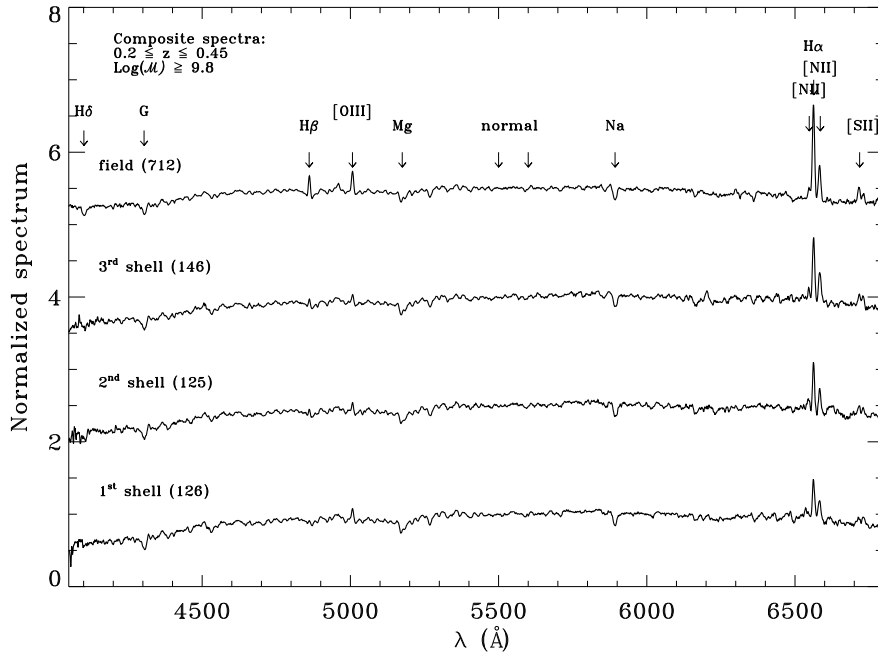


Figure 7.7: Mean stacked spectra of the typical galaxy with $\log(\mathcal{M}_{gal}/\mathcal{M}_{\odot}) > 9.8$ which populates, from top to bottom, the field, the outer, intermediate and the core region of the low- z SG.

7 Segregation effects: further insights from spectra and morphologies

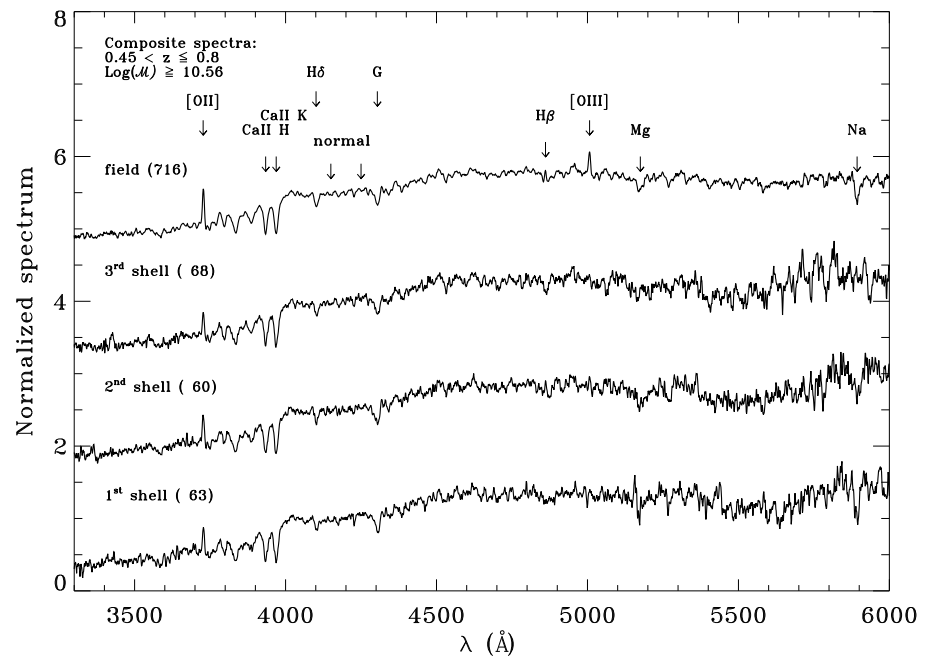


Figure 7.8: Same as Fig. 7.7 but for $\log(\mathcal{M}_{gal}/\mathcal{M}_{\odot}) > 10.56$ in the high-z SG.

7.3 Morphological and Spectral segregation

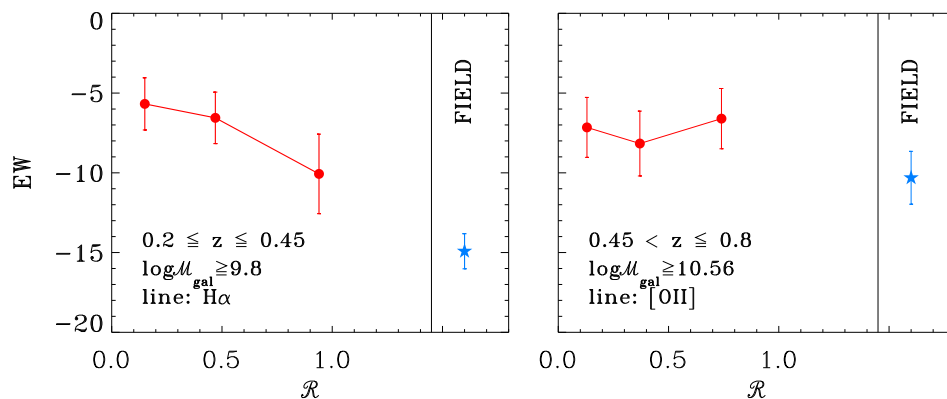


Figure 7.9: EW of H α ([OII]) in the mean stacked spectra of the typical galaxy with $\log(\mathcal{M}_{gal}/\mathcal{M}_{\odot}) > 9.8(10.56)$ as a function of the group-centric distance for the low-z (left panel) and high-z (right panel) SGs. Red circles refer to the group values, while cyan stars refer to the field ones.

in different environments, we measured the EW of the most important emission lines at each redshift bin: H α and [OII] for the low-z and high-z bin respectively. By convention, feature in emission have negative EW values. In Fig. 7.9 we show the EW of the mean stacked spectra of the typical galaxy with $\log(\mathcal{M}_{gal}/\mathcal{M}_{\odot}) > 9.8(10.56)$ as a function of the group-centric distance for the low-z (left panel) and high-z (right panel) SGs. Red circles refer to the group values, while cyan stars refer to the field ones. The error bars are the sum in quadrature of (1) the measurement uncertainty provided by the linebackfit procedure and (2) a 500 bootstrap resampling of the data. We notice that in this case no attempt to account for interlopers has been made, therefore the true trends might be somewhat shallower than those presented here.

Let us first focus on the low-z bin: there is a clear trend of increasing EW while moving far away from the core region out to the peripheral one and then to the field.

Since the EW of H α is strongly correlated to the SSFR, Fig. 7.9 shows that the average star formation properties of galaxies strongly depend on the environment they live in. In the outermost region of the SG the EW is still somewhat smaller than that of field galaxies, suggesting that entering the group environment has a significant impact in quenching the star formation.

On the contrary in the high- z bin we do not detect any radial trend of the EW of the typical galaxy, but we still find a difference between the EW of the mean stacked spectrum of group and field galaxies. We shall underline once again that at this redshift we are observing only the most massive galaxies for which differences between group and field are less prominent.

These results are in good agreement with what we found in our color segregation analysis, see Fig. 6.2.

The observed trend of increasing EW as a function of the group-centric distance in the low- z SG can either be the result of an actual increase of EW among the SF galaxies depending on the region they live or it can simply reflect the trend of increasing F_{blue} we found in Sect. 6.2.

To better understand this point, we now concentrate on the properties of blue active galaxies both at fixed stellar mass and environment in the low- z bin, where we are able to separate the role of these two quantities. In Fig. 7.10 we show the distribution of EWs of group galaxies (empty circles) as a function of their group-centric distance and that of field galaxies (empty stars). We overlaid the EW of the mean stacked spectra of galaxies with low masses (triangles) and of galaxies with high masses (squares) in each group region (red symbols) and in the field (cyan symbols). This plot shows that the EW correlates with the galaxy stellar mass, galaxies with $9.8 \leq \log(\mathcal{M}_{gal}/\mathcal{M}_{\odot}) \leq 10.56$ having larger EWs than most massive ones. This has already been observed in terms of SSFR with low mass galaxies having a higher SSFR than high mass ones (Muzzin et al. 2011, and references therein). This correlation is independent of the environment the galaxies live in: group and field galaxies show the same EW at fixed stellar mass. The lack of dependence of SF galaxy properties on environment as already been observed in previous work (Balogh et al. 2004; Kauffmann et al. 2004; Peng et al. 2010; Muzzin et al. 2011). As a consequence the radial trend in EW we observed is a reflection of the color radial trend we found in Sect. 6.2.

This result hints to two important properties of environmental effects: (1) the group environment regulates the fraction of blue/active galaxies rather than their actual SSFR, (2) for this to happen, the environmental quenching process must be rapid enough to prevent us from detecting a fading of the blue active group galaxies EWs.

In the next Section we will discuss in more details the results we found in our

7.3 Morphological and Spectral segregation

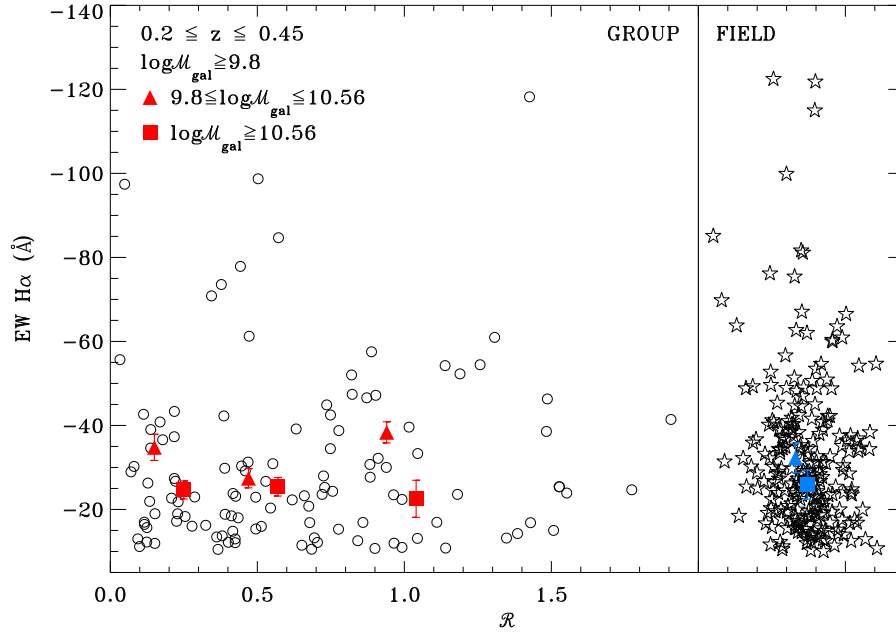


Figure 7.10: Distribution of EWs of blue active, i.e., $EW(H\alpha) \leq -10$, group galaxies (empty circles) as a function of their group-centric distance and that of field galaxies (empty stars). We overlaid the EW of the mean stacked spectra of low mass galaxies (triangles) and of high mass galaxies (squares) in each group region (red symbols) and in the field (cyan symbols).

morphological and spectral segregation analysis.

7.4 Low mass galaxies: the key to understand the rapid *nurture* effects

In this Chapter we tried to further investigate the main conclusions we drew in Chapt. 6.

First of all poorer groups bear memory of their recent accretion history and therefore we are able to detect color radial trends as a result of environmental processes in act. These processes must affect galaxy properties on short time-scales since richer structures, which are in a more advanced dynamical stage, have already wiped out color trends and the absence of a large-scale trend confirms that the processes should be rapid and act on group size scales.

In Sect. 7.3.3 we have shown that there is an homology between blue fraction trends and EW trends: in the low- z SG, where we are complete down to $\log(\mathcal{M}_{gal}/\mathcal{M}_{\odot}) = 9.8$, we are able to detect a change in the $H\alpha$ EW of the mean stacked spectrum as a function of the group-centric distance out to the field, see Fig. 7.9. On the contrary in the high- z SG there is no radial trend while the difference with the EW of the mean stacked field spectrum is still present. Once again this can be the result of both the richness and the mass, but as we are now using only the spec- z sample we do not have enough statistic to disentangle between the two. Reassured by the similarity of the general trends we decided to focus on the effect of environment on the blue active galaxies.

To disentangle whether the environment causes a fading of the mean EW of star forming galaxies or it simply regulates their fraction, we measured the EW of blue active galaxies at fixed mass and environment. Fig. 7.10 showed that EW correlates with the galaxy stellar mass but it is independent of environment. In other words star forming galaxies share the same properties among all environments and at any group-centric distance. This means that we are not able to detect galaxies with a blue color/continuum but lacking a prominent emission feature. This would be the transition status from blue star forming field-like galaxies and red quenched group-like galaxies. The absence of this kind of galaxies implies that the transition between the two status should be rapid enough (see also Muzzin et al. 2011).

This result is in perfect agreement with our conclusions in Chapt. 6 where we suggested a time-scale shorter than 1.5-2 Gyrs.

The second important conclusion of Chapt. 6 is that lower mass galaxies in poorer

7.4 Low mass galaxies: the key to understand the rapid nurture effects

groups hold the smoking gun of environmental effects in action. These are the galaxies that clearly display a gradual change in the blue fraction and that mostly differ from their counterpart in the field. To further investigate this issue, we selected all spiral galaxies and we looked for differences in both their structural parameters, i.e., their bulgeness, and their emission properties, i.e., the fraction of passive galaxies. The statistic allowed us to perform this analysis in stellar mass bins only for the low- z SG.

Fig. 7.5 showed that at fixed galaxy stellar masses, differences between environments arise only for galaxies with $9.8 \leq \log(\mathcal{M}_{\text{gal}}/\mathcal{M}_{\odot}) \leq 10.56$, while most massive galaxies, $\log(\mathcal{M}_{\text{gal}}/\mathcal{M}_{\odot}) > 10.56$, share the same bulge distribution. On average lower mass galaxies have a dominant bulge in group environment, while they are mainly bulgeless in the field. This result confirms once again the importance of galaxy stellar mass as a key parameter in driving the galaxy evolution together with the environment. It also highlights that we might be able to detect strong morphological changes for galaxies with lower masses as a function of environment.

This is confirmed by Fig. 7.4, where the fraction of F_{late}^{GR} and F_{early}^{GR} group galaxies with lower masses is significantly different from that of the field sample. This plot suggests that part of the late-type galaxies with low mass has suffered morphological changes while entering the group potential well. On the contrary, the difference between F_{late}^{GR} and F_{early}^{GR} in group and field for most massive galaxies is less prominent, but still in place. Once inside group environment, both galaxies with low and high mass show a morphological segregation as a function of group-centric distance. The radial trend is mild and for the most massive galaxies is exclusively driven by the $F_{\text{late}}^{GR}/F_{\text{early}}^{GR}$ values in the core region. Bamford et al. (2009) found a similar small, steady increase in early-type fraction as a function of distance at fixed stellar mass. Our results at high- z , where we are complete only for this mass range, are in good agreement with those at low- z in the same mass bin.

The connection between the spectro-morpho segregation analysis and our previous results might be summarized by Fig. 7.6. It shows that there is a considerable fraction of red-passive late-type galaxies, more than 10%, both in the group and in the field. At fixed stellar mass the only difference between environments is still for lower mass galaxies. Bamford et al. (2009) made a similar exercise by studying the fraction of red spirals as a function of group-centric distance. They found a strong dependence on the explored region with a peak towards $0.4 R_{\text{vir}}$. At higher densities or in the cores of groups they found that the red spiral fraction declines sharply. We do not find any group-centric dependence of the red passive spirals, but we shall remind that we specifically select only quenched red spirals, while there is a considerable fraction of red active galaxies. We plan to analyze these peculiar objects in the future.

Adding the morphological and spectroscopic information to our analysis has confirmed that the group environment shares an important role in galaxy evolution with galaxy stellar mass. In particular, *nurture* effects in act can be highlighted exploring lower mass galaxies in poor groups, where the short environmental processes are still visible and detectable due to the recent accretion history of these systems.

7.5 Conclusions

In this Chapter I presented the preliminary results on how galaxy morphologies and spectral properties vary as a function of the distance from the group center. The analysis was performed using mass-complete samples to disentangle the obvious galaxy stellar mass/spectro-morphological dependencies.

The main results are:

(i) In both the redshift bins explored we detect morphological segregation both as a function of group-centric distance and as a function of the environment. For massive galaxies, i.e., $\log(\mathcal{M}_{gal}/\mathcal{M}_{\odot}) \geq 10.56$, the morphological segregation is mainly driven by the core region where F_{late}^{GR} and F_{early}^{GR} differ significantly from that in the outskirts and field. Galaxies with lower stellar mass, i.e., $9.8 \leq \log(\mathcal{M}_{gal}/\mathcal{M}_{\odot}) < 10.56$, have only a mild group-centric dependence of F_{late}^{GR} and F_{early}^{GR} , while they show the strongest differences with respect to the field.

(ii) Group spirals with low mass have a bulge distribution peaked towards bulge dominated types, while their field counterpart are significantly shifted towards bulge-less types. At higher masses this differences is erased.

(iii) Globally most massive galaxies are more bulge dominated than low mass galaxies irrespective of the environment.

(iv) There is a considerable fraction of red-passive late-type galaxies in both group and field. Group galaxies with low masses show an excess of these strangled spirals with respect to the field.

(v) In the low- z bin we detect a variation of the $H\alpha$ EW of the mean stacked spectrum as a function of group-centric distance out to the field. On the contrary in the high- z bin there is no radial trend in the intensity of the [OII] EW.

(vi) Blue active galaxies have the same EWs at fixed stellar mass irrespective of the environment they live in. On the mean low mass galaxies show higher EWs than high mass galaxies at fixed environment.

All these observations confirm the scenario we proposed in the previous Chapter and suggest that the group environment determines the fraction of blue active galaxies and not their properties. The process that regulates the transition from blue-active to red-

passive should be short enough to prevent us detecting variation in the properties of the blue active sample as a function of environment and to keep a strong bimodality distribution of galaxy colors. Lower mass galaxies seem to be the witnesses of the *nurture* effects in act as they show the strongest segregation effects.

This spectro-morpho analysis is far from being exhaustive and there is a lot of work that can be done. For example we are going to investigate the dependence of peculiar objects, e.g., post starburst galaxies and red active galaxies, on environment, and we plan to study also absorption lines.

8 Conclusions and future prospects

In this last Chapter, I will summarize my overall findings and give a brief outlook for further investigations.

8.1 Conclusions

The aim of this thesis was to provide a significant contribution to our understanding of galaxy evolution, specifically focusing on the role of group environment in affecting galaxy properties. It is well established that the environment of a galaxy correlates with its properties, e.g., denser environments host a higher fraction of red/early-type galaxies. However, there are several key questions that are still open: the so-called *nature/nurture* debate, i.e., are the differences between galaxy population in group and field the result of two distinct evolutionary tracks (*nurture*), or do they just reflect the initial conditions and general evolution of galaxies irrespective of environment (*nature*)? Furthermore, if the environment plays a key role in galaxy evolution, which are the environmental processes which cause the galaxy transformations? And, finally, are we able to reconstruct the accretion history of groups through the star formation history of their member galaxies?

This thesis attempts to address these important questions by exploring segregation effects of group galaxies over a wide redshift range. The thesis is based on the unique data set from both COSMOS and zCOSMOS survey, which enable me to study group galaxies out to $z=0.8$ on a mass complete sample.

Here I summarize the main results of my thesis:

1. Using realistic mock galaxy catalogs, properly designed to match our observed data set I developed an algorithm to incorporate into groups those galaxies brighter than $I_{AB} = 22.5$ and missing the spectroscopic redshift information. Thus providing statistically reliable sample, i.e., $\sim 90\%$ complete with only $\sim 3\%$ of interlopers, to study galaxy evolution in group environment. The code was specifically designed in order to not introduce any significant radial trend of the contamination from interlopers, thus allowing a reliable study of the variation of group member galaxy properties as a function of the group-centric distance.

8 Conclusions and future prospects

2. Aming at building a composite group I developed a new technique to define group centers and central galaxies. The new centers get as close as $40 h_{70}^{-1} Kpc$ to the real center of the groups, as tested on the mocks. The new estimator to retrieve the central galaxy of a group works correctly in 60% of the cases, an improvement when compared to simpler definitions. Furthermore it can be used as the center of the group, with an overall median distance to the real group center of $16 h_{70}^{-1} Kpc$.
3. I studied color and mass segregation effects at fixed stellar mass in two composite groups at $0.2 \leq z \leq 0.45$ and $0.45 < z \leq 0.8$. The blue fraction of most massive galaxies, i.e., $\log(\mathcal{M}_{gal}/\mathcal{M}_{\odot}) \geq 10.56$, does not display strong group-centric dependence, despite displaying a clear lower blue fraction in groups than in the field. This result holds irrespective of group richness. On the contrary for galaxies of lower masses, i.e., $9.8 \leq \log(\mathcal{M}_{gal}/\mathcal{M}_{\odot}) < 10.56$, there is a radial dependence in the changing mix of red and blue galaxies, red galaxies being found preferentially in the group center. This trend is stronger for poorer groups, while it disappears for richer groups. Mass segregation shows the opposite behavior with respect to galaxy colors trends: it is visible only in rich groups, while poorer groups have a constant mix of galaxy stellar masses as a function of group-centric distances. Therefore the observed color trends cannot be simply explained as caused from different stellar masses distribution in different group regions.
4. From the morphological and spectral segregation analysis I found that the early type fraction at fixed stellar mass is a strong function of environment, especially for galaxies with $\log(\mathcal{M}_{gal}/\mathcal{M}_{\odot}) \geq 10.56$, and there is a dependence of morphology on group-centric radius at fixed stellar mass. Overall the main morphological differences between group and field arise when studying spirals with low mass, i.e., their bulge distribution is much more peaked towards bulge dominated types than their field counterpart. The galaxies with low mass also show an excess of red-passive late-type galaxies, the so called strangled spirals, with respect to the field. We observed spectral segregation, i.e., the emission line EW of the mean stacked spectrum changes as a function of group-centric distance out to the field. Nevertheless, blue active galaxies have the same EWs at fixed stellar mass irrespective of the environment they live in.
5. I identified in both starvation and collisions the possible physical processes that causes the transformation of galaxy properties in groups. We do not detect any radial trend of the blue fraction in the proximity of group environment, i.e., no large scale trends in the blue fraction. This means that the physical length-

scale on which the environment plays its role coincides with the group physical scales. Furthermore the processes should act on short time-scales, less than 1.5-2 Gyrs to keep the observed strong bimodality distribution of galaxy colors. This short time-scale processes regulate the changing fraction of blue active galaxies between different environments.

6. Our results can be interpreted in a scenario in which environmental effects are superimposed over galaxy secular evolution and group dynamical evolution. The parallel absence(/presence) of color segregation in rich(/poor) groups hints to the fact that nurture effects are still in action in poorer structures, whereas in richer systems have already exhausted their effects, so that all galaxies are uniformly red irrespective of their position within the group (at least down to the galaxy stellar masses we explored). The corresponding presence(/absence) in rich(/poor) groups of mass segregation suggests that richer systems have been in place for time long enough so that more massive galaxies have sank to the group center, something that has yet to happen for the poorer groups, that still keep memory of their more recent growth history.

7. In this scenario our chance to observe *nurture* in act resides in lower mass galaxies in poorer groups. These galaxies still display gradually bluer colors moving from group center to more external regions and show an excess of stragles spirals than in the field, as a consequence of the still recent accretion history of these groups.

8.2 Future plans

This thesis has exploit only part of the possible studies this powerful data set can allow. Here I list some of the projects that can be pursue using the algorithms and SG I constructed:

1. First of all the algorithms I developed can be applied to any kind of spectroscopic survey with ancillary photometric data to implement group catalogs. For example the spectroscopic survey VIPERS is an ongoing ESO large program to measure 100000 redshifts for galaxies with $I_{AB} \leq 22.5$ over an area of 24 square degrees. At completion, this survey is supposed to reach a high effective spectroscopic sampling rate ($> 50\%$) and to cover the CFHTLS W1 and W4 fields.

8 Conclusions and future prospects

2. In the recent years galaxies has been divided into two categories: centrals and satellites. Many studies have highlighted differences of properties between the two of them (Skibba 2009; Peng et al. 2010). The new estimator of the central galaxy I developed can be used to separate the zCOSMOS data set into these two classes. This allows a detailed analysis of the dependence of these differences at fixed group richness, an issue that has barely been addressed in these kind of studies. Furthermore a detailed comparison of the properties of central galaxies with those of simulations can help to investigate the so called central galaxy paradigm. Skibba et al. (2011) has tested this assumption at low redshift, finding discrepant results between observed and mock centrals. Here we can extend this analysis to higher redshift.
3. Another interesting topic that we can explore with these SGs is the group-close pair connection and its dependence on both galaxy colors, group richness, and group-centric distance. This may shed further light on the accretion history of the groups and on the role of collisions, mergers as environmental process driving the migration from the blue cloud to the red sequence (López-Sanjuan et al. 2010; Kampczyk et al. 2011).
4. These SGs allow to study on a statistically way the peculiar objects such as post starburst, i.e., recently-quenched galaxies (Poggianti et al. 2009; Vergani et al. 2010; Kampczyk et al. 2011; Muzzin et al. 2011), red active galaxies, i.e., galaxies showing a different stellar/gaseous behaviour, and the galaxies in the green valley, i.e., the population of transition galaxies in their migration from the blue cloud to the red sequence (Balogh et al. 2011).
5. From the stacked spectra we can perform a detail analysis of the absorption features of both the typical galaxy and the red inactive galaxy as a function of both galaxy stellar mass and environment.
6. Since this work has highlighted the importance of galaxies with low mass as witnesses of *nurture* in act, a follow-up of with a K band selection to reach completeness down to lower masses may help us to understand the role and impact of environment on these galaxies.
7. Most of this work was dedicated to study galaxy evolution in the environment, but the environment itself was not explored in detail. A comprehensive study of group global properties would include their morphologies, i.e., do they show regular or elongated shapes? how does it depend on their richness? Is there any connection with their central galaxy properties?

8.2 *Future plans*

8. There were some groups for which the algorithm did not add any photo-z. These groups have a smaller projected radius than the others. It would be interesting to further analyze this sub-set of groups.

This is a short list of possible proposals, but there are many more projects that are worth to be undertaken using my algorithms and the SGs I constructed.

Bibliography

- Abadi, M. G., Moore, B., & Bower, R. G. 1999, MNRAS, 308, 947
- Abell, G. O., Corwin, Jr., H. G., & Olowin, R. P. 1989, ApJS, 70, 1
- Bai, L., Rasmussen, J., Mulchaey, J. S., et al. 2010, ApJ, 713, 637
- Baldry, I. K., Balogh, M. L., Bower, R. G., et al. 2006, MNRAS, 373, 469
- Baldry, I. K., Glazebrook, K., Brinkmann, J., et al. 2004, ApJ, 600, 681
- Balogh, M., Eke, V., Miller, C., et al. 2004, MNRAS, 348, 1355
- Balogh, M. L., McGee, S. L., Wilman, D., et al. 2009, MNRAS, 398, 754
- Balogh, M. L., McGee, S. L., Wilman, D. J., et al. 2011, MNRAS, 412, 2303
- Balogh, M. L., Morris, S. L., Yee, H. K. C., Carlberg, R. G., & Ellingson, E. 1999, ApJ, 527, 54
- Balogh, M. L., Navarro, J. F., & Morris, S. L. 2000, ApJ, 540, 113
- Bamford, S. P., Nichol, R. C., Baldry, I. K., et al. 2009, MNRAS, 393, 1324
- Berlind, A. A., Frieman, J., Weinberg, D. H., et al. 2006, ApJS, 167, 1
- Bertoldi, F., Carilli, C., Aravena, M., et al. 2007, ApJS, 172, 132
- Biviano, A., Katgert, P., Thomas, T., & Adami, C. 2002, A&A, 387, 8
- Blanton, M. R., Eisenstein, D., Hogg, D. W., Schlegel, D. J., & Brinkmann, J. 2005, ApJ, 629, 143
- Blanton, M. R., Eisenstein, D., Hogg, D. W., & Zehavi, I. 2006, ApJ, 645, 977
- Blanton, M. R., Hogg, D. W., Bahcall, N. A., et al. 2003, ApJ, 594, 186
- Blanton, M. R. & Moustakas, J. 2009, ARAA, 47, 159
- Bolzonella, M., Kovač, K., Pozzetti, L., et al. 2010, A&A, 524, A76+

Bibliography

- Boselli, A. & Gavazzi, G. 2006, *PASP*, 118, 517
- Bottini, D., Garilli, B., Maccagni, D., et al. 2005, *PASP*, 117, 996
- Brinchmann, J., Charlot, S., White, S. D. M., et al. 2004, *MNRAS*, 351, 1151
- Bruzual, C. & Charlot, S. 2007, in Prep.
- Bruzual, G. & Charlot, S. 2003, *MNRAS*, 344, 1000
- Capak, P., Abraham, R. G., Ellis, R. S., et al. 2007a, *ApJS*, 172, 284
- Capak, P., Aussel, H., Ajiki, M., et al. 2007b, *ApJs*, 172, 99
- Carlberg, R. G., Yee, H. K. C., & Ellingson, E. 1997, *ApJ*, 478, 462
- Carlberg, R. G., Yee, H. K. C., Morris, S. L., et al. 2001a, *ApJ*, 563, 736
- Carlberg, R. G., Yee, H. K. C., Morris, S. L., et al. 2001b, *ApJ*, 552, 427
- Chabrier, G. 2003, *ApJL*, 586, L133
- Chandrasekhar, S. 1943, *ApJ*, 97, 255
- Cowie, L. L., Songaila, A., Hu, E. M., & Cohen, J. G. 1996, *AJ*, 112, 839
- Croton, D. J., Springel, V., White, S. D. M., et al. 2006, *MNRAS*, 365, 11
- Cucciati, O., Iovino, A., Marinoni, C., et al. 2006, *A&A*, 458, 39
- De Lucia, G. & Blaizot, J. 2007, *MNRAS*, 375, 2
- Diaz, E., Zandivarez, A., Merchan, M. E., & Muriel, H. 2005, *ApJ*, 629, 158
- Domínguez, M., Muriel, H., & Lambas, D. G. 2001, *AJ*, 121, 1266
- Domínguez, M. J., Zandivarez, A. A., Martínez, H. J., et al. 2002, *MNRAS*, 335, 825
- Dressler, A. 1980, *ApJ*, 236, 351
- Dressler, A., Oemler, Jr., A., Couch, W. J., et al. 1997, *ApJ*, 490, 577
- Eisenstein, D. J., Hogg, D. W., Fukugita, M., et al. 2003, *ApJ*, 585, 694
- Eke, V. R., Baugh, C. M., Cole, S., et al. 2004, *MNRAS*, 348, 866
- Feldmann, R., Carollo, C. M., Porciani, C., et al. 2006, *MNRAS*, 372, 565

- Font, A. S., Bower, R. G., McCarthy, I. G., et al. 2008, *MNRAS*, 389, 1619
- Francis, P. J., Hewett, P. C., Foltz, C. B., et al. 1991, *ApJ*, 373, 465
- Franzetti, P., Scodreggio, M., Garilli, B., Fumana, M., & Paiero, L. 2008, in *Astronomical Society of the Pacific Conference Series*, Vol. 394, *Astronomical Data Analysis Software and Systems XVII*, ed. R. W. Argyle, P. S. Bunclark, & J. R. Lewis, 642
- Frei, Z., Guhathakurta, P., Gunn, J. E., & Tyson, J. A. 1996, *AJ*, 111, 174
- Gavazzi, G., Pierini, D., & Boselli, A. 1996, *A&A*, 312, 397
- Gehrels, N. 1986, *ApJ*, 303, 336
- George, M. R., Leauthaud, A., Bundy, K., et al. 2011, *ApJ*, 742, 125
- Gerke, B. F., Newman, J. A., Davis, M., et al. 2005, *ApJ*, 625, 6
- Gerke, B. F., Newman, J. A., Faber, S. M., et al. 2007, *MNRAS*, 376, 1425
- Gill, S. P. D., Knebe, A., & Gibson, B. K. 2005, *MNRAS*, 356, 1327
- Girardi, M., Rigoni, E., Mardirossian, F., & Mezzetti, M. 2003, *A&A*, 406, 403
- Gunn, J. E. & Gott, III, J. R. 1972, *ApJ*, 176, 1
- Hansen, S. M., Sheldon, E. S., Wechsler, R. H., & Koester, B. P. 2009, *ApJ*, 699, 1333
- Hao, J., McKay, T. A., Koester, B. P., et al. 2010, *ApJS*, 191, 254
- Hashimoto, Y. & Oemler, Jr., A. 1999, *ApJ*, 510, 609
- Hasinger, G., Cappelluti, N., Brunner, H., et al. 2007, *ApJS*, 172, 29
- Hogg, D. W., Blanton, M. R., Eisenstein, D. J., et al. 2003, *ApJL*, 585, L5
- Huchra, J. P. & Geller, M. J. 1982, *ApJ*, 257, 423
- Ilbert, O., Capak, P., Salvato, M., et al. 2009, *ApJ*, 690, 1236
- Iovino, A., Cucciati, O., Scodreggio, M., et al. 2010, *A&A*, 509, A40+
- Kampczyk, P., Lilly, S. J., de Ravel, L., et al. 2011, *ArXiv e-prints*
- Katgert, P., Biviano, A., & Mazure, A. 2004, *ApJ*, 600, 657
- Kauffmann, G. & Charlot, S. 1998, *MNRAS*, 297, L23

Bibliography

- Kauffmann, G., Heckman, T. M., White, S. D. M., et al. 2003, *MNRAS*, 341, 54
- Kauffmann, G., White, S. D. M., Heckman, T. M., et al. 2004, *MNRAS*, 353, 713
- Kimm, T., Somerville, R. S., Yi, S. K., et al. 2009, *MNRAS*, 394, 1131
- Kitzbichler, M. G. & White, S. D. M. 2007, *MNRAS*, 376, 2
- Knobel, C., Lilly, S. J., Iovino, A., Porciani, C., & Kovač, K. 2011, in Prep.
- Knobel, C., Lilly, S. J., Iovino, A., et al. 2009, *ApJ*, 697, 1842
- Koekemoer, A. M., Aussel, H., Calzetti, D., et al. 2007, *ApJS*, 172, 196
- Komatsu, E., Smith, K. M., Dunkley, J., et al. 2011, *ApJS*, 192, 18
- Kovač, K., Lilly, S. J., Cucciati, O., et al. 2010a, *ApJ*, 708, 505
- Kovač, K., Lilly, S. J., Knobel, C., et al. 2010b, *ApJ*, 718, 86
- Lamareille, F., Brinchmann, J., Contini, T., et al. 2009, *A&A*, 495, 53
- Le Fèvre, O., Vettolani, G., Garilli, B., et al. 2005, *A&A*, 439, 845
- Lewis, I., Balogh, M., De Propris, R., et al. 2002, *MNRAS*, 334, 673
- Lilly, S. J., Le Brun, V., Maier, C., et al. 2009, *ApJs*, 184, 218
- Lilly, S. J., Le Fèvre, O., Renzini, A., et al. 2007, *ApJS*, 172, 70
- López-Sanjuan, C., Balcells, M., Pérez-González, P. G., et al. 2010, *A&A*, 518, A20
- Mahdavi, A., Geller, M. J., Böhringer, H., Kurtz, M. J., & Ramella, M. 1999, *ApJ*, 518, 69
- Margoniner, V. E., de Carvalho, R. R., Gal, R. R., & Djorgovski, S. G. 2001, *ApJL*, 548, L143
- Marinoni, C., Davis, M., Newman, J. A., & Coil, A. L. 2002, *ApJ*, 580, 122
- McCarthy, I. G., Frenk, C. S., Font, A. S., et al. 2008, *MNRAS*, 383, 593
- McGee, S. L., Balogh, M. L., Bower, R. G., Font, A. S., & McCarthy, I. G. 2009, *MNRAS*, 400, 937
- McGee, S. L., Balogh, M. L., Wilman, D. J., et al. 2011a, *MNRAS*, 413, 996

- McGee, S. L., Balogh, M. L., Wilman, D. J., et al. 2011b, *MNRAS*, 413, 996
- Mignoli, M., Cimatti, A., Zamorani, G., et al. 2005, *A&A*, 437, 883
- Mo, H. J. & White, S. D. M. 2002, *MNRAS*, 336, 112
- Moore, B., Katz, N., Lake, G., Dressler, A., & Oemler, A. 1996, *Nat*, 379, 613
- Muzzin, A., Wilson, G., Yee, H. K. C., et al. 2011, *ArXiv e-prints*
- Oesch, P. 2011, in *Prep.*
- Oesch, P. A., Carollo, C. M., Feldmann, R., et al. 2010, *ApJL*, 714, L47
- Peebles, P. J. E. 1982, *ApJL*, 263, L1
- Peng, Y., Lilly, S. J., Kovač, K., et al. 2010, *ApJ*, 721, 193
- Poggianti, B. M., Aragón-Salamanca, A., Zaritsky, D., et al. 2009, *ApJ*, 693, 112
- Postman, M. & Geller, M. J. 1984, *ApJ*, 281, 95
- Pozzetti, L., Bolzonella, M., Zucca, E., et al. 2010, *A&A*, 523, A13+
- Presotto, V., Iovino, A., Scodeggio, M., et al. 2012, *ArXiv e-prints*
- Press, W. H. & Schechter, P. 1974, *ApJ*, 187, 425
- Ribeiro, A. L. B., Lopes, P. A. A., & Trevisan, M. 2010, *MNRAS*, 409, L124
- Rix, H.-W. & Rieke, M. J. 1993, *ApJ*, 418, 123
- Sanders, D. B., Salvato, M., Aussel, H., et al. 2007, *ApJS*, 172, 86
- Scarlata, C., Carollo, C. M., Lilly, S., et al. 2007, *ApJs*, 172, 406
- Schinnerer, E., Smolčić, V., Carilli, C. L., et al. 2007, *ApJS*, 172, 46
- Scodeggio, M., Franzetti, P., Garilli, B., et al. 2005, *PASP*, 117, 1284
- Scoville, N., Aussel, H., Brusa, M., et al. 2007, *ApJS*, 172, 1
- Shapley, H. 1933, *Proceedings of the National Academy of Science*, 19, 591
- Skibba, R. A. 2009, *MNRAS*, 392, 1467
- Skibba, R. A., van den Bosch, F. C., Yang, X., et al. 2011, *MNRAS*, 410, 417

Bibliography

- Snowden, S. L., Mushotzky, R. F., Kuntz, K. D., & Davis, D. S. 2008, *A&A*, 478, 615
- Springel, V. 2005, *MNRAS*, 364, 1105
- Tanaka, M., Goto, T., Okamura, S., Shimasaku, K., & Brinkmann, J. 2004, *AJ*, 128, 2677
- Taniguchi, Y., Scoville, N., Murayama, T., et al. 2007, *ApJS*, 172, 9
- Thomas, T. & Katgert, P. 2006, *A&A*, 446, 31
- Toomre, A. & Toomre, J. 1972, *ApJ*, 178, 623
- Tran, K., Simard, L., Zabludoff, A. I., & Mulchaey, J. S. 2001, *ApJ*, 549, 172
- Treu, T., Ellis, R. S., Kneib, J.-P., et al. 2003, *ApJ*, 591, 53
- van der Wel, A., Bell, E. F., Holden, B. P., Skibba, R. A., & Rix, H.-W. 2010, *ApJ*, 714, 1779
- Vanden Berk, D. E., Richards, G. T., Bauer, A., et al. 2001, *AJ*, 122, 549
- Vergani, D., Zamorani, G., Lilly, S., et al. 2010, *A&A*, 509, A42
- Weinmann, S. M., Kauffmann, G., van den Bosch, F. C., et al. 2009, *MNRAS*, 394, 1213
- Weinmann, S. M., van den Bosch, F. C., Yang, X., & Mo, H. J. 2006, *MNRAS*, 366, 2
- White, S. D. M. & Rees, M. J. 1978, *MNRAS*, 183, 341
- Wilman, D. J., Oemler, A., Mulchaey, J. S., et al. 2009, *ApJ*, 692, 298
- Wilman, D. J., Zibetti, S., & Budavári, T. 2010, *MNRAS*, 406, 1701
- Yang, X., Mo, H. J., van den Bosch, F. C., et al. 2007, *ApJ*, 671, 153
- Zucca, E., Bardelli, S., Bolzonella, M., et al. 2009, *A&A*, 508, 1217

Acknowledgements

I want to thank my supervisor, Dott. Angela Iovino, for proposing me this interesting project for my Ph.D. thesis, which gave me the chance to add my piece of understanding to the evolution of galaxies. It has been a long journey throughout difficulties and interesting findings, thank you for showing me always the bright side of each moment. Choosing such a comprehensive approach to the topic allowed me to learn computational skills, reduction techniques and different analysis approaches. These will be the solid basis I will rely on in the next years, thank to you.

In these three years Marco Scodiggio and Olga Cucciati have been of great support both during scientific/technical discussions and in sharing experience and suggestions. Thank you both.

I wish to thank the zCOSMOS collaboration for the immediate and warm welcome, this whole thesis would not have been possible without the effort of all of you. This collaboration provided me scientific and financial support during the entire Ph.D. period. Among all people working in zCOSMOS, there are few that I would like to mention and thank: Micol Bolzonella, you are the best example of a present and helpful collaborator, Alexis Finoguenov, you are such an inspiring person, and Christian Knobel with whom I shared most of the work.

The first year of my Ph.D. was dedicated to a different project and thank to Emanuela Pompei I had the chance to spend few months at ESO Chile. This changed my life and I want to thank you for giving me this unique opportunity and for being always such a stimulating person.

I want to thank also those people I spent most of my time with in Brera: first of all this thesis has been possible thank to the technology support of Cristina Bernasconi, you saved me and my thesis so many times. A special thank to Stefano Andreon for stimulating discussion on both astronomy and music. Thank to Marcella Longhetti for sharing her knowledge on synthetic models with me and for her genuine approach to this life, it's inspiring. Thank to Paolo and Paola for sharing our lives out of Brera and supporting me in many ways. Then I would like to thank Adriana, Ilaria, Maria Angela, and Sonia for those fundamental breaks during long working days and for the creation of parallel fancy worlds. Francesca: *breakfast at Sniffo's* was such a great

Acknowledgements

movie!

Davide, I don't know how I could have made this without you. You were present day and night, whenever I needed advices, suggestions and comments. Sharing this hard journey, the doubts, the exhalting moments, the questions, the many awake night hours with you made it easier and worth the effort. Mi raccomando: sgranda la mela!

To all my friends that don't even know what a galaxy is: thank you, without you I would have become insane! To the most patient man, Forrest Gump: let's go to Brazil!

Thank to my laptop, which didn't crash after falling from the table a week before thesis submission.

Finally, I want to thank my family for giving me unconditional support and love. I am a lucky person, I always knew it, these years made it only more evident. To you, and to your daily effort in showing me that is worth living this life, is dedicated this thesis.

CV of Valentina Presotto

PERSONAL DATA

Name:	Valentina
Surname:	Presotto
Date of Birth:	11-04-1983
Place of Birth:	Milan, Italy
Nationality:	Italian
e-mail:	valentina.presottobrera.inaf.it

EDUCATION

- 2008 November-present day, Ph.D. student in Astronomy and Astrophysics at the University of Insubria, Como. I am working at the Observatory of Brera, Milan, with Dr. A. Iovino and Dr. M. Scodreggio as supervisor. As part of the zCOSMOS project I am studying the environmental dependence of galaxy star formation. In details I am focusing on group environment trying to define a relation between group global properties and those of galaxies (including star formation rates, colours and masses). The work comprises analysis of both spectroscopic and photometric data and comparison with simulations.
- 30/09/2008, Master Degree in Astrophysics and Physics of Space at University of Milano Bicocca: vote 109/110; Thesis title: "Young and Dynamic: the galaxies of the southern compact group SCG0018-4854" During my thesis I worked at the Observatory of Brera, Milan, with Dr. A. Iovino as supervisor. I also collaborate with Dr. E. Pompei (ESO) and Dr. G. Temporin (Institut für Astro- und Teilchenphysik, Innsbruck). The work dealt with galaxies interactions in compact groups on the basis of high resolution photometric and spectroscopic data. The aim of the work was to investigate and analyse kinematics, morphology and activity of the galaxies of SCG0018-4854 and the effects of interactions on them.

- 26/10/2005, Bachelor Degree in Physics at University of Milano Bicocca: vote 100/110; Thesis' title: "Photometric studies of galaxies in the Virgo Cluster". I worked at the university with Prof. G. Gavazzi as supervisor. The work consisted in preparing the necessary instruments and software to identify and crosscorrelate the radio sources in the ALFALFA catalog with optical galaxies from the SDSS catalog in order to inquire into the relation between HI-mass and the mass of formed stars in optical galaxies.
- 2002, Secondary-level degree at Scientific Secondary-School Leonardo da Vinci Milano.

ATTENDED MEETINGS AND TALKS

- 14-25 November 2011, "XXIII Canary Islands Winter School of Astrophysics", Canary - Spain: I attended the school that this year focuses on the secular evolution of galaxies. I contributed with the poster: "When a galaxy catches the train to the core of groups"
- July 2011, Invited talk at the Observatory of Trieste, Trieste - Italy.
- 4-8 July 2011, "Alpine Cosmology Workshop" Innsbruck - Austria with a talk contribution. Title: "A journey from the outskirts to the cores of groups I: Colour and Mass Segregation in the 20k-zCOSMOS group sample."
- July 2009, Invited talk at ESO/Santiago - Chile, Thirty Minutes Talk (TMT)
- 24-29 May 2009, School of Astrophysics "Francesco Lucchin" - X Cycle, III Course, Bertinoro - Italy with talk contribution.
- 12-15 May 2009, "Galaxies in isolation: exploring nature vs nurture", Granada -Spain with poster contribution. In this occasion I won the competition of 'Best Conference Poster'.
- September 2008, "3D-NTT proposal meeting", Montreal - Canada 2008, I contributed to the talk: "The multiple faces of interactions in compact groups: tidal tails, free floating HII regions, new galaxies and galactic outflows", authors E. Pompei, A. Iovino, M. Dahlem, V. Presotto e S.G. Temporin
- September 2008, JENAM, Vienna - Austria with poster contribution.

- I also attended several international meetings of the zCOSMOS collaboration during which I exposed my work, (Marseille 2009, Milano 2010, Bologna 2010, Zurich 2011)

EMPLOYMENTS AND GRANTS

- 2008 November-present day, Ph.D. grant in Astronomy and Astrophysics at the University of Insubria, Como - Italy, granted by INAF.
- 4 July - 4 October 2009, Three month short term studentship DGDF 09/39 awarded by the European Southern Observatory (ESO) Chile. Project title: Strong mergers in compact groups of galaxies. Proposer: E. Pompei. During my staying at ESO I studied the photometric and morphological properties SCG0018-4854 galaxies, focusing on the likely age of the stellar populations and their correlation with morphological structures.

OBSERVATIONAL AND TECHNICAL EXPERIENCE

- July 2009, During the short term at ESO Chile I participate in the observatory run (6 nights) at the Very Large Telescope (VLT) using VIMOS. Target: deep spectroscopy of intragroup medium in compact groups of the Local Universe.
- April 2006, I participate in the observatory run (10 nights) at the Mexican National Telescope S.P.M. with Prof. G. Gavazzi of University of Milano Bicocca. Target: H α Narrow-Band imaging spectrophotometry to study recent star formation regions in local galaxies.
- February 2006, I participate in the observatory run (2 nights) at the Loiano Telescope as an additional activity of laboratory's classes. Target: nuclear spectroscopy of local galaxies to study their activity.
- Optical spectra reduction (long slits, MOS, MXU modes) and photometric data reduction (broad band), with IRAF standard packages, VIPGI (VIMOS Data Reduction Interactive Pipeline), GASGANO (ESO data handling/reduction tool), and SWARP (images co-adding and resampling program).
- Experience in handling and fitting simple stellar population (SSP) models to observed spectra using GOSSIP (Interactive SED fitting Program).

- Basic knowledge of Bayesian analysis of statistical models with JAGS (Just Another Gibbs Sampler).
- Wide experience in writing codes using IDL language. In particular I developed: 1) a code to retrieve group galaxy membership, 2) a code for group centering, 3) a code to stack spectra of galaxies and handling templates.
- Experience in extracting/handling catalogs from both galaxy survey database (zCOSMOS) and simulation database (MILLENIUM)

INTERESTS

- Large and small scale environment (compact/fossil groups, galaxy groups and clusters)
- Environmental effects on galaxy properties
- Galaxy formation and evolution
- Spectral analysis of galaxy properties: Star Formation, Spectral Indices
- Galaxy-galaxy interactions

List of publications

Heavily involved into:

1. Presotto, V., Iovino, A., Scodeggio, M., et al. 2012, ArXiv e-prints
2. Tanaka, M., Finoguenov, A., Lilly, S. J., et al. 2011, ArXiv e-prints
3. Peng, Y.-J., Lilly, S. J., Kovač, K., et al. 2010, ApJ, 721, 193
4. Presotto, V., Iovino, A., Pompei, E., & Temporin, S. 2010, A&A, 510, A31+

Marginally involved into:

1. Bordoloi, R., Lilly, S. J., Knobel, C., et al. 2011, ArXiv e-prints
2. de la Torre, S., Guzzo, L., Kovač, K., et al. 2010, MNRAS, 409, 867